COMPLEX NETWORK APPROACH FOR INVESTIGATING THERMOACOUSTIC SYSTEMS

A THESIS

submitted by

MEENATCHIDEVI MURUGESAN

for the award of the degree

of

DOCTOR OF PHILOSOPHY

DEPARTMENT OF AEROSPACE ENGINEERING
INDIAN INSTITUTE OF TECHNOLOGY MADRAS

MARCH 2016

THESIS CERTIFICATE

This is to certify that the thesis titled **COMPLEX NETWORK APPROACH FOR INVESTIGATING THERMOACOUSTIC SYSTEMS**, submitted by **Meenatchidevi Murugesan**, to the Indian Institute of Technology, Madras, for the award of the degree of **Doctor of Philosophy**, is a bona fide record of the research work done by him under our supervision. The contents of this thesis, in full or in parts, have not been submitted to any other Institute or University for the award of any degree or diploma.

Prof. R. I. Sujith
Research Guide
Professor
Dept. of Aerospace Engineering
IIT-Madras, 600036

Dr. Sridharakumar Narasimhan
Research Co-Guide
Assistant Professor
Dept. of Chemical Engineering
IIT-Madras, 600036

Place: Chennai
Date: 29th March 2016

Place: Chennai
Date: 29th March 2016

To my father

ACKNOWLEDGEMENTS

I would to like to thank and acknowledge the support and help of many people, without them this thesis would not have been possible:

First of all, I am much indebted to my Ph. D. supervisor, Prof. R. I. Sujith for his valuable guidance and continuous support. His vigorous enthusiasm for research kept me constantly engaged with my research. His exceptional passion for looking for new insights and comprehend the results has been an inspiration for me. He has been there for me with tireless encouragement in all the tough times. I have learned a lot of things from him, both technical and non-technical, that have helped and would help me to continue research as my career in the future.

I would like to express my sincere gratitude to my co-guide Dr. Sridharakumar Narasimhan from Chemical Engineering department for his exceptional comments and suggestions. I would like to thank the members of my Doctoral Committee, Dr. Sunetra Sarkar, Dr. Nandan Kumar Sinha and Dr. Preeti Aghalayam for their valuable comments and suggestions during the meetings. I am much thankful to the Head of the Aerospace Engineering department, Prof. K. Bhaskar for his support and encouragement throughout my Ph. D. period. I would also like to thank my teachers, Prof. M. Ramakrishna, Dr. Amit Kumar, Dr. T. M. Muruganandam, Prof. S. R. Charavarthy, Dr. Santanu Ghosh, Dr. N. R. Panchapakesan from the Department of Aerospace Engineering, Prof. V. S. Ramachandra Rao (Chemical Engineering), Prof. Arul Lakshminarayan and Prof. Neelime Gupte from the Department of Physics.

I am much thankful to the constant support of the administrative staffs, Mrs. Y. Mekala, Mr. A. Robin Kennedy, Mrs. K. Aruna Kumari, Mr. Manikandan, Mrs. T. R. Yamuna and Mrs. S. Nirmala. I would like to thank Mr. E. Sankara Kumaraswamy, Mr. John George, Mr. M. Divakaran, Mr. A. Thayalan and Mr. B. Biju Kumar for their great help in workshop. I would like to acknowledge Mr. Ranganathan (passed away) for his great help in fabrication of most of the components in my experimental setups.

I would like to acknowledge the financial assistance rendered by Ministry of Human Resource Development (MHRD) to present the papers in an International conference and Institute for Advanced Studies (IAS), Munich, Germany to support my travel to TU Munich. I would like to thank Prof. W. Polifke and Mr. Thomas Emmert from TU Munich for teaching me new tools of TAX software.

This section would never be complete, if I do not mention my lab friends who have supported me in all the times. I would like to thank my senior colleagues, Dr. Sathesh Mariappan, Dr. Priya Subramanian, Dr. Lipika Kabiraj, Mr. J. Vivekanadan, Dr. Vineeth Nair and Dr. Gireesh K. Thampi for motivating and mentoring me to get started with my research. The major parts of the experimental setup which I have used in my Ph. D. work were fabricated for the M. S. work of Mr. J. Vivekanadan. I would like to sincerely acknowledge him for teaching me to perform experiments. I am also much thankful to Dr. Vineeth Nair and Mr. Vishnu R. Unni for providing the unsteady pressure data that are used in the present thesis.

Next, I would like to sincerely thank Mr. E. A. Gopalakrishnan for his selfless help at the right times. He has helped me a lot in both technical and non-technical aspects. He has patiently offered continuous support and motivation to me throughout my Ph. D. period. I am also thankful to my lab mates Samadhan, Mani, Abin, Prabodh, Sirshendu, Mridula, Akshay, Tony, Sreelekha, Vishnu R. Unni, Nitin, Syam, Dileesh, Rama and Hashir. Mr. Dileesh has helped in performing experiments and drawing the schematic of the experimental setups.

Finally, I should acknowledge my family members for their love and constant support. My father and husband has always encourgaged and supported me in all the decisions which I have made. I would like to acknowledge the tremendous sacrifices that my parents made to ensure that I had an excellent education. For this and much more, I dedicate this thesis to my father and husband. I thank the Almighty for giving me the strength and patience to work through all these years.

ABSTRACT

KEYWORDS: Thermoacoustic instability; Blowout; Combustion noise; Complex networks; Visibility graph; Threshold grouping method; Scale-free network; Regular network; Pattern formation; Precursors; Intermittency; Flame-flow-acoustics interaction.

Combustion is a major source of energy production for a wide range of applications to meet the increasing demand for power. In recent times, there has been a drive towards clean energy and lower emissions. Towards this goal, engines are operated under fuel lean conditions, where the temperature of the products is low, thereby reducing the production of oxides of nitrogen, which are harmful. However, the development and operation of such engines are marred by the occurrence of combustion instability (also known as thermoacoustic instability) and blowout of flame.

Inherent fluctuations in the flow get amplified when the unsteady heat release rate from combustion interacts in phase with the acoustic field of the combustion chamber. Consequently, detrimental, high-amplitude, pressure oscillations known as thermoacoustic instability occurs in combustion systems. These oscillations often cause losses in billions of dollars to the engine companies. Meanwhile, the blowout of flame is another dangerous problem which can even cause sudden descent of an airplane, in addition to the financial losses. These detrimental thermoacoustic instability and flame blowout occur in the system when combustors are operated in a fuel-lean condition. However, clean combustion as well cannot be avoided to meet the stringent emission norms. Hence, an understanding of the transition to thermoacoustic instability and blowout is absolutely critical.

Traditionally, thermoacoustic systems are analyzed from a reductionist approach which attempts to analyze a complex system in terms of its constituent elements. Recently, it was shown that the combustion noise and the near blowout dynamics display multifractal characteristics. The presence of multifractality in the combustion dynamics is a reflection of the complexity of the

thermoacoustic systems. The traditional reductionist approach fails to explain the complex behaviours in the thermoacoustic systems.

In the present thesis, the complex behaviours in the dynamics of thermoacoustic systems are investigated in the framework of complex networks. First, the pattern in the dynamics of the combustion noise generated during the stable operation of the combustor is investigated. The unsteady pressure data from a backward-facing step combustor is converted into obtain complex networks using the visibility condition. The scale invariance of combustion noise in a confinement is hard to discern from the frequency spectra due to the presence of low-amplitude peaks, arising from the coupling of combustion noise with the confinement modes. The complex network representation reveals the scale invariance of combustion noise as scale-free structure in the topology of the complex network. The dynamics of the combustion noise is mapped as nodes and links between them and the power-law behavior in the distribution of links in the network is a clear reflection of the scale invariant property of the combustion noise generated in a turbulent environment.

Further, the structure of the complex network during thermoacoustic instability possess regular topology that represent order. The transition to thermoacoustic instability from combustion noise is reflected as a transition from scale-free to order in the networks topology. The measures for quantifying the topological features of the networks such as clustering coefficient, characteristic path length, network diameter and global efficiency are calculated at each operating conditions during the transition from combustion noise to thermoacoustic instability. These network measures change significantly well before the onset of thermoacoustic instability and can be used as the precursors to thermoacoustic instability.

The transition in the system dynamics from combustion noise to the onset flame blowout is investigated in the framework of complex networks. The regular structure in the complex networks during thermoacoustic instability transition to scale-free structure at the onset of blowout. The network properties are computed and used as the early warning measures to the onset of blowout.

The transition to thermoacoustic instability and blowout from the stable operation happened via intermittency. In order to investigate the physical reasons for such transitions in thermoacoustic systems, we investigated the intermittent dynamics that presages the onset of thermoacoustic instability and blowout in a turbulent lifted jet flame combustor. The simultaneous measurement of acoustic pressure, chemiluminescence images and Mie scattering images are performed in order to characterize the acoustics-flame-flow interactions during intermittency.

The intermittent dynamics prior to the onset of thermoacoustic instability occurs due to the alternating (either positively or negatively) coupled interaction of the flame, flow and duct acoustics. In contrast, the intermittency that presages the onset of blowout is caused by the interplay between the blowout precursor events and the driving of high-amplitude pressure oscillations as the flame propagate towards the fuel tube. Alternatively, the commonality between the intermittency prior to thermoacoustic instability and blowout is investigated using first return maps and recurrence plots.

TABLE OF CONTENTS

LIST OF FIGURES

ABBREVIATIONS

LPG	Liquefied Petroleum Gas
SLPM	Standard Litres Per Minute
RMS	Root Mean Square
MFDFA	MultiFractal Detrended Fluctuation Analysis
BVK	Benard Von Karman
RP	Recurrence plot

NOTATION

$x(t)$	Time series to be converted into complex network
$p(t)$	Local peaks in the time series
$A_{i,j}$	Adjacency matrix
δ	Threshold in the threshold grouping method
x_{n+1}	$(n+1)^{\text{th}}$ iterate of a function x in the Henon map
x_n	n^{th} iterate of a function x in the Henon map
a, b	Variables in the Henon map
k	Degree of a node
$P(k)$	Percentage of nodes having degree of k in the network
γ	Power-law exponent in the plot of $P(k)$ Vs k
Re	Reynolds number
M	Size of the adjacency matrix
k_v	Degree of a node v
C_v	Clustering coefficient of node v
N_v	Number of links in the neighborhood of a node v
$K_v(K_v - 1)/2$	Maximum possible number of links in the neighborhood of a node v
C	Clustering coefficient of a network
$L_{i,j}$	Short path length
L	Characteristic path length
D	Diameter of the network
E	Global efficiency
H	Hurst exponent
E	Threshold in the visibility condition
C_0	Maximum value of the clustering coefficient
L_0	Maximum value of the characteristic path length
D_0	Maximum value of the network diameter
C_0	Maximum value of the global efficiency
φ	Equivalence ratio
P_{max}	Maximum value of the unsteady pressure
x_f	Location of the inner copper tube inside the quartz tube
p'	Unsteady pressure
I	Intensity of CH^* chemiluminescence

I_0	Maximum value of the intensity of CH^* chemiluminescence
St	Strouhal number
f	Characteristic frequency
L	Thickness of the hexagonal nut
U	Velocity of the co-flowing air in the quartz tube
t	Time
X_n	Vector consists of local maxima in the time series data
X_{n+1}	Vector consists of local maxima in the time series data
$R_{i,j}$	Recurrence matrix
Θ	Heaviside step function
σ	Threshold for the maximum distance between a pair of states in the phase space to treat them as recurrent
Z	Time delayed vectors indicating the state of the system in the phase space
u, v	Time instants when the distance is calculated
N	Length of the unsteady pressure data
d_0	Embedding dimension
τ_{opt}	Optimum time delay
D	Diameter of the attractor in the phase space

CHAPTER 1

INTRODUCTION

1.1 Motivation

Thermoacoustic instability and blowout of flame are the most challenging problems faced in the development of practical combustion systems of aero-engines and land-based gas turbines (Mcmanus *et al*., 1993; Lieuwen, 2012; Nair and Lieuwen, 2005). Thermoacoustic instability refers to the occurrence of large-amplitude, self-excited, self-sustained pressure oscillations in the combustion systems. Thermoacoustic instability occurs as a consequence of coupled interaction of the unsteady heat release rate from combustion with the acoustic field of the combustion chamber (Lieuwen, 2012).

Inherent fluctuations in the flow create oscillations in the heat release rate from combustion (Lieuwen, 2012). As an example, the changes in the flame surface area and consequently, the oscillations in the heat release rate from flame are modeled to occur due to the upstream velocity fluctuations in the study of premixed flames (Schuller *et al*., 2003; Subramanian and Sujith, 2011). The oscillations in the heat release rate produce volumetric expansion and compression of the fluid in the vicinity of the flame. Thus, the flame is often modeled as a series of monopole sources of sound (Subramanian and Sujith, 2011). The acoustic waves originated from the combustion source travel downstream of the combustion chamber and reflect back towards the flame at the boundaries. When the acoustic waves establish this feedback coupling positively (i.e., in phase) with the oscillatory heat release rate, the amplitude of the acoustic oscillations begins to grow (Rayleigh, 1878). When the acoustic oscillations reach certain large-amplitude, nonlinearity comes into picture. The acoustic oscillations saturates to large-amplitude, self-sustained, limit cycle oscillations as the driving from the positive coupling of the heat release rate and the acoustics balances the damping (or acoustic losses) in the system.

The existence of self-sustained, large-amplitude, acoustic oscillations causes excessive vibrations, increased thermal and structural loading on the propulsive systems (Mcmanus *et al.*, 1993; Lieuwen, 2012). Eventually, this can lead to structural damage or even complete failure of the systems. Therefore, prediction and control of thermoacoustic instability is an important problem in the design and development of combustors for practical systems. The complex interactions of the acoustic field of the combustion systems with the processes that cause fluctuations in the heat release rate are hard to understand and the problem of thermoacoustic instability remains challenging. Further, combustion systems are required to operate in a fuel-lean condition to meet the stringent emission norms. Combustion systems are more prone to thermoacoustic instability if operated in a fuel-lean condition (Annaswamy *et al.*, 1997).

In addition to thermoacoustic instability, fuel-lean operation makes the combustion systems to be prone to blowout of the flame as well (Nair and Lieuwen, 2005; Muruganandam *et al.*, 2005). When the combustion takes places in a fuel-lean condition, the temperature of the reaction zone is low and consequently, the speed at which the flame propagates into reactive mixture is low. The stabilization of the flame inside the combustion systems is a challenging task in such situations where the flame speed is slower than the incoming flow speed to the combustion chamber. As a general practice, the flame is stabilized using flame holding devices which creates low-velocity zones or using a pilot flame which increases the reaction rate to stabilize the flame. However, in the case of a fuel-lean combustion, the common flame stabilization practices fails and the flame propagates out of the combustion systems, which is traditionally referred as blowout of the flame. The value of equivalence ratio at which the flame blowout happens is specified as the lean blowout limit.

The blowout of flame causes unexpected power loss to the aero-engines. In land-based power plants, in addition to this power loss, the blowout creates emergency shut down and re-ignition processes which are highly expensive. In aero-engines, the blowout leads to loss in thrust and the re-ignition of flame could be difficult which can even cause sudden descent of an airplane. In military applications, blowout can be disastrous during the high-thrust requirements. Currently, the occurrence of blowout is avoided by roughly estimating the blowout limit based on the time scales of flow speed and flame speed and restricting the combustor operators to conservative safe operating range. However, inherent turbulent fluctuations in the flow and large-amplitude acoustic oscillations during thermoacoustic instability can alter the stable operating regime and trigger blowout. The classical stability analysis uses linear relations to detect the onset of thermoacoustic instability and blowout of flame in combustion systems.

1.2 Classical stability analysis

In the classical stability analysis of combustion systems, the onset of flame blowout and the onset of thermoacoustic instability from the stable operation (i.e., combustion noise) are viewed as two different phenomena. As an example, the flame behaviors such as flashback or blowout when the flame cannot stabilize inside the combustor are treated as static instability of the flame (Nair, 2006; Muruganandam, 2006). The statistically stable operating regime are estimated by determining the range of operating conditions over which the flame does not flashes back or blows out of the combustor.

The stabilization of the flame inside the combustor is associated with the balance between the flame speed and the flow speed. Based on this principle, many different theories are proposed to provide a condition for the onset of blowout (Zukoski and Marble, 1955; Longwell *et al*., 1948; Splading, 1955). Despite their difference, all the approaches lead to a similar condition for the blowout in terms of Damkohler number ($Da = \frac{\tau_{res}}{\tau_{chem}}$). Here, τ_{res} represents the flow residence time and τ_{chem} represents the chemical reaction time. According to this condition, the flame blowout occurs when the flow residence time is faster than the chemical reaction time. Alternatively, the flame blowout condition is framed in terms of the turbulent flame speeds and the local flow velocities (Lewis and Von Elbe, 2012; Wohl, 1953). The flame is treated as a number of flamelets and the blowout occurs if the turbulent flame speeds of all the flamelets are slower than the local flow velocities (Lewis and Von Elbe, 2012; Wohl, 1953).

Despite the complications in computing the turbulent flame speeds for each flamelet, the underlying principle of the condition for the onset of blowout is the same as the Damkohler number correlations. These conditions implicitly assume that the blowout is an abrupt event. The occurrence of blowout is, however, not an instantaneous process. The onset of blowout is most often preceded by seemingly random oscillations in the flame and the acoustic characteristics of the combustion systems. Nicholson and Field (1948) reported that the blowout is presaged by the events of flame detachment and reattachment to the flame holding device. Therefore, the classical static stability analysis of blowout, which have not accounted for these complex behaviors in combustion systems, fails to accurately detect the onset of blowout.

In the classical analysis, in contrast to blowout, the onset of thermoacoustic instability is considered as a dynamic instability of the combustion systems (Nair, 2006; Muruganandam, 2006). The existence of self-excited acoustic oscillations in combustion systems was the reason to view thermoacoustic instability as a dynamic instability. Most often in the classical analysis of thermoacoustic instability, the time evolution of the combustion systems are mathematically represented as a number of linearized ordinary differential equations. This linearization is based on the assumption that the amplitude of fluctuations in the system is small. Lieuwen (2002) reported that the amplitudes of acoustic pressure oscillations in the gas turbine combustors are less than 5% of the mean pressure. Therefore, the linear stability tools are often used to find whether the combustion system is dynamically stable or not. In the linear analysis, the system of governing linear equations are arranged in the standard form as, $\frac{dx}{dt} = Ax$. The system is linearly stable if the real parts of all the Eigen values of the linear matrix A are negative. The linearly stable operating regimes (i.e., dynamic stability) are identified for different combustor configurations by determining the operating conditions for which the real parts of all the eigenvalues are negative.

Alternatively, in the frequency domain, the linear stability analysis is performed by modelling the combustion systems as a network of a number of subsystems (Paschereit *et al.*, 2002). The interactions between the subsystems are specified in terms of their transfer functions. As an example, the transfer function describing the response of acoustic field of the combustion system to unsteady combustion is specified as the ratio of acoustic variables (acoustic velocity) to the heat release rate oscillations at given operating conditions. The acoustic response to the heat release rate fluctuations at different forcing frequencies are specified using flame describing functions. The eigenvalues of these transfer functions or flame describing functions are then used to determine the linear stability of the combustors.

The amplitude of acoustic oscillations is expected to grow exponentially even for infinitesimally small disturbances in a linearly unstable system. However, in practical combustion systems, the nonlinear mechanisms cause the acoustic oscillations to saturate to a finite, large-amplitude limit cycle oscillations. Therefore, the classical linear analysis can only provide information about the growth or decay rate of the acoustic oscillations from the eigenvalues. The classical linear analysis cannot predict the amplitude and the frequency of limit cycle oscillations during thermoacoustic instability. The characteristics (amplitude and frequency of limit cycle oscillations) of thermoacoustic instability, however, need to be estimated accurately during the design phase of the gas turbine combustors (Zinn and Lieuwen, 2006).

Further, the fluctuations in the system are assumed to be small in the linear analysis. When the amplitude of fluctuations in the system is above a certain threshold value, nonlinear processes can trigger thermoacoustic instability even if the system is linearly stable. The amplitude levels of fluctuations in the combustion system depend on many factors such as turbulent intensity levels, fuel-air ratio and geometry of the combustor etc. The classical linear theory is simple which have not accounted for the initial state of the combustor, fails to explain such triggering of thermoacoustic instability. Hence, to predict the onset of thermoacoustic instability and the onset of flame blowout as well, one has to understand the nonlinear processes involved in the combustion systems.

1.3 Literature review

The stability analysis of the combustion systems are performed in order to understand the mechanisms that cause thermoacoustic instability and blowout of flame. The phenomenon of flame blowout was studied as a flame stabilization problem. Based on the incoming flow velocity, the flame is considered to be stable, flashes-back and blows out of the combustor. Lewis and Von Elbe (2012) reported that the flame blows out as the air flow velocity is increased. The mechanism of flame stabilization in most of the practical combustors is as follows. The fresh mixture of reactants enters the recirculation zone created by the bluff-body and mixes with the hot combustion products. As the temperature of the fresh reactants increases above a certain threshold, combustion takes place. The part of the hot reactive mixture travels downstream in the flow and the remaining part of the hot combustion products in the recirculation zone increases the temperature of the incoming fresh reactants. This feedback process between the hot combustion products and the cold reactants is necessary to stabilize the flame inside the combustion systems.

Zukoski and Marble (1955) developed a condition for the onset of flame blowout based on such flame stabilization mechanisms. They assumed that the stream of incoming flow is in contact with the recirculation zone for a time interval (τ_{res}) based on the velocity of the incoming flow and the length of the recirculation zone. They suggested that the flame blowout occurs if the time spent by the incoming flow in contact with the hot recirculation zone is less than the time required for ignition. They formulated this blowout condition in terms of Damkohlar number ($Da = \frac{\tau_{res}}{\tau_{chem}}$) as, Da is 1 at the condition of flame blowout. Similar to Zukoski and Marble (1955), ; Longwell *et al*. (1948) and Splading (1955) provided a similar condition for the onset of blowout.

Alternatively, the blowout conditions are developed by considering flamelet-like combustion properties (Lewis and Von Elbe, 2012; Wohl, 1953). In this approach, the flame stabilization is related to the flame propagation in the reactive mixture. The flame is treated as a number of flamelets. Each flamelet propagates with its own flame speed (S_L). Blowout occurs if the flame speeds of all the flamelets are slower than the local flow velocities ($S_L < U_{local}$) (Lewis and Von Elbe, 2012; Wohl, 1953). Here, the calculation or measurement of turbulent flame speeds for each flamelet is complicated and related to the composition of the fuel-air mixtures.

The effect of fuel composition on the characteristics of blowout was investigated (Schefer *et al*., 2002; Griebel *et al*., 2007; Yoshimura *et al*., 2005). Studies showed that the addition of H_2 delays the onset of blowout. The addition of H_2 results in increase in the concentration of OH^* radicals. This increase, in turn, increases the reaction rate and the flame speed to delay the onset of blowout. This delay in blowout was shown to be linearly correlated with the percentage of H_2

addition. In addition to the delay in blowout, the addition of H_2 reduces the emission level of CO and NO_x (Schefer *et al.*, 2002; Griebel *et al.*, 2007; Yoshimura *et al.*, 2005).

Most of these approaches treated blowout as an instantaneous event. However, Nicholson and Field (1948) reported that the onset of flame blowout is associated with the dynamic behaviors in flame. The flame detachment and reattachment from the flame holder is reported prior to blowout. The dynamic behavior of flame close to blowout condition can be found in Nair and Lieuwen (2005), Muruganandam *et al.* (2005) and Nair and Lieuwen (2007).

Nair and Lieuwen (2005) reported that the time-localized intermittent events are seen prior to blowout. They measured the acoustic signals and flame images in combustors with different flame stabilization methods, pilot, swirler and bluff-body, to characterize the dynamical behaviours prior to blowout. They reported that the time-localized intermittent events become more frequent as the combustion systems approach blowout (Nair and Lieuwen, 2005; Muruganandam *et al.*, 2005). These changes in dynamics are used to develop threshold-based precursors to identify the onset of blowout (Nair and Lieuwen, 2005; Muruganandam *et al.*, 2005). Muruganandam *et al.* (2005) measured the OH^* chemiluminescence and developed precursors to blowout. As the onset of blowout is detected, the fuel flow distribution was altered to change the equivalence in order to control the occurrence of blowout. The active control of blowout was demonstrated in a swirl-stabilized combustor (Muruganandam *et al.*, 2005).

Further, the flow-field dynamics prior to blowout are investigated (Nair and Lieuwen, 2007; Shanbhogue *et al.*, 2009; Muruganandam and Seitzman, 2012). They reported that the blowout of flame occurs in a two stage process. First, as the equivalence ratio is reduced towards the condition of flame blowout, they showed that the vortices close to bluff-body have higher magnitudes of vorticity. These vortices of higher vorticity magnitude introduces higher fluid mechanical stretch rate to the flame. If such increase in flame stretch rate exceeds above a flame extinction stretch rate, holes are formed in the flame during the first stage of flame blowout process. As the equivalence is further reduced, these flame holes are formed in many regimes of flame and a violent detachment and reattachment of flame to the bluff-body was observed before the flame completely blows out.

Nair and Lieuwen (2007) and Shanbhogue *et al*. (2009) observed that the flow-field prior to blowout is characterized by the presence of vortices that shed due to the von Karman type hydrodynamic instability which is similar to the vortices that are shed in the non-reacting flow. Such interactions of hydrodynamic instability with the flame are inevitably nonlinear. Hence, nonlinear analysis of blowout could bring more insight into the dynamic processes prior to blowout of flame.

Meanwhile, in the context of thermoacoustic instability, the nonlinear analysis have been performed to understand thermoacoustic instability encountered in various practical systems including rocket motors, gas turbine combustors, ducted laminar premixed and non-premixed flames. Since 1930, Culick attempted to investigate the influence of nonlinear processes to understand the thermoacoustic instability occurring in the solid and the liquid rocket motors. In rocket motors, when the unsteady heat release rate from the burning of propellants form a positive feedback coupling with the acoustic field, large-amplitude thermoacoustic pressure oscillations are developed. Typically in the rocket motors, the amplitude of unsteady pressure increases up to the order of magnitude of 20% to 50% of the mean pressure levels. This led Culick to consider that the nonlinear mechanisms in thermoacoustic instability could be arising from such gas dynamic effects (Culick, 1970, 1976).

The nonlinear equations for the acoustics are solved with the assumption that the combustion process is linear and the condition for the occurrence of thermoacoustic instability are calculated. Later, the nonlinear processes arising from the gas dynamic effects are shown to be insignificant to cause triggering of thermoacoustic instability. In contrast, the nonlinear effects arising from the combustion processes were considered as a possible cause for the triggering (Culick, 1994). The nonlinearity was introduced in the interaction between the heat release rate (i.e., burn rate of propellant) and the acoustic velocity.

Similar to the nonlinear analysis of thermoacoustic instabilities in rocket motors, the nonlinear mechanism that cause thermoacoustic instability in the gas turbine combustors is also considered to arise from the interaction between the heat release rate oscillations and the acoustic velocity oscillations (Dowling, 1997; Lieuwen, 2002). The amplitude of the unsteady pressure in the gas turbine combustors is reported to be less than 1% to 5% of the mean pressure. In non-premixed flames, the interaction of heat release rate fluctuations with the acoustic field of the combustion systems is identified to be nonlinear (Tyagi *et al*., 2007). Tyagi *et al*. (2007) used the model of non-premixed flame with finite rate chemistry and infinite rate chemistry to illustrate the nonlinear interaction of flame and acoustics.

In the experimental investigation of premixed flames, the response of premixed flames to the acoustic excitation is shown to be nonlinear (Karimi *et al*., 2009; Noiray *et al*., 2006, 2008). The premixed flames were forced with acoustic excitations of different frequencies and amplitudes. The response of the flame to such excitation of different frequencies and amplitudes are used to formulate the nonlinear describing function for the particular combustor configuration. This nonlinear describing function is treated as a response function for the flame and the interaction of this flame response with the acoustic field of the combustor is investigated to understand the onset of thermoacoustic instability (Noiray *et al*., 2006, 2008). The interaction of premixed flame with the acoustics is considered to be nonlinear in the numerical and analytical approach to thermoacoustic instability as well.

The approach to understand thermoacoustic instability based on the flame transfer function relies on the response of the flame to acoustic forcing. However, in engineering systems, thermoacoustic instability is self-excited. Therefore, investigating the nonlinear aspects which cause self-excited thermoacoustic instability in the absence of forcing could bring more understanding. Further, the nonlinear processes at the onset of blowout are still not clear. The dynamical systems approach is a framework to investigate the nonlinear dynamics of the systems.

1.4 Dynamical systems approach

Culick considered that the nonlinearity arises from the gas dynamic processes and showed that the amplitude of the acoustic oscillations nonlinearly saturate to a limit cycle oscillations (Culick, 1970, 1976). Later, the nonlinearity from gas dynamic processes was shown to be not significant to cause thermoacoustic instability. The nonlinear interaction between the heat release rate and the acoustic field was modeled as a time delayed coupling.

Jahnke and Culick (1994) used tools from dynamical systems theory such as continuation methods and showed that the pitchfork and torus bifurcation are possible in the dynamics of thermoacoustic systems. Further, they showed that in addition to limit cycle oscillations, quasi-periodic oscillations dominated by two incommensurate frequencies are also possible in the thermoacoustic systems (Jahnke and Culick, 1994). Dynamically complex behaviors, as an example chaos, are reported in the numerical (Sterling, 1993; Lei and Turan, 2009) and the experimental (Fichera *et al*., 2001) investigation of thermoacoustic systems.

Recently, Sujith and coworkers used the dynamical systems approach to systematically investigate the nonlinear behaviors of the thermoacoustic systems. In a horizontal Rijke tube, Subramanian *et al*. (2010) investigated the bifurcation to thermoacoustic instability using numerical continuation methods. Further, Subramanian *et al*. (2010) reported that the quasi-periodicity and the period doubling route to chaos are observed in the dynamics of a horizontal Rijke tube from their numerical analysis. Similar to the numerical investigation of a horizontal Rijke tube, Subramanian and Sujith (2011) showed that the dynamical behaviors such as subcritical bifurcation, quasi-periodicity and route to chaos are possible in the numerical analysis of a ducted laminar premixed flame.

In parallel to these numerical studies, Kabiraj and Sujith (2012) experimentally investigated the dynamics of the thermoacoustic systems from the framework of dynamical systems approach. The quantities describing the dynamics of a practical systems are a few in case of experimental studies. Therefore, the nonlinear time series analysis tools such as phase space reconstruction are used to unravel the dynamical features of a system hidden in the time series data. Kabiraj and Sujith (2012) reported that the dynamical behaviors such as quasi-periodicity, period doubling, chaos in a ducted laminar premixed flame. Similar results are reported in the numerical investigation by Kashinath and Juniper (2013), Kashinath *et al*. (2013), Waugh *et al*. (2014) and Kashinath *et al*. (2015).

All these approaches investigated the dynamics of the thermoacoustic systems operated in laminar flow conditions. However, most of the practical systems operate in a turbulent environment. The thermoacoustic instability in a gas turbine combustors was analyzed from a dynamical systems perspective (Lieuwen, 2002; Gianni *et al*., 2003). Lieuwen (2002) considered the stable state of the thermoacoustic system as a fixed point and the birth of limit cycle oscillations is explained as a loss in stability of that fixed point. The transition to instability is explained as a bifurcation due to the change in operating conditions of the system. Traditionally, thermoacoustic systems are considered to have two states – stable and unstable. The stable state corresponds to a fixed point and the unstable state corresponds to a limit cycle (Lieuwen, 2002).

Recently Nair *et al*. (2013) showed that the stable regime of a combustor with turbulent flow does not correspond to a fixed point. They suggested that the low-amplitude aperiodic pressure fluctuations during the stable operation of the combustor (known as combustion noise in the community) are deterministic and have chaotic behavior. During thermoacoustic instability, the acoustic pressure is characterized by large-amplitude, self-sustained, periodic oscillations. In contrast with chaos, these periodic oscillations represent order. The transition from combustion noise to order (i.e., periodic oscillations) happens via intermittency; a state composed of bursts of large-amplitude periodic oscillations amidst regions of low-amplitude chaotic fluctuations (Nair *et al*., 2013; Nair *et al*., 2014).

Intermittency is a state composed of alternating appearances of both chaotic and quiescent/periodic states in an apparently irregular manner (Pomeau and Manneville, 1980). They used measures quantifying intermittency as precursors to detect the onset of impending thermoacoustic instability (Nair and Sujith, 2014; Nair *et al*., 2014).

Kabiraj and Sujith, (2012) reported intermittency before the onset of blowout in a simple thermoacoustic system that consists of a ducted laminar premixed flame. The tools from nonlinear time series analysis such as phase space reconstruction and recurrence plots are used to characterize the intermittency. Gotoda *et al*. (2014) reported that the relatively regular pressure fluctuations during thermoacoustic instability transitioned to intermittency before lean blowout with respect to decreasing equivalence ratio in a model gas turbine combustor.

Unni and Sujith (2015), Nair and Sujith (2015), Thampi and Sujith (2015) and Nair (2014) and also observed intermittent bursts of periodic oscillations as they varied the Reynolds number further past the condition of thermoacoustic instability towards the condition of lean blowout. Unni *et al*. (2013) invented a system and method to detect blowout in combustion systems which relies on the appearance of intermittency prior to blowout. Measures from time series analysis such as Hurst exponent, recurrence rate and burst count etc. are used to detect blowout. Gotoda *et al*. (2014) used a quantity called translation error from dynamical systems theory to detect lean blowout

Thus, intermittency precedes both blowout and thermoacoustic instability when the combustion systems are operated in a turbulent environment (Nair and Sujith, 2014; Nair *et al*., 2014; Gotoda *et al*., 2011, 2012, 2014; Unni and Sujith, 2015; Nair, 2014).

From a dynamical systems perspective, intermittency prior to thermoacoustic instability (Nair and Sujith, 2013) and lean blowout (Nair 2014) are shown to arise from the formation of homoclinic orbits in the reconstructed phase space. Homoclinic orbit is a phase space trajectory in which an unstable manifold of a fixed point of the system merges with its own stable manifold (Strogatz, 2014). This results in switching of the system dynamics back and forth between the stable and unstable orbits in the phase space. In time series data, such dynamics manifest as the alternative appearance of bursts of high-amplitude periodic oscillations and low-amplitude chaotic fluctuations in the unsteady pressure. The presence of chaos and intermittency reflects the complexity of the dynamics of thermoacoustic systems.

1.5 Complex systems approach

Complexity is a characteristic of real physical systems. Our day-to-day dynamical systems, for example, economic systems, our language or biological systems are ‘complex’ systems, because a great number of interacting elements are involved. The behavior of a thermoacoustic system for example arises from a variety of factors such as molecular mixing, turbulent transport that involves a wide range of scales, chemical kinetics and acoustic wave interaction etc., giving rise to a rich variety of dynamics, giving rise to the possibility of chaotic fluctuations on one hand to ordered periodic oscillations on the other hand.

Despite the many differences in the nature of complex systems, they often display similar dynamical behavior. The traditional reductionist approach, which attempt to analyze a complex system in terms of its constituent elements, hits its limit in explaining these similarities in fundamentally different physical systems (Barabasi, 2011). In this context, a new approach to science has emerged in recent years that investigate how interaction between parts (or elements) gives rise to the collective behavior of the system. This approach is defined as complex systems approach, where a complex system is reviewed as a system with "multiple interacting components whose behavior cannot be simply inferred from the behavior of the components" (http://www.necsi.edu).

In complex systems approach to thermoacoustic systems, Nair and Sujith (2014) have shown that combustion noise displays a multifractal signature and this disappears at the onset of thermoacoustic instability. A fractal time series has portions that look similar to the whole time series and have non-integer dimension. In a multifractal time series, fluctuations of different amplitudes scale differently. Multifractality of combustion noise confirmed the absence of a single characteristic scale in thermoacoustic systems (Nair and Sujith, 2014).

Gotoda *et al*. (2012), and Domen *et al*. (2015) characterized the complexities in the dynamics of thermoacoustic systems close to blowout of flame. Gotoda *et al*. (2012) and Domen *et al*. (2015) showed that the relatively regular pressure oscillations generated by thermoacoustic instabilities transition into low-dimensional intermittent chaos prior to blowout with as the equivalence ratio is reduced. They used measures from nonlinear time series analysis such as permutation entropy, fractal dimension and short-term predictability. They reported that the dynamics close to blowout of flame possess self-similar fractal structure.

Unni and Sujith (2015) investigated the complex multifractal characteristics of both self-excited thermoacoustic instability and blowout of flame in a single framework. They showed that the onset of blowout from thermoacoustic instability can be viewed as an increase in the width of the multifractal spectrum.

Multifractality in combustion dynamics; combustion noise and blowout, reflects the complex nature of the dynamics involved in combustion systems that arises due to the nonlinear interaction between combustion, flow and duct acoustics. Statistical theory of complex networks is a tool very recently devised to study complex systems (Lesne and Lagues, 2011). Complex network approach represents complex systems as large-scale networks with complex topologies, heterogeneous structures and provides a comprehensive understanding of complex connectivity patterns in dynamical systems.

Dramatic advances have been made in the past few years in the field of complex networks since the discovery of small-world network by Watts and Strogatz (1998) and scale-free network by Barabasi and Albert (1999). Watts and Strogatz (1998) proposed a network model, where starting with a regular topology, with the random addition of few links, the average distance between nodes reduced drastically. Such a network is known as small-world network. The small-world network model is successful in describing the transition from regular to random topology, popularly known as the Watts and Strogatz (WS) model. Both small-world and random networks follow exponential distribution of connectivity in the network.

Later, in 1999, Barabasi and Albert (1999) discovered that most of the real world networks such as the Internet, World-Wide Web and scientific collaboration networks have a heavy-tailed distribution of connectivity with no characteristic scale; such networks are called 'scale-free' networks. Surprisingly, despite their differences, most of the complex systems such as biological systems (Alm and Arkin, 2003; Barabasi and Oltvai, 2004), world wide web (Barabasi *et al*., 1999; Albert *et al*., 2000) and power grids (Arianos *et al*., 2009; Chen *et al*., 2010; Pagani and Aiello, 2013) possess scale-free topological structure.

Time series data are the reflection of the underlying spatio-temporal dynamics of any system. For example, the time series data of fluctuating quantities measured in the flow are shown to have direct correlation with the features of flow patterns in two phase flows (Rouhani and Sohal, 1983; Das and Pattanayak, 1993). In nonlinear sciences, complex networks are used to understand the dynamics underpinning the time series data (Zhang and Small, 2006; Lacasa *et al*., 2008; Donner *et al*., 2010). The information hidden in the dynamics of a time series is visualized as different structures in the corresponding complex networks.

It has been recently demonstrated that complex networks can be used to distinguish the flow patterns in gas-liquid two phase flows (Gao and Jin, 2009; Gao *et al*., 2010) and various regimes of turbulent jet flows (Charakopoulos *et al*., 2014). Detecting the patterns or structures in the complex network obtained from a thermoacoustic system may enable us to obtain an alternative definition and characterization of thermoacoustic transition. In another study, Okuno *et al*. (2015) used the complex networks to examine the nature of thermoacoustic oscillations. They found that the thermoacoustic oscillations possess pseudo-periodicity, high-dimensional nature, power-law behaviour in the degree distribution and small-world like nature.

In the present thesis, we make a first attempt to investigate signals generated by the interaction between acoustics, combustion and turbulence from the complex networks perspective, with the hope that tools from the field of complex networks can stimulate the study of dynamical features or pattern in the combustion dynamics prior to thermoacoustic instability and blowout of flame from an alternative perspective.

1.6 Scale-freeness of combustion noise

To investigate the transition to thermoacoustic instability and blowout, one should first understand the stable operation of the combustor. The low-amplitude, aperiodic fluctuations in the unsteady pressure during the stable operation is called combustion noise.

Combustion noise is generated by unsteady combustion processes in propulsion and power producing systems. Combustion noise is considered as a pollutant. Unlike other chemical pollutants, combustion noise is found to have direct impact on the listeners (Strahle 1978). Noise can cause physiological changes and even impede the efficiency of the listeners. Exposure of such noise for longer times can even lead to physiological disorders such as hearing loss and interrupted sleep (Dowling and Mahmoudi, 2015). Combustion noise is identified to be an important source of noise in industrial furnaces, aero and land based gas turbine engines. Control of noise emission is of critical importance in view of the increased public concern and increasing stringent regulations.

Combustion noise arises due to the unsteady burning of reacting gases, producing volumetric expansion and compression of fluid near the flame zone. The first explicit analysis of the source of combustion noise was performed by Bragg (1963). He modeled flame as a distribution of monopole sound sources of combustion noise. The flame propagation is described as a locally laminar process and the effect of turbulence is included through the wrinkled flame surface area. However, Bragg's model was based on heuristic arguments and does not rigorously follow the principles of fluid mechanics. A more rigorous analysis was then performed by Strahle (1971) which closely followed Lighthill's theory of aerodynamic noise. An excellent review of the advancements in understanding the sources of combustion noise can be found in (Dowling and Mahmoudi, 2015).

Spectral analyses of combustion noise generated from open turbulent flames have shown that the acoustic energy spectrum of combustion noise is broadband and involves power law scaling. Abugov and Obrezkov (1978) showed that the combustion noise spectrum exhibits power law scaling with a scaling exponent of -5/2 in the frequency range of 2 *kHz* to 10 *kHz*. Belliard (1997) also arrived at the power law scaling with a similar exponent.

In the low frequency range, the acoustic power spectrum is found to have f^{β} dependence and in the intermediate and high frequency range, the power spectrum is given $f^{-\alpha}$ (Rajaram and Lieuwen, 2009), where α and β are positive numbers. The power law scaling ($f^{-\alpha}$) in the high frequency side of the acoustic power spectrum was shown to have a $P(\omega) \sim \langle|q(\omega)|^2\rangle$ behavior, where $P(\omega)$ is acoustic power and $q(\omega)$ is heat release rate fluctuations (Rajaram, 2007).

Clavin and Siggia (1991) and Clavin (2000) related the power law in the acoustic power spectrum of combustion noise to the Kolmogorov spectrum of turbulence. The existence of power laws is an indication of scale invariance that is often seen in physical systems (Lovejoy and Schertzer, 1986; Davis *et al*., 1995; Lesne and Lagues, 2011).

In practical combustors, flames exist in confined environments. The confinement modes preferentially amplify the sound emitted from the flames at time scales close to their natural time scales (frequencies) and hence lead to multiple peaks in the acoustic power spectrum (Chiu and Summerfield, 1974; Kumar, 1975; Strahle, 1978; Hegde *et al*., 1987). As a consequence of these peaks in the acoustic power, the scale invariance of combustion noise in a confined environment is hard to discern in the power spectrum.

1.7 Transitions to thermoacoustic instability and blowout from combustion noise

Further, positive coupling of the heat release rate fluctuations from combustion with the acoustic field in the combustion chamber can lead to large-amplitude pressure oscillations called thermoacoustic instability. A review of acoustically coupled combustion driven oscillations can be found in Dowling and Stow (2003). In addition to acoustics and combustion, vortices that are shed due to hydrodynamics play a key role in driving thermoacoustic instability (Schadow *et al*., 1989; Coats, 1996). The vortices shed, grow and impinge at the combustor walls at the instability frequency and the heat release rate fluctuations closely follow the vortex history (Rogers, 1956; Yu *et al*., 1991).

Most of these studies individually investigate and contrast the states of the system during its stable operation (combustion noise) and full blown thermoacoustic instability (Smith and Zukoski, 1985; Poinsot *et al*., 1987; Yu *et al*., 1991). However, studies focusing on the transition to thermoacoustic instability in a turbulent combustor from a stable regime (combustion noise) in response to the systematic variation of operating conditions of the combustor remain very few in number. Chakravarthy and co-workers (Chakravarthy *et al*., 2007*a*; Charavarthy *et al*., 2007*b*) studied the onset of thermoacoustic instability as a transition from combustion noise to thermoacoustic instability by systematically varying the operating conditions.

Currently, we know that transition to thermoacoustic instability from combustion noise is associated with change in acoustic amplitude spectrum from one which is broad with shallow peaks to one with sharp peaks at acoustic instability modes (Nair and Sujith, 2014; Nair *et al.*, 2014). However, there is some vagueness associated with this definition as it is difficult to define what constitutes a shallow peak or a sharp peak. To arrive at a better definition, the pattern or dynamical features emerging during this transition to thermoacoustic instability and blowout of flame via intermittency needs to be identified and formalized. This involves formalising the process of pattern discovery (Barabasi, 2011).

On the other hand, the transition to the onset of blowout from combustion noise is viewed as a loss of static stability of flame. Traditional analysis considers that flame blows out when the chemical reactions are slower than the convection of flow in the combustion systems. However, Muruganandam *et al.*, (2005) and Nair and Lieuwen (2005) reported that blowout is associated with complex dynamical processes in the combustion and the acoustic characteristics of the combustion system. The fluid mechanical changes during the onset of blowout are investigated by Shanbhogue *et al.*, (2009). Most of the studies focused on characterizing the acoustic, combustion and flow characteristics near blowout conditions. The changes in the dynamics during the transition from combustion noise to blowout and thermoacoustic instability are still not clear and are of importance to understand the transitions.

1.8 Precursors to thermoacoustic instability and blowout

The possibility of detecting an impending thermoacoustic instability and blowout, well before its onset, provides the engine operator an indication such that the necessary control actions can be implemented to avoid the occurrence of thermoacoustic instability and blowout in the fielded systems.

Lieuwen (2005) proposed a method for online detection of thermoacoustic instability. He calculated the damping rate using autocorrelation function of the unsteady pressure signal. The damping rate approaches zero at instability which is treated as a precursor. Yi and Gutmark (2008) extended Lieuwen's method to the frequency domain. Both these methods have a few drawbacks. First, the system has to reach instability (or very close to it) for the detection system and methods to work, which is not affordable. In addition, the methods may not be effective for combustors exhibiting noise induced transition to instability. Further, the existence of several frequencies in the spectrum makes the estimation of damping difficult.

Similar to precursors for thermoacoustic instability, Nair and Lieuwen (2005) developed precursors for the blowout detection based on spectral, statistical and threshold-based analysis of the acoustic signal. Muruganandam *et al*. (2005) used OH^* chemiluminescence and threshold-based identification strategy to obtain blowout precursors. The precursors from both these methods (Nair and Lieuwen, 2005; Muruganandam *et al*., 2005) work on the principle that the frequency of intermittent events increases as the combustor approaches blowout.

Recently, Nair *et al*., (2014) observed that intermittency presages the onset of thermoacoustic instability. The measures quantifying intermittency are used as early warning signals to thermoacoustic instability. They calculated the recurrence behavior of different dynamical states of the combustor using recurrence quantification analysis. These recurrence quantities are treated as early warning measures for the onset of detrimental periodic oscillations.

Further, adopting a complex systems approach to thermoacoustic systems, Nair and Sujith (2014) showed that the dynamic pressure data measured during combustion noise have a multifractal signature. They showed that the multifractal nature of the combustion noise is no longer present during combustion instability. Measures such as Hurst exponent are used to detect the proximity to the onset of thermoacoustic instability.

Unni and Sujith (2015) used the Hurst exponent to detect the onset of blowout in turbulent combustors. Gotoda *et al*. (2012) used the quantity called translation error for the online detection of blowout. Domen *et al*. (2015) proposed permutation entropy which characterizes the complexities in the dynamics of thermoacoustic systems close to blowout of flame as a precursor.

Most of the above described precursors to detect the onset of thermoacoustic instability and blowout rely on single measure. Reliance on a single measure to obtain early warning about thermoacoustic instability and blowout can lead to false positives and negatives. In addition to these instability and blowout detection methods, the early warning from a number of measures could enables us to eliminate false positives and negatives, thereby making the warning system more robust.

1.9 Current understanding on physical mechanisms that cause transitions in combustion systems

Alternatively, from the perspective of reacting flow physics, thermoacoustic instability and blowout are two different behaviors in a thermoacoustic system. The behavior of a thermoacoustic system arises from the nonlinear interaction of flow, flame and duct acoustics. The role of flow-acoustics-flame interaction during combustion noise and full blown combustion instability are fairly well studied. During the occurrence of combustion noise, the combustion chamber acoustics and vortex dynamics do not lock and results in broadband, low-amplitude oscillations in the acoustic pressure (Strahle, 1978; Charavarthy *et al*., 2007*a*).

In contrast, the lock-in of vortex dynamics and duct acoustics plays a prominent role in the excitation of combustion instabilities (Schadow *et al*., 1989; Coats, 1996). Large-scale coherent vortex structures are formed at the natural time scales (or frequencies) of the combustion chamber (Smith and Zukoski, 1985; Poinsot *et al*., 1987; Yu *et al*., 1991). Oscillatory heat release rate follows the vortex history (Rogers, 1956; Yu *et al*., 1991). The positive coupling of the periodic heat release rate fluctuations from combustion with the acoustic field in the combustion chamber leads to large-amplitude pressure oscillations during thermoacoustic instability.

Meanwhile, the physical mechanisms that cause blowout of flame are explained as a three-stage process (Chaudhuri *et al*., 2010; Chaudhuri and Cetegen, 2008). In the first stage, the vortices in the flow-field introduce straining of the flame (Nair and Lieuwen, 2007; Shanbhogue *et al*., 2009). The holes are formed in the flame at the locations where the flame strain rate is higher than the flame extinction strain rate. The number of holes formed in the flame increases along with the repeated detachment and reattachment of the flame from the flame holding device, as the equivalence is decreased further towards the condition of flame blowout (Nair and Lieuwen, 2007; Shanbhogue *et al*., 2009). Meanwhile, the flow-field becomes progressively non-reactive as the blowout limit is approached (Chaudhuri *et al*., 2010; Chaudhuri and Cetegen, 2008; Chaparro and Cetegen, 2006). In the partial extinction of the flame, part of the flow-field becomes non-reactive, while the other part of the flow-field remains reactive where the flame re-ignites. The flame extinction and re-ignition events occur intermittently in the regions of non-reactive and reactive flow-field. In the final stage, when the flow-field becomes completely non-reactive, the flame fails to re-ignite and the flame blows out (Chaudhuri *et al*., 2010).

From the perspective of reacting flow physics, thermoacoustic instabilities and blowout are two different phenomena. Intermittency precedes both these phenomena and gives a hint that there is some commonality in the physics of transition to thermoacoustic instability and blowout. Therefore, we investigate the flow physics during intermittency in order to understand the physical mechanisms that cause the transitions to thermoacoustic instabilities and blowout. On the other hand, from a dynamical systems perspective, we need to investigate if there are any commonalities between the intermittency that presages thermoacoustic instability and the intermittency that presages blowout.

1.10 Objectives and overview of the thesis

The objectives of the present thesis are focused on the analysis of thermoacoustic instability and blowout from the stable operation of the combustion systems operated under turbulent flow conditions. The outstanding questions are identified from the above discussions and the objectives of the present thesis are summarized as follows.

1. First, we investigate the scale invariance of combustion noise in a confined environment using complex networks. The scale invariance of combustion noise is hard to discern from the frequency spectrum due to the presence of multiple peaks near the frequencies at

which thermoacoustic instability happens. We show that low-amplitude, aperiodic pressure fluctuations during combustion noise can be represented as a scale-free network. A network is called scale-free if it follows a power law behavior in the distribution of connections (Barabasi, 2011). These power laws are related to the scale invariance of combustion noise.

2. We show that the scale-free behavior of combustion noise transitions to an orderly behavior at the onset of thermoacoustic instability (periodic oscillations). We calculate the network properties which quantify the topological changes in a complex network during the transition from combustion noise (scale-free) to thermoacoustic instability (regular). We propose the variation of number of network properties as the early warning measures to detect the onset of impending thermoacoustic instability.

3. We also illustrate that as the system dynamics transitions to the onset of blowout from thermoacoustic instability, the transition again happens from regular to scale-free structure in the networks. The distribution of connections in the networks transitions from a single discrete point to power law behavior during the onset of blowout. The network properties are used to detect the onset of blowout as well.

4. Alternatively, in order to understand the physical reasons for such transitions in a thermoacoustic system, we investigate the coupling of duct acoustics, flame and flow during the occurrence of intermittent dynamics that presages both thermoacoustic instability and blowout. We acquire the simultaneous measurements of acoustic pressure, CH^* chemiluminescence images and Mie scattering images to understand the interactions.

The present thesis has two aspects based on the indentified objectives. First, the complex network analysis is performed to investigate the dynamical features or pattern in the dynamics of thermoacoustic systems. Second, the flow physics during intermittency is investigated in order to understand the physical mechanisms that cause the transitions in thermoacoustic systems.

The rest of the thesis is organized as follows. A brief introduction to complex networks and the characteristics of various complex networks are described in **Chapter 2**. Further, Chapter 2 describes the existing methods to obtain the complex networks from the time series data such as visibility graphs and horizontal visibility graphs. The drawbacks of these methods to represent the intermittent dynamics as the clusters in a complex network's topology are discussed. The threshold grouping method which helps in visualizing the intermittency is introduced. The bursts of periodic oscillations in the time series data corresponding to intermittency is represented as clusters of nodes in the network using the threshold grouping method. Further, the definitions of network properties which can quantify the structural features of the complex networks along with their implications are provided in Chapter 2.

In **Chapter 3**, the complex network analysis of thermoacoustic systems are discussed. The unsteady pressure data which are same as one reported by Nair and Sujith (2014) and Unni and Sujith (2015) are used in the network analysis. The unsteady pressure is measured from a bluff-body stabilized backward-facing step combustor operated in a turbulent environment with LPG as the fuel. The schematic of the experimental setup and the details of the experiments are provided in the Sections 3.3 and 3.4 respectively. The complex networks are mapped from the unsteady pressure data using the visibility algorithm which is described in Section 3.2.

First, the amplitude spectrum of combustion noise is shown to indicate that the power laws are not discernable due to the presence of multiple peaks near the instability frequencies (Section 3.5). In Section 3.6, the results on complex networks corresponding to combustion noise are then presented highlighting that the power law behavior is observed in the distribution of connections in the network. The onset of thermoacoustic instability via intermittency (Section 3.7.1) and the structural changes in the topology of the complex network during the onset of thermoacoustic instability (Section 3.7.2) are discussed in Section 3.7. The network properties such as clustering coefficient, network diameter, characteristic path length and global efficiency are computed. These network properties are proposed as the precursors to thermoacoustic instability and the implications for the change in network properties during the onset of thermoacoustic instability are described in Section 3.7.3. The conclusions from the investigation of the onset of thermoacoustic instability are summarized in Section 3.8.

Further, the complex network analysis of the onset of blowout of flame from the stable operation of the combustor via thermoacoustic instability is discussed in Section 3.9. The complex network representation of the dynamics at the onset of blowout and the network properties as the precursors are provided.

Chapter 4 describes the experimental investigation performed in order to understand the physical reason for such transitions to thermoacoustic instability and blowout. The details of the experimental setup (i., turbulent lifted jet flame combustor) and the methods of data acquisition are provided in Sections 4.3 and 4.4 respectively. The physical mechanism that causes intermittency prior to thermoacoustic instability and blowout are investigated by studying the flow-flame-acoustic behavior in Sections 4.5 and 4.7 respectively. Alternatively, the commonality between the intermittent dynamics prior to thermoacoustic instability and blowout are examined using the recurrence plots and first return maps.

In **Chapter 5**, the conclusions are summarized in detail and the scope for the future works are presented that could stimulate further investigations based on complex networks.

CHAPTER 2

BACKGROUND ON COMPLEX NETWORKS

The present chapter provides a background on complex networks and an introduction to the terminologies and the tools to be used in the following chapters. The tools from complex networks are applied in various scientific disciplines after the discovery of small-world and scale-free networks. This chapter provide the characteristic features of small-world and scale-free networks in this chapter. Further, complex networks can be mapped from time series data which reflect the spatio-temporal dynamics in the systems. A number of methods that are used to obtain complex networks from the time series data are described. In particular, the visibility graph and horizontal graph to obtain complex networks are illustrated.

Further, a new method proposed by us to derive complex networks from time series data are described. Each data point in the time series is treated as a single node and nodes are connected if their values differ by a value less than a threshold δ. The method is easy to implement and transforms periodic time series into regular networks, and random time series into random networks. Network specific properties such as scale freeness, small world effects and the presence of hubs are captured by this method. The method converts a chaotic time series into a scale-free network.

The method is applied on a model time series (a chaotic time series of Henon map, a periodic time series and a random time series) and an experimental time series (fluctuating pressure time series measured from the combustor involving turbulent flow). The complex network derived from the Henon map obeys a power law degree distribution, highlighting the scale free behavior of the associated chaotic state. The motivation for proposing the present method is that the method is able to convert specific patterns in the dynamics of a time series into spatial structures in the complex network. We show this specialty of the present method by constructing a complex network from a time series of acoustic pressure measured from a combustor involving turbulent flow that exhibits intermittency. The intermittent bursts in the considered time series are converted into clusters in the corresponding complex network.

The structural features of the complex networks can be quantified in terms of calculating the properties of the complex network. The definitions of network properties such as clustering coefficient, characteristic path length, network diameter and global efficiency are provided along with their implications.

2. 1 Background

The network science has emerged from the graph theory. In 1736, Euler provided the solutions for a bridge problem by formulating the problem as a graph made up of set of nodes and the links between the nodes. In this bridge problem, the nodes represent the landscapes and the links represent the bridge that connect the landscapes. In 1950's, the challenging question of "How small is the world" was answered by considering the networks underlying the social interactions (Milgram, 1967; de Sola Pool and Kochan, 1978). Meanwhile, the two mathematicians, Paul Erdös and Alfréd Rényi proposed the mathematical models for the networks (Rényi and Erdös, 1959). The model was originally developed by Solomonoff and Rapport (1951). In Erdös and Rényi's model, the links between the nodes are connected in a random manner to mimic the real complicated networks. The ER model predicted that the average distance between any two persons in the social interaction network is three (de Sola Pool and Kochan, 1978). However, Milgram (1967) showed that the average separation is six by performing experiments on hand-delivering a letter through the acquaintances.

Meanwhile, Price (1965) reported that the citations between the scientific journals does not follow a distribution similar to that of the random ER network model with a peak near the average value. In contrast to ER model, a large number of articles had a few citations and a few articles had a large number of citations. In 1990's, Barabasi and Albert (1999) discovered that the links in the WWW network follow power-law distribution similar to that of the one observed by Price (1965). The networks with power-law distribution in their connections are called scale-free networks (Barabasi and Albert, 1999) because there is no single characteristic scale associated with the distribution of links in the network.

At the same Watts and Strogatz (1998) proposed a network model, where starting with a regular topology, with the random addition of few links, the average distance between nodes reduced drastically. Such a network is known as small-world network. The small-world network model is successful in describing the transition from regular to random topology, popularly known as the Watts and Strogatz (WS) model. The small-world network follow exponential distribution of connectivity as in the random networks.

The breakthrough in the network science has originated since the discovery of small-world network by Watts and Strogatz (1998) and scale-free network by Barabasi and Albert (1999). The discovery of small-world and scale-free network revealed that the network structures underlying the complex systems are not random. The patterns emerges out of the interactions and reflect in the distribution of links in the complex networks.

2. 2 Time series to complex networks and vice-versa

The behavior of a dynamical system can be understood by analyzing the time series data of its evolution. Linear time series analysis is very helpful in understanding the nature of a linear system. The nonlinear aspects such as fractality, multifractality, self-organization and the presence of multiple scales etc. arising out of complex systems are studied using the tools from nonlinear time series analysis (Tan *et al.*, 2009; Zorick and Mandelkern, 2013; Eser *et al.*, 2014).

The representation of a time series from such complex systems as a complex network can provide a better way to visualize hidden patterns in the time series. The presence of multiple scales, fractal behavior etc. can be visual in terms of connections between the nodes in the network representation. The features of the network can be characterized using the properties of the network. The network measures can be useful in quantifying the information present in the time series.

Zhang and Small (2006) proposed a method for constructing complex networks from pseudo-periodic time series. Each cycle in the time series is considered as a single node. For an experimental time series, the connection between any two nodes are formed when the distance between the corresponding two cycles in phase space is less than a threshold. For simple toy models, connectivity is based on the temporal correlation between the two cycles. This method is applicable only for time series with dominant peaks in the power spectra. The partition of a time series into sequence of cycles depends on the dominant frequency in power spectra. Further, in this method, the process of finding connectivity requires either reconstruction of the phase space or a complex calculation of the temporal correlation coefficient between different cycles (Zhang *et al.*, 2008).

In an alternative scheme, complex networks called recurrence networks are constructed from time series data based on the recurrence behavior of state points in the phase space (Donner *et al.*, 2010). The phase space is reconstructed from the time series and each state point in the phase space is considered as a node. The nodes are connected if the state space distance between them is less than a certain threshold. This method is also complicated because it requires embedding and reconstruction of the state space.

Algorithms for constructing complex networks called visibility graphs and horizontal visibility graphs, based on the visibility of nodes are presented by Lacasa *et al.* (2008) and Luque *et al.* (2009) respectively. In both these methods, data points in the time series are converted into nodes. In a visibility graph, two nodes are connected if a straight line can be drawn between these nodes without intersecting the data points lying between them. Horizontal visibility graph is a special case of visibility graph (Luque *et al.*, 2009). If a horizontal line can be drawn between the two nodes without intersecting any node between them, the nodes are treated as connected.

Complex calculations are involved in the construction of a network from time series using the methods proposed in references (Zhang and Small, 2006; Zhang *et al.*, 2008; Donner *et al.*, 2010). In contrast, the visibility graph and horizontal visibility graphs are simple. We explain the visibility graphs, the horizontal visibility graphs and a threshold grouping method proposed by Murugesan and Sujith (2014).

2. 2. 1 Visibility graphs

According to the visibility condition, each data bar or data value in the time series is considered as a node. Any two nodes are connected when a straight line can be drawn between these two nodes without intersecting any intermediate data bars. In the visibility graph, connections from a given node to any other nodes are made based on the visibility of other nodes from the top of the given node. The method can be better understood from Fig. 2.1.

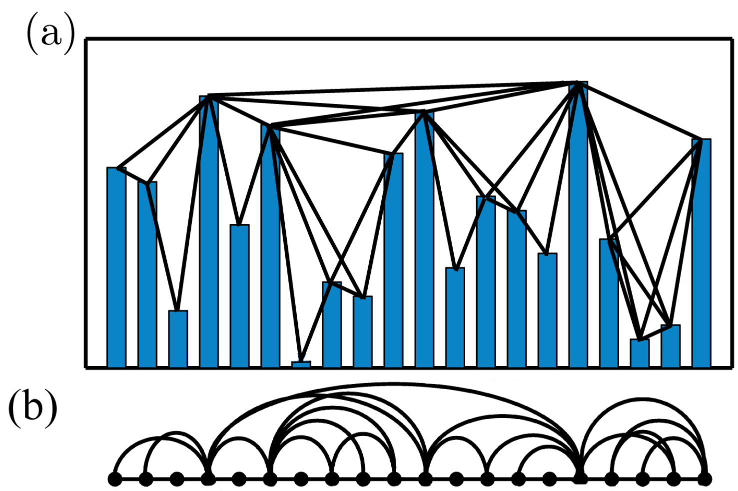

Figure 2.1: Illustration of visibility graph to convert a time series into a complex network. *a*) The time series to be converted into a complex network is represented as vertical bars. Each data point in the time series $p(t)$ is converted into a node appearing as a black dot in Fig. 2.1(*b*). If a straight line can be drawn between any two nodes (i.e. data heights i and j) without intersecting any nodes ($i<k<j$) between them, nodes i and j are connected. If two nodes are connected, a connection is drawn between them in the network as shown in Fig. 2.1(*b*). *b*) The complex network with nodes and connections derived from the time series shown in Fig. 2.1(*a*), using the visibility condition.

Two nodes (i and j) are connected if the intermediate nodes ($i<k<j$) satisfy the following condition,

$$\text{if } p_i < p_j + (p_i - p_j)\frac{t_i - t_k}{t_j - t_i}, \qquad A_{i,j} = 1; \tag{2.1}$$

$$\text{else,} \qquad A_{i,j} = 0;$$

2. 2. 2 Horizontal visibility graphs

The horizontal visibility graph is a special case of visibility graph where the connection from a node to any other node is made based on the horizontal visibility between these nodes. If a horizontal line can be drawn between the two nodes without intersecting any node between them, the nodes are treated as connected. The concept of horizontal visibility is shown in Fig. 2.2.

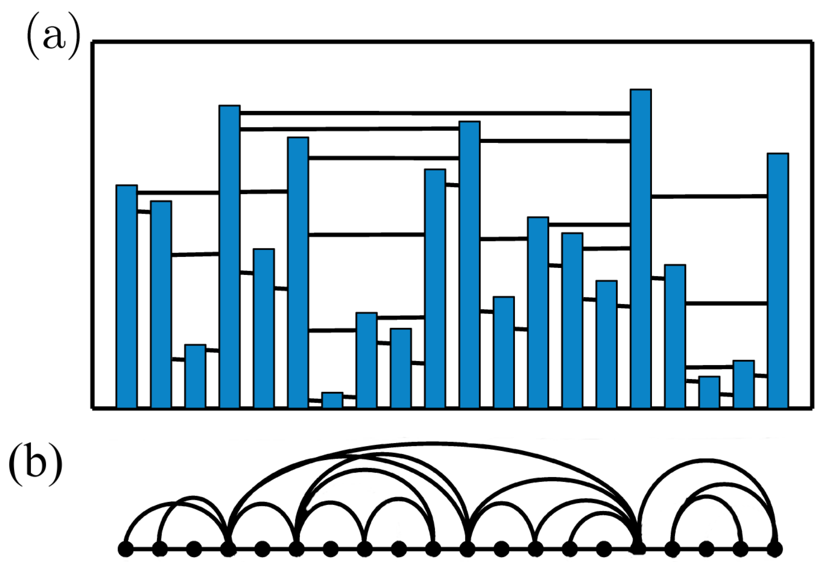

Figure 2.2: Illustration of horizontal visibility graph to convert a time series into a complex network. *a*) The time series to be converted into a complex network is represented as vertical bars. Each data point in the time series $p(t)$ is converted into a node appearing as a black dot in Fig. 2.2(*b*). If a horizontal line can be drawn between any two nodes (i.e., data heights i and j) without intersecting any nodes ($i<k<j$) between them, nodes i and j are connected. If two nodes are connected, a connection is drawn between them in the network as shown in Fig. 2.2(*b*). *b*) The complex network with nodes and connections derived from the time series shown in Fig. 2.2(*a*), using the horizontal visibility condition.

Two nodes (i and j) are connected if the intermediate nodes ($i<k<j$) satisfy the following condition,

$$\text{if } p_i, p_j > p_k, \qquad A_{i,j} = 1; \qquad (2.2)$$

$$\text{else,} \qquad A_{i,j} = 0;$$

2. 2. 3 Threshold grouping method

Threshold grouping method to derive complex networks from time series data is proposed by us (Murugesan and Sujith, 2014). The construction of a complex network using threshold grouping method is illustrated using the Henon map at chaotic state after removing the transients (Al-Shameri, 2012). A new time series called $p(t)$ is constructed from the peaks (crest of each cycle) in $x(t)$. In the threshold grouping method, each data bar or data value in the time series is treated as a node. If the difference between the values of two data points is less than a threshold δ, they are connected. Any two nodes with a difference more than ε are not connected. Nodes that are not connected to their neighbors are treated as not connected to other nodes also.

For i and j to be connected, the values of i, j and k ($i<k<j$, k denotes the points between i and j) should have approximately same value for all values of k. The condition is given as,

$$\text{if } |p_i - p_j|, |p_i - p_k|, |p_k - p_j| < \delta, \qquad A_{i,j} = 1; \qquad (2.3)$$

$$\text{else,} \qquad A_{i,j} = 0;$$

The method is illustrated in Fig. 2.3. The basic idea is that nodes of approximately the same value are connected together forming a group. Within any group, the nodes are different only by a value less than δ.

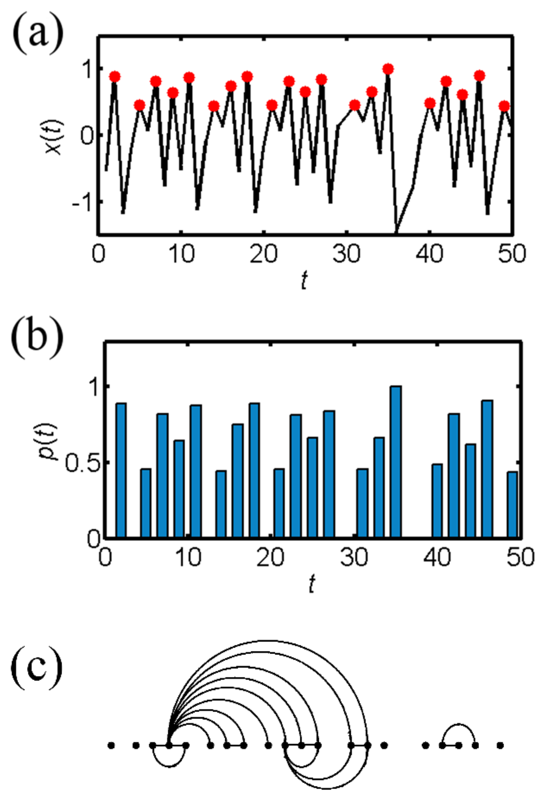

Figure 2.3: Illustration of threshold grouping method to convert a time series into a complex network. *a*) *x*(*t*) represents the time series to be converted into a complex network (For illustration, we show the first 50 observations of chaotic time series from the Henon map ($x_{n+1} = 1 - a{x_n}^2 + bx_n$) (Al-shameri, 2012) at chaotic state ($a = 1.4, b = 0.3$)), *b*) The peaks in *x*(*t*) are shown as *p*(*t*), *c*) Each peak is considered as a node. Two nodes (*i* and *j*) are connected if p_i, p_j and p_k ($i<k<j$, *k* denotes the points between *i* and *j*) have approximately the same value for all values of *k*. Here, $\delta = 0.25$.

Edges in the obtained network do not have direction and weight. However, the method can be extended by assigning weights to edges based on the value of nodes connected by those edges. The edges connecting the nodes with higher values can be assigned higher weights and edges connecting the nodes with lower values can be assigned lower weights. The complex network with weights to edges is not constructed in the present work.

Application of the proposed method on model time series

Chaotic time series of Henon map

The proposed algorithm is applied to 10,000 observations of the classical Henon map ($x_{n+1} = 1 - ax_n{}^2 + bx_n$) (Al-shameri, 2012) at chaotic state ($a = 1.4, b = 0.3$). The first 1000 observations are discarded to remove the transients in the iterations. The number of edges that are connected with every node is specified as the degree of that node k. The probability of nodes having k number of connections is represented using $P(k)$.

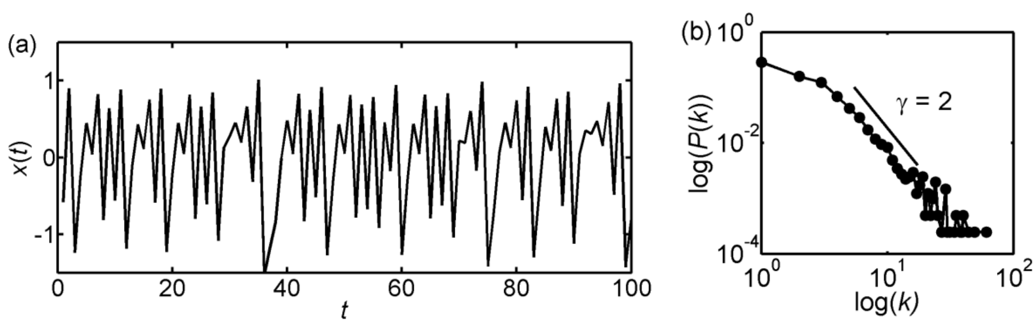

Figure 2.4: Chaotic time series obtained from the Henon map is converted into a scale-free network using the threshold grouping method. *a*) The first 100 observations of the Henon map (Al-Shameri, 2012) ($x_{n+1} = 1 - ax_n{}^2 + bx_n$) at chaotic state ($a = 1.4, b = 0.3$) after removing the transients, (b) degree distribution of the complex network obtained from the Henon map with $\delta\ = 0.25$.

The degree distribution of the obtained network follows a power law behavior ($P(k)\sim k^{-\gamma}$), thereby indicating that the constructed network is "scale free". In addition to the scale free behavior, small world effects are captured by the present method. Small world behavior implies that the network has a high clustering coefficient and small characteristic path length (Watts and Strogatz, 1998; Watts, 1999). The complex network obtained from the first 50 observations of the chaotic time series from the Henon map is illustrated in Fig. 2.3(*c*). In this figure, node 4 is connected to a large number of nodes in the networks. Meanwhile, there are other nodes with fewer connections and nodes with even no connection. The nodes that have the largest number of connections are important and are called hubs. The presence of such hubs (nodes that are highly connected) is captured with the present method.

Periodic time series

The method is then applied on a periodic time series ($x(t) = \sin(t)$). There are 20 peaks in the time series. All the nodes (peaks) have the same value. All the nodes are connected to all other nodes. All the nodes have the same number of connections (number of connections is 19). This implies that the obtained network is 'regular' (Quenell, 1994). The periodic time series and the degree distribution of the corresponding complex network are shown in Fig. 2.5(a) and 2.5(b) respectively.

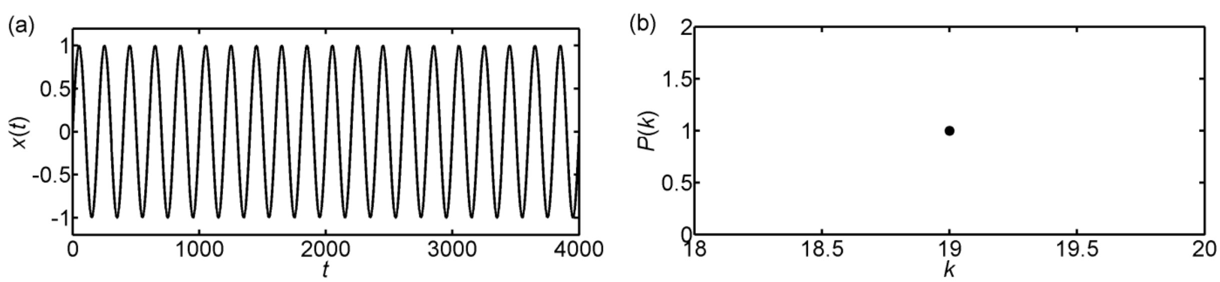

Figure 2.5: A regular network is obtained from a periodic time series using the threshold grouping method. a) Periodic time series ($x(t) = \sin(t)$) with 4000 data points, there are 20 peaks in the time series and are converted into nodes, (b) degree distribution of the corresponding complex network. All the nodes have equal number of connections (number of connections is 19).

Random time series

A random noisy series is generated using the Matlab command called randn. The degree distribution of the obtained complex network follows a Poisson distribution, indicating that the corresponding network is a random network (Zhang and Small, 2006). Random time series and degree distribution of the random network are shown in Fig. 2.6(a) and 2.6(b) respectively.

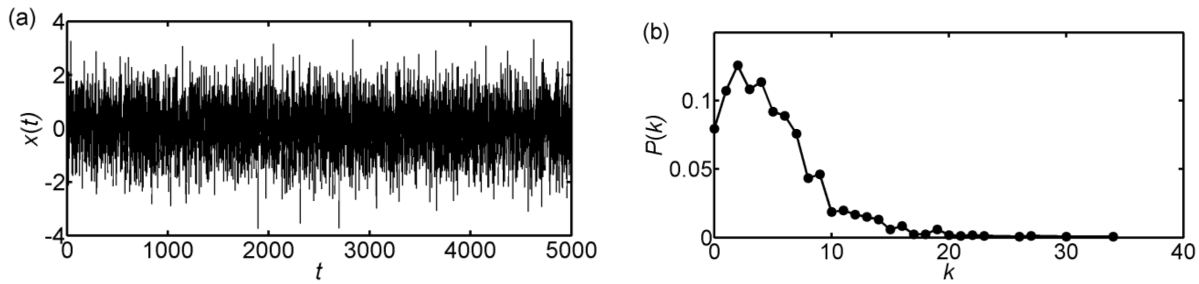

Figure 2.6: Random time series is converted into a random network *a*) Random time series generated using the Matlab command called randn with 5000 data points, *b*) degree distribution of the corresponding complex network.

The present method is able to convert a periodic time series into a regular network, a random time series into a random network and a chaotic time series into a scale-free network.

In addition, the present method is successful in highlighting specific patterns in the time series in the corresponding complex network. We illustrate this by converting a time series obtained from an experiment (fluctuating pressure time series from a combustor involving turbulent flow) into complex network (Nair *et al.*, 2014).

Application of proposed algorithm to a time series that exhibits intermittency

The present method is applied to the times series data of fluctuating pressure measured from a combustor with turbulent flow that exhibits intermittency. The obtained network is visualized using the software called Gephi (Bastian *et al.*, 2009).

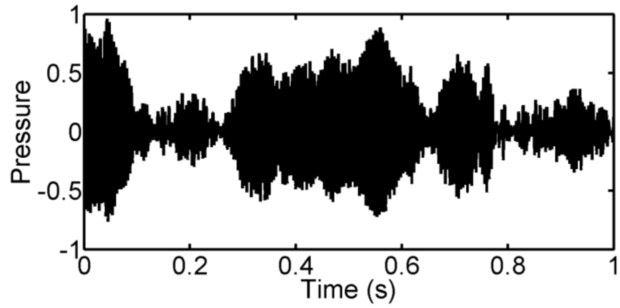

Figure 2.7: Time series data of the fluctuating pressure is measured from a combustor involving turbulent flow. The combustor is 700 *mm* long with square cross section (90 *mm* × 90 *mm*). Fuel (LPG) and oxidizer (air) are flowing at high Reynolds number ($Re = 25812$). The flame is stabilized using a flame holding device called a circular bluff body. Further details of the experiments can be found in (Nair *et al.*, 2014). Intermittent periodic bursts are observed in the time series data in a near random manner.

The complex networks derived from three different methods namely, visibility graph, horizontal visibility graph and threshold grouping method are shown (Fig. 2.8*a*, 2.8*b* and 2.8*c* respectively) for comparison. The nodes are appearing as small circles filled with colors in the obtained networks. The edges are shown as the lines connecting the nodes. The nodes are colored based on the degree of that node. For example, green color in the visibility and horizontal visibility graph implies that the corresponding node has a degree of 2.

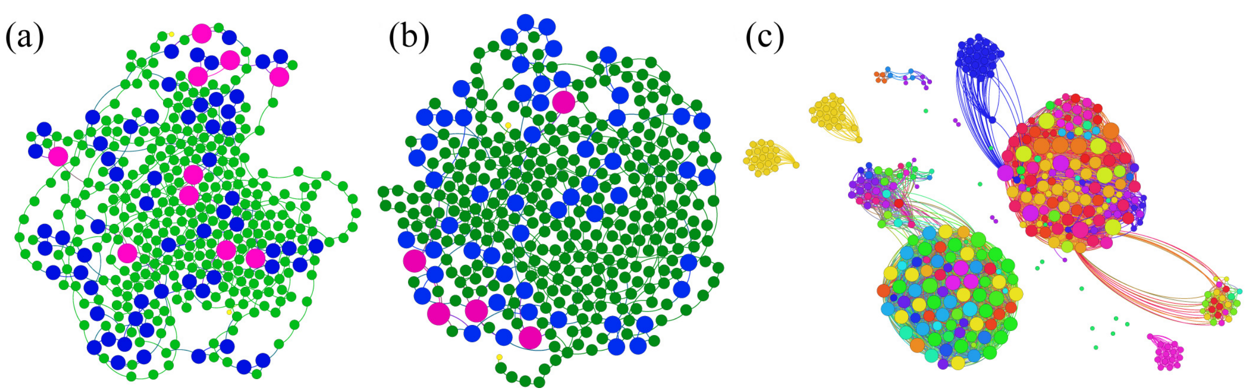

Figure 2.8: The complex networks are derived from a time series shown in Fig. 2.7 using *a*) visibility condition, *b*) horizontal visibility condition and *c*) threshold grouping method. The visualization of the complex networks are accomplished using the software called as Gephi (Bastian *et al.*, 2009).

The intermittent time series shows periodic bursts. In the visibility and horizontal visibility graph, the nodes in the periodic bursts are connected only with nodes which are next to it and have a degree of 2. The number of nodes with green color is more compared to nodes with other colors in the visibility and horizontal visibility graphs. This is due to the presence of periodic bursts in the time series.

The threshold grouping method converts the intermittent bursts in the experimental time series into different clusters in the complex network. The clusters of various sizes can be seen in the network corresponding to the bursts in the time series. The proposed algorithm is thus able to capture the structure (pattern) that corresponds to the intermittent bursts present in the time series. Further, the properties of the complex network (for example clustering coefficient, short path length etc.) can be calculated. The variation of these network properties for different dynamical states (for example chaos, limit cycle oscillations etc.) is useful in studying the dynamical transitions.

2. 3 Topological measures of complex networks

The pervasiveness of complex networks in a wide range of scientific disciplines have led to the formulation of a number of statistical measures and topological quantifiers to characterize the distinct features of the complex networks. In this section, we provide the definition and significance of four statistical measures namely, clustering coefficient, characteristic path length, global efficiency and network diameter which have been employed in the present thesis for the detection of onset of impending thermoacoustic instability and blowout of flame.

A complex network can be represented in an adjacency matrix ($A_{i,j}$ is a M by M matrix, where M is the total number of nodes in a network). If a pair of nodes i and j are linked in a network, the element $A_{i,j}$ attains a value of 1; otherwise $A_{i,j}$ is 0. The nodes are not self-connected (i.e., $A_{i,i} = 0$). Therefore, an adjacency matrix is a symmetric matrix with 0's and 1's as its elements.

The degree of a node v (k_v) is defined as the number of nodes that are directly linked to it and can be calculated from,

$$k_v = \sum_{i=1}^{M} A_{i,v} \tag{2.4}$$

The degree of a node signifies its connectedness to receive an information spread in the network. The fraction (or percentage) of nodes with a k number of nodes that are directly connected to it are computed as a frequency distribution $P(k)$. The graph plotted between k and $P(k)$ is important to characterize a complex network. The degree distribution plot can be employed to check whether the transformed complex network inherit the underlying dynamics of the associated time series or not.

2. 3. 1 Clustering coefficient

The clustering coefficient of a node v (C_v) is defined to characterize the connectedness of the clusters in a network. It can be computed as,

$$C_v = \frac{2N_v}{K_v(K_v - 1)} \tag{2.5}$$

Here, N_v represents the number of links available in the neighborhood of a node v and $K_v(K_v - 1)/2$ refers to the maximum possible number of links in the neighborhood of a node v. The clustering coefficient is proposed by Watts and Strogatz (1998) and indicates the density of links in the neighborhood of that node.

The clustering coefficient of a network (C) is computed as the average of clustering coefficients of all the nodes in the network.

$$C = \frac{1}{M} \sum_{v=1}^{M} C_v \tag{2.6}$$

The value of clustering coefficient ranges between 0 and 1. The clustering coefficient is a measure of cliquishness of the nodes (Watts and Strogatz, 1998). The term cliquishness was introduced to quantify whether the nodes in the neighborhood of any node are also neighbors (i.e connected) or not. For example, consider a node connected to two other nodes. The maximum possible number of connections in the neighborhood of a given node is 1. If two other nodes are connected with each other, then the clustering coefficient attains its maximum value of 1. The value of 1 for the clustering coefficient for any node implies that all the nodes in the neighborhood of a given node are connected to each other.

2. 3. 2 Characteristic path length

Path length of a pair of nodes is an important network measure which is defined as the number of links in the sequence of nodes connecting the given pair of nodes. A pair of nodes in the network can be connected in a number of ways. The shortest path length of nodes *i* and *j* ($L_{i,j}$) is a path length of the shortest path connecting those nodes *i* and *j*. The average of shortest path lengths of all the pairs of nodes in the network is defined as the characteristic path length.

$$L = \frac{1}{M(M-1)} \sum_{i=1}^{M} \sum_{\substack{j=1 \\ i \neq j}}^{M} L_{i,j} \qquad (2.7)$$

The value of characteristic path length tells how fast the information can be transferred in the network. For directly connected nodes, $L_{i,j}$ is 1 and for an isolated node $L_{i,j}$ is ∞.

2. 3. 3 Network diameter

The maximum value of the shortest path lengths of all the pairs of nodes in the network is defined as the network diameter (D)

$$D = max(L_{i,j}) \qquad (2.8)$$

2. 3. 4 Global efficiency

The global efficiency (E) is calculated as the average of inverse of the shortest path lengths of all the pairs of nodes in the network.

$$E = \frac{1}{M(M-1)} \sum_{i=1}^{M} \sum_{\substack{j=1 \\ i \neq j}}^{M} \frac{1}{L_{i,j}} \qquad (2.9)$$

For a disconnected node, the value of short path length becomes infinity. The global efficiency is defined to avoid infinity in the calculations for the network with disconnected nodes. The global efficiency is an indicator of efficiency of information transfer in the network. If the short path length is small, the global efficiency becomes high indicating that nodes are highly connected. This quantity is very useful for networks with disconnected nodes. Further details on the network measures can be obtained from Donner *et al.* (2010).

CHAPTER 3

COMPLEX NETWORK ANALYSIS OF THERMOACOUSTIC SYSTEMS

The present chapter discusses the complex network approach to unravel the pattern or dynamical features in the dynamics of the thermoacoustic systems. The transition to thermoacoustic instability and blowout are investigated. First, the scale invariance of combustion noise generated from turbulent reacting flows in a confined environment is investigated using complex networks. The time series data of unsteady pressure, which is the indicative of spatio-temporal changes happening in the combustor, is converted into complex networks using the visibility algorithm which is explained in the previous chapter. The complex network obtained from the low-amplitude, aperiodic pressure fluctuations during combustion noise has a scale-free structure. The power law distributions of connections in the scale-free network are related to the scale invariance of combustion noise.

Further, the use of complex networks enables us to formalize the identification of the pattern during the transition from combustion noise to thermoacoustic instability as a structural change (i.e., scale-free to order) in topology of the network. The statistical topological measures of the complex networks are used to quantify the structural changes during the onset of thermoacoustic instability from combustion noise. The variation of these network measures are used to detect the onset of an impending thermoacoustic instability.

Further, the complex networks approach to flame blowout reveals that combustion dynamics close to flame blowout exhibits a scale-free topological structure in the complex networks. The changes in dynamical behaviour of the system during the transition to flame blowout via self-excited thermoacoustic instability can be represented as a transition from regular to scale-free structure in complex networks. The topological measures such as clustering coefficient, network diameter, characteristic path length and global efficiency are evaluated to quantify the changes in combustion dynamics. These topological measures of networks that vary significantly well before the transition to flame blowout are used as the precursors to detect an impending blowout in the combustion systems.

3.1 Introduction

In the combustors operated in a turbulent environment, the transition from stable operation of the combustor (usually referred to as combustion noise) to thermoacoustic instability and blowout of flame happen via intermittency (Nair *et al.*, 2014; Unni and Sujith, 2015). Further, Nair and Sujith (2014) showed that combustion noise has multifractal characteristics and the transition to thermoacoustic oscillations from combustion noise can be viewed as a loss of multifractality. Unni and Sujith (2015) explained the complex multifractal characteristics of both self-excited thermoacoustic instability and flame blowout in a single framework.

The presence of multifractal signature and intermittency reflects the complexity of the dynamics of thermoacoustic systems. The dynamical behaviours of thermoacoustic systems; blowout and thermoacoustic instability, in fact occur due to the complex interplay of various factors such as reaction kinetics, molecular mixing, turbulent transport and acoustic wave interaction etc.

A complex system is composed of number of subsystems interacting in a way that its collective behavior is not a sum of the individual subsystems behavior. Craig Reynolds described the complex behavior in a group of birds as “A flock is not a big bird” (Waldrop, 1992). The collective phenomena of a complex system can go beyond the system. The traditional reductionist viewpoint that breaks a complex system into parts had been a powerful tool. The behavior of parts were explained with the governing laws. However, the reductionist viewpoint fails to explain the emergence of pattern or emergent behavior in a complex system (Barabasi, 2011).

The complex networks are a new way to characterize the complexity in different natural and engineering systems. A complex network maps a complex system in terms of its subsystems and the interactions between the subsystems. The intrinsic practice in the network approach is to treat a whole complex system as a sum of the interacting parts and the interaction between the parts. The interactions between parts are essential to understand the complexity in different systems. Therefore, the complex networks are inevitably used to understand the interactions in internet, power-grids, social interactions, cellular and ecological systems.

In fluid mechanics, the complex networks approach have been used to understand and distinguish the various regimes of turbulent jet flows (Charakopoulos *et al*., 2014) and energy dissipation rates in three-dimensional fully developed turbulence (Liu *et al*., 2010). Recently, Okuno *et al*. (2015) used the complex networks to examine the nature of thermoacoustic oscillations. They found that the thermoacoustic oscillations possess pseudo-periodicity, high-dimensional nature, power-law behaviour in the degree distribution and small-world like nature.

The power-law distributions and the small-world behavior imply that the network representing the underlying dynamics of the thermoacoustic systems possess non-random structures. The main goal of the present chapter is to formulate quantities to quantitatively describe the pattern or topological aspects of the thermoacoustic systems.

3. 2 Mapping complex networks from the time series data

A complex network consists of nodes and connections between the nodes. Many different methods can be used to construct a complex network from a time series. As an example, conditions based on temporal correlation of pseudo-periodic cycles (Zhang and small, 2006), recurrence of states in phase space (Donner *et al.*, 2010), visibility of nodes (Lacasa *et al.*, 2008) are used to connect the nodes in a network. We use the visibility graph to represent a thermoacoustic system as a complex network which is explained in the previous chapter. We then show the topological changes in complex networks during the transition from combustion noise to thermoacoustic instability and blowout of flame via intermittency.

From the acquired data, we construct a new time series by considering only the peaks in the time series data. As an example, let $x(t)$ be the acoustic pressure time series and $p(t)$ be the vector that consists of data points belonging to the crest of each cycle in the time series. Each data point in the vector $p(t)$ is considered as a node. Information about the connectivity between nodes is stored in an adjacency matrix (Donner *et al.*, 2010). As an example, if two nodes i and j are connected, $A_{i,j}$ is one; otherwise $A_{i,j}$ is zero. To avoid self connections, $A_{i,i}$ is chosen as 0 in the adjacency matrix.

Visibility graph

According to the visibility condition, each data bar or data value in the time series $p(t)$ is considered as a node (Lacasa *et al.*, 2008). Any two nodes are connected when a straight line can be drawn between these two nodes without intersecting any intermediate data bars. Two nodes (i and j) are connected if the intermediate nodes ($i<k<j$) satisfy the following condition,

$$\begin{aligned} &\text{if,} \quad p_k < p_i + (p_j - p_i)\frac{t_k - t_i}{t_j - t_i}, \qquad && A_{i,j} = 1; \\ &\text{else,} && A_{i,j} = 0; \end{aligned} \tag{3.1}$$

The method discussed above is employed to extract a complex network from the time series data of unsteady pressure measured from a combustor described in the following section.

3.3 Description of the backward-facing step combustor

The unsteady pressure data used in the complex network analysis are same as the data used by Nair and Sujith (2014) and Unni and Sujith (2015). The experiments are carried out on a backward-facing step combustor operated in turbulent flow conditions (Re > 16,000) with a circular bluff-body as a flame-holding device. The schematic of the experimental setup and the flame-holding device are shown in Figures 3.1(a) and 3.1(b) respectively.

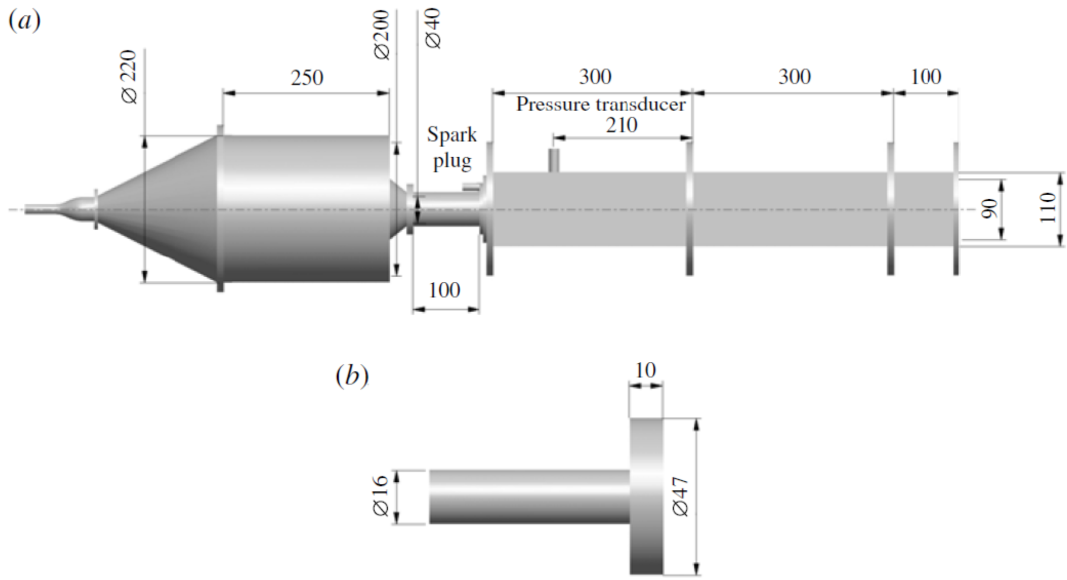

Figure 3.1: Schematic of the *a*) experimental configuration and *b*) the flame holding device. The combustion chamber has a square cross-section of 90 *mm* × 90 *mm* and a length of 700 *mm* with three extension ducts. The flame is stabilized using a circular bluff-body. The unsteady pressure is measured at 90 mm from the back-ward facing step using a piezoelectric sensor.

The setup mainly composed of three parts; a settling chamber, a burner and a combustion chamber with extension ducts. The settling chamber has a diameter of 220 *mm* and a length of 250 *mm*. The burner has a circular cross-section with a diameter of 40 *mm*. The combustion chamber is 700 *mm* long with extension ducts having a square cross-section of 90 *mm* × 90 *mm*. The flame holding device is a circular disk having a diameter of 47 *mm* and a thickness of 10 *mm*. The bluff-body is positioned into the combustion chamber using a circular shaft having a diameter of 16 *mm* and a length of 30 *mm*.

The circular shaft is attached to the rack and pinion mechanism to change the position of the bluff-body along the length of the combustion chamber with a least count of 1 *mm*. The bluff-body is then positioned at 50 *mm* downstream of the backward step for stabilizing the flame. The circular shaft which supports the bluff body is also used to inject the fuel (Liquefied Petroleum Gas) into the combustion chamber through four radial holes. These radial holes have a diameter of 1.7 *mm* and are positioned at a location of 160 *mm* upstream of the rear end of the bluff-body.

The air is supplied into the chamber from a high-pressure tank through a moisture separator. The volumetric flow rates of the fuel and the air are digitally measured and controlled using mass flow controllers (Alicat Scientific, MCR Series) with an uncertainty of ± 0.8% of reading + 2% of full scale.

3. 4 Unsteady pressure measurements

The increase in air flow rate increases the Reynolds number and decreases the equivalence ratio. The nonlinear interaction of the hydrodynamics with chamber acoustics and combustion dynamics results in various oscillatory states in the system. The system dynamics at each air flow rate is captured by acquiring the unsteady pressure signal using a pressure sensor (PCB piezotronics, Model Number 103B02, sensitivity 217.5 *mV/kPa*, 0.14 *Pa* uncertainty). The acoustic sensor is mounted at a location of 90 *mm* from the upstream end of the combustion chamber using a Teflon adapter at the combustion chamber wall. The measured pressure signal is stored in a computer system using a 16 bit analog to digital conversion card (NI-6143) through a signal conditioner.

For all the experiments, the exponential decay rates of the acoustic pressure in the system were obtained to be -37 $s^{-1}$with ± 3% variation. These cold decay rates are estimated by introducing an acoustic pulse at a fundamental acoustic frequency of 135 *Hz* with a loudspeaker (Ahuja AU60) that is mounted at the exit of the combustion chamber and measuring the decay in amplitude when the pulsing was switched off. Data acquisition is made at each equivalence ratio condition at a sampling rate of 10 *kHz* for duration of 3 seconds.

3. 5 Spectral analysis of combustion noise

The acoustic pressure measurements during the occurrence of combustion noise acquired from turbulent combustor with a circular bluff body as flame holding device is shown in Fig. 3.2(*a*). The acoustic pressure exhibits low-amplitude, seemingly random, irregular fluctuations. The corresponding acoustic pressure amplitude spectra (Fig. 3.2*b*) are broadband with shallow peaks near the acoustic modes of the combustor.

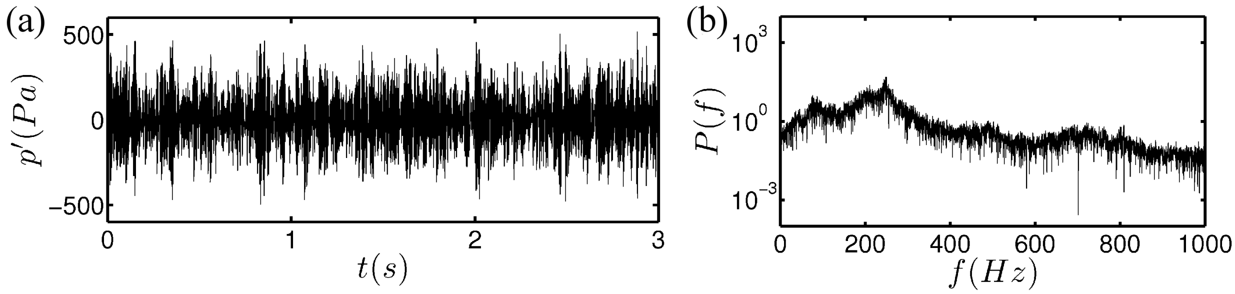

Figure 3.2: *a*) Acoustic pressure time series data acquired during combustion noise in a combustor with bluff body (Re = 1.8 × 10^4) as flame holding device. The unsteady pressure exhibits low-amplitude, seemingly random, irregular fluctuations. *b*) The amplitude spectrum of combustion noise from bluff-body stabilized configuration. The amplitude spectra of acoustic pressure are broadband with shallow peaks in the vicinity of the acoustic modes of the combustor.

Assuming linear acoustics, the sound emission at each frequency from open turbulent flames is shown to be generated from heat release process at that frequency (Rajaram, 2007). When such turbulent flames are confined in a combustion chamber, the confinement modes preferentially amplify the sound emitted from the flames at time scales close to its natural time scales (frequencies) and gives rise to the shallow peaks in the amplitude spectrum. The presence of multiple peaks in acoustic power spectrum during combustion inside a confinement is reported in literature (Chiu and Summerfield, 1974; Kumar, 1975; Strahle, 1978; Hegde *et al*., 1987). However, combustion chamber acoustics and hydrodynamics do not lock on during combustion noise and hence do not lead to the excitation of self sustained combustion instabilities (Chakravarthy *et al*., 2007*a*; Charavarthy *et al*., 2007*b*).

As we have already mentioned in Sec. 3.1, the acoustic power spectrum of combustion noise from open turbulent flames involves a power law scaling. The physical reason for the power law scaling in the acoustic power spectrum in combustion noise is turbulence. Clavin and Siggia (1991) and Clavin (2000) showed that if the turbulence have Kolmogorov spectrum, the acoustic power spectrum varies as $\omega^{-5/2}$. Power laws are an indication of scale invariance often seen in physical systems (Lovejoy and Schertzer, 1986; Davis *et al*., 1995; Lesne, 2011).

Scale invariance is an important feature of turbulent flows (Pocheau, 1994; Frisch, 1995; Lesne, 2011). However, such power law scaling is not discernable in the amplitude spectrum for combustion noise in a confined environment (see Fig. 3.3b) due to the presence of narrow peaks near the duct modes. To unveil scale invariance of combustion noise in a confined environment, we employ the statistical theory of complex networks.

3. 6 Combustion noise is scale-free

The time series data of acoustic pressure representing the dynamics of combustion noise is mapped into complex networks using visibility algorithm which is explained in Sec. 3.2. If any two nodes (i and j) are connected $A_{i,j}$ is one, otherwise $A_{i,j}$ is zero. Any node ($i = 1$ to N, N is the total number of nodes in the network) can be connected to a number of other nodes ($j = 1$ to N-1) present in the network. The total number of nodes that are connected with a given node v is specified as the degree of that node ($k_v = \sum_{i=1}^{N} A_{i,v}$). The percentage of nodes with k number of connections in a complex network can be represented using a distribution $P(k)$. The variation of $P(k)$ with respect to k is important in distinguishing the different types of complex networks. As an example, if the variation of $P(k)$ with respect to k follows a random distribution (Poisson distribution, exponential distribution etc.), the corresponding network is classified as a random network (Zhang and Small, 2006).

The degree distribution of complex networks mapped from the unsteady pressure time series during combustion noise acquired from a bluff-body configuration is shown in Fig. 3.3(a).

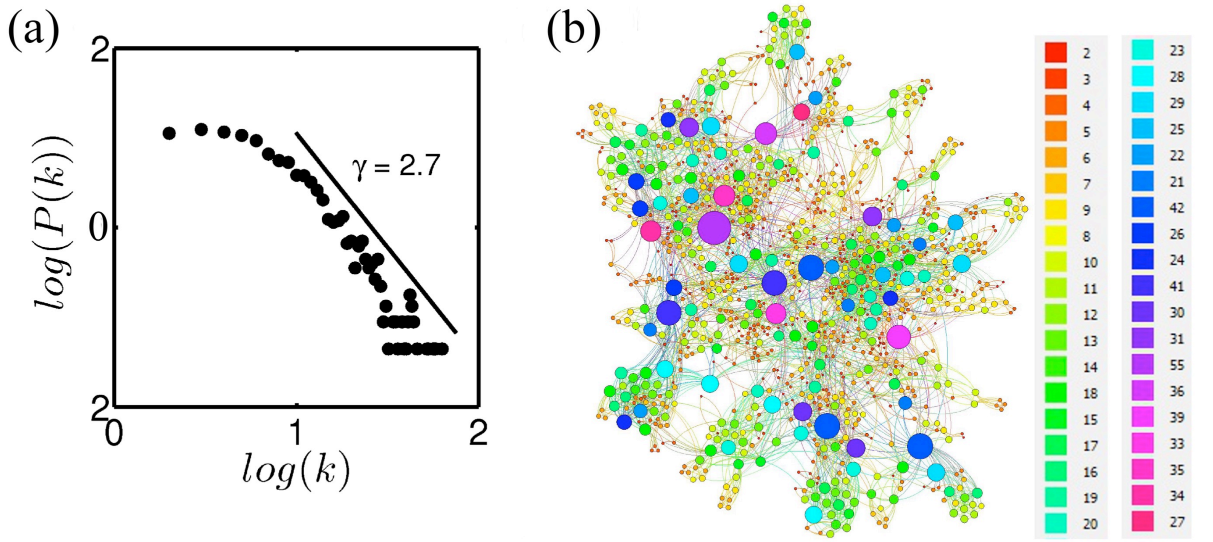

Figure 3.3: *a*) Degree distributions ($P(k)$ Vs k) of the complex network during combustion noise acquired from a bluff-body configuration (Re = 1.8 × 10^4). It is evident from Fig. 3.3(*a*), that the degree distribution curve has a power law behavior highlighting that networks during combustion noise are scale-free. The physical mechanism underlying scale-free nature (scale invariance) of combustion noise is the turbulence involving vortices that span a range of scales in the inertial regime. *b*) Complex networks during combustion noise acquired from bluff-body configuration is plotted using the Gephi software. Nodes are shown as circles and colored based on their degree (degree of a node is the number of nodes connected with that node). The sizes for nodes are assigned based on their degree. A few large nodes that are connected with highest number of nodes (called hubs) in a network correspond to a few large vortices in the flow. It can be seen that blue and pink colored nodes are connected with largest number of nodes and are the hubs in a scale-free network of combustion noise. Nodes with fewer degrees are due to the intermediate and small scale vortices in the flow. The complex network during combustion noise possesses heterogeneity of degrees of nodes with no characteristic degree.

As can be seen from Fig. 3.3(*a*), the degree distribution of complex networks mapped from time series data during combustion noise has a power law behavior.

$$P(k) \sim k^{-\gamma}$$

The power law exponents are measured to be $\gamma = 2.7$ for bluff-body configuration with uncertainty of ± 0.1. For all the data that we obtained in the bluff body configurations and in another swirler configuration, the power law exponent of scale-free network during combustion noise was in the range of 2.5 to 2.7. This highlights the fact that the power law exponent ($\gamma = 2.7$ & 2.5) are nearly identical for two different (bluff body & swirler) configurations.

From the power law trend, we discover that the complex networks obtained during combustion noise are scale-free networks. This is the first time in thermoacoustics literature that time series data acquired during combustion noise is represented as scale-free network. Time series obtained from turbulent systems have been recently represented as scale-free networks (Liu *et al.*, 2010; Charakopoulos e*t al.*, 2014).

Scale-free behavior of complex network during combustion noise represents the scale invariance of combustion noise. The power law distributions of scale-free network are related to the fractality (scale invariance) of the original time series (Zhang and Small, 2006; Lacasa *et al.*, 2008). For non-stationary time series, Lacasa *et al.* (2009) proposed a linear correlation between the power law exponent and the Hurst exponent. In statistical analysis, non-stationary time series is the one for which statistical properties (for example mean, variance, central moments etc.) does not remain constant in time. The acoustic pressure time series data acquired during combustion noise is non-stationary since pressure measurements acquired at a given instant is not only a function of the previous instant, but also depends on the changes happening at some other locations in the reacting flow. If we crudely apply the equation relating Hurst exponent and power law exponent ($\gamma = 3.1 - 2H$) given by Lacasa *et al.* (2009) and Ni *et al.*, (2009), we get Hurst exponent of $H = 0.2$ for bluff body configuration and $H = 0.3$ for swirler configuration.

The value of the Hurst exponent ($0 < H = 0.2, 0.3 < 0.5$) implies that combustion noise data is anti-persistent. For anti-persistent time series, a large data value is followed by a small value and a small value is followed by a large value. For anti-persistent signals, the value of Hurst exponent lie between 0 and 0.5. The results on Hurst exponent are consistent with the results reported by Nair and Sujith (2014).

The networks derived during the occurrence of combustion noise are plotted (Fig. 3.3*b*) using the Gephi software (Bastian *et al.*, 2009). The nodes are shown as circles and nodes of different degrees are shown in different colors (degree of a node is the number of nodes connected with that node). Further, nodes are shown in different sizes based on their degree. As can be seen from Fig. 3.3*b*, the complex networks during combustion noise possess heterogeneity of degrees of nodes. There is no characteristic degree in this network which is the reason why they are scale-free networks.

The heterogeneity in degrees of nodes can be directly linked to the physical state of combustion noise. Turbulent reacting flows involve scales that span a range from large scales of the order of the characteristic dimension of the flow to Kolmogorov scales. A few large vortices in the reacting flows produce fluctuations of large magnitudes which are reflected as large fluctuations of data values in the time series. As we move towards the intermediate and small vortices, the number of small scale, short-living vortices increases. These high frequency small eddies in the reacting flows produce fluctuations of small magnitude which result in small fluctuations of data values in the time series. Nodes that correspond to larger data values in the time series have visibility to many other nodes that correspond to small data values in the time series. Therefore, nodes with large data values are connected with more number of other nodes in a network. Such nodes that are connected directly with a very large number of other nodes in a network are called hubs.

Hubs are the key nodes in the network and only few numbers of such hubs can be found in a network. These hubs are the reflection of large scale vortices in the turbulent flow. In the degree distribution, nodes with the highest degree occur in minimum percentage to the total number of nodes (occupies the tail portion of the power law curve). As an example, in a scale-free network of combustion noise (Fig. 3.3*b*), a few hubs (nodes that are colored in blue and pink) connected with a large number of other nodes can be seen.

In contrast, nodes having small data values can see only few of their neighbors and are connected with only a few other nodes. These nodes with lower degrees occur as large population and are a reflection of short-living, large number of small scale eddies in the flow. In the degree distribution, we can see a higher percentage of nodes having fewer degrees. In complex networks (Fig. 3.3*b*), these nodes can be seen as large number of small size nodes with fewer connections.

The cascade of vortices of different scales leads to the absence of a single characteristic scale and is the physical reason for scale-free behavior in combustion noise. The scale-invariance (i.e. power law distribution) of combustion noise in a confined environment is unraveled in the complex network representation as scale-free behavior, though such scale invariance cannot be discerned in the amplitude spectrum.

3. 7 Onset of thermoacoustic instability

3.7.1 Intermittency route to thermoacoustic instability

The scale-free behavior of combustion noise gives a hint that the addition of heat in turbulent flows (corresponding to the case of combustion in turbulent flows) preserves the scale invariance which is in fact a property of turbulent flows. However, the transition to the onset of combustion instability from combustion noise is associated with the change in system dynamics from one dominated by the presence of multiple scales to one dominated by a few discrete scales. The transition in system dynamics during this transition (combustion noise to combustion instability) for increasing flow Reynolds number in a bluff-body stabilized turbulent combustor is illustrated in terms of changes in the time series data of acoustic pressure (Fig. 3.4).

As we have already discussed in Sec. 3.4, the acoustic pressure measured during combustion noise is characterized by aperiodic fluctuations (Fig. 3.2*a*). However, as we increase the Reynolds number further past the condition of combustion noise, ordered periodic oscillations appear intermittently amidst regimes of aperiodic fluctuations.

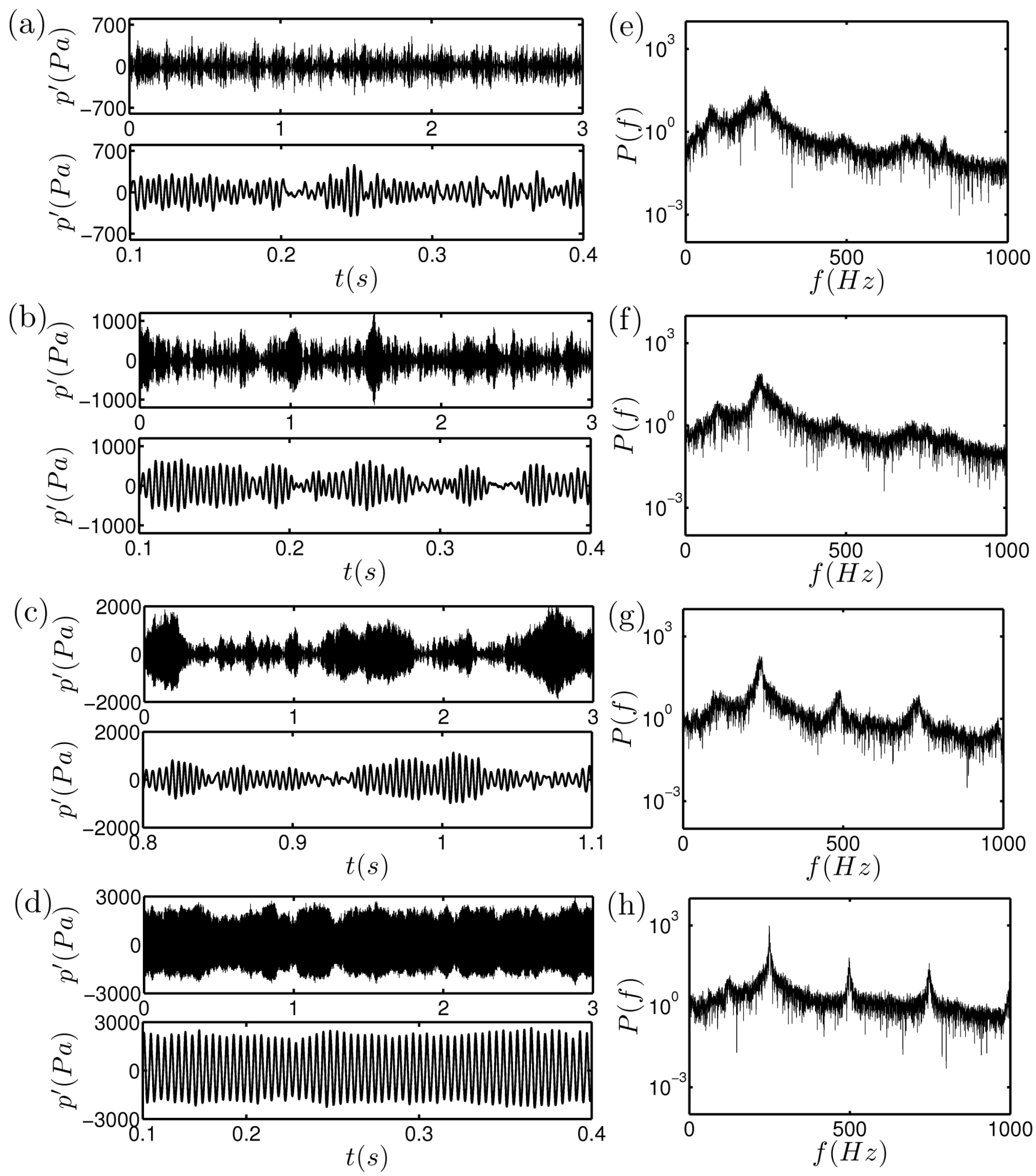

Figure 3.4: Unsteady pressure time series measured in bluff-body configuration during *a*) combustion noise ($Re = 1.7 \times 10^4$), intermittency when *b*) $Re = 2.2 \times 10^4$ and *c*) $Re = 2.5 \times 10^4$. Intermittent bursts of high-amplitude periodic oscillations amidst regimes of chaotic fluctuations last longer in time as we increase the Reynolds number towards the condition of combustion instability. Finally, when *d*) $Re = 2.8 \times 10^4$, self-sustained, high-amplitude, ordered periodic oscillations happen during full blown combustion instability. Transition from combustion noise to combustion instability is reflected as a transition from chaos to limit cycle in the time series of acoustic pressure. The accumulation of acoustic energy, reflected as growth in acoustic pressure amplitude in the amplitude spectrum in the vicinity of acoustic instability modes, is observed during this transition to combustion instability.

This intermediate state characterized by alternating appearances of bursts of periodic and chaotic fluctuations is identified to be 'intermittency' (shown in Figures 3.4*b* and 3.4*c*) (Nair *et al.*, 2014). Such an intermittent state is a dynamical state different from combustion noise and combustion instability and is observed consistently every time during the transition from combustion noise to combustion instability and persists in time. Intermittency is not a transient state, but a distinct state described by dynamical systems theory.

From a dynamical systems perspective, intermittency is explained as a result of homoclinic orbits in the phase space by Nair and Sujith (2013). A homoclinic orbit is a trajectory in phase space in which an unstable manifold of a fixed point of the system merges with its own stable manifold (Nair and Sujith, 2013). The equilibrium state of the system during intermittency switches between stable and unstable states in phase space. This corresponds to the alternate switching of bursts of high-amplitude periodic oscillations and low-amplitude chaotic fluctuations in the unsteady pressure time series data (see Figures 3.4*b* and 3.4*c*).

These intermittent bursts of high-amplitude periodic oscillations last longer in time as we increase the Reynolds number towards the condition of combustion instability. Finally, self-sustained, high-amplitude, ordered periodic oscillations happen during full blown combustion instability (Fig. 3.4*d*). Therefore, the transition from combustion noise to combustion instability is reflected as a transition from chaos to limit cycle (order) in the acoustic pressure time series.

3.7.2 Transition from scale-free to order at the onset of thermoacoustic instability

Complex networks are constructed from the time series data of acoustic pressure acquired during this transition. The degree distributions of the complex networks during intermittency (shown in Figures 3.5*a* and 3.5*b*) have a power law behavior. This shows that time series acquired during intermittency are also converted into scale-free networks. The scale-free networks during intermittency are plotted with the help of the Gephi software (Bastian *et al.*, 2009) and as one would expect, these networks also has no characteristic degree (Figures 3.5*d* and 3.5*e*).

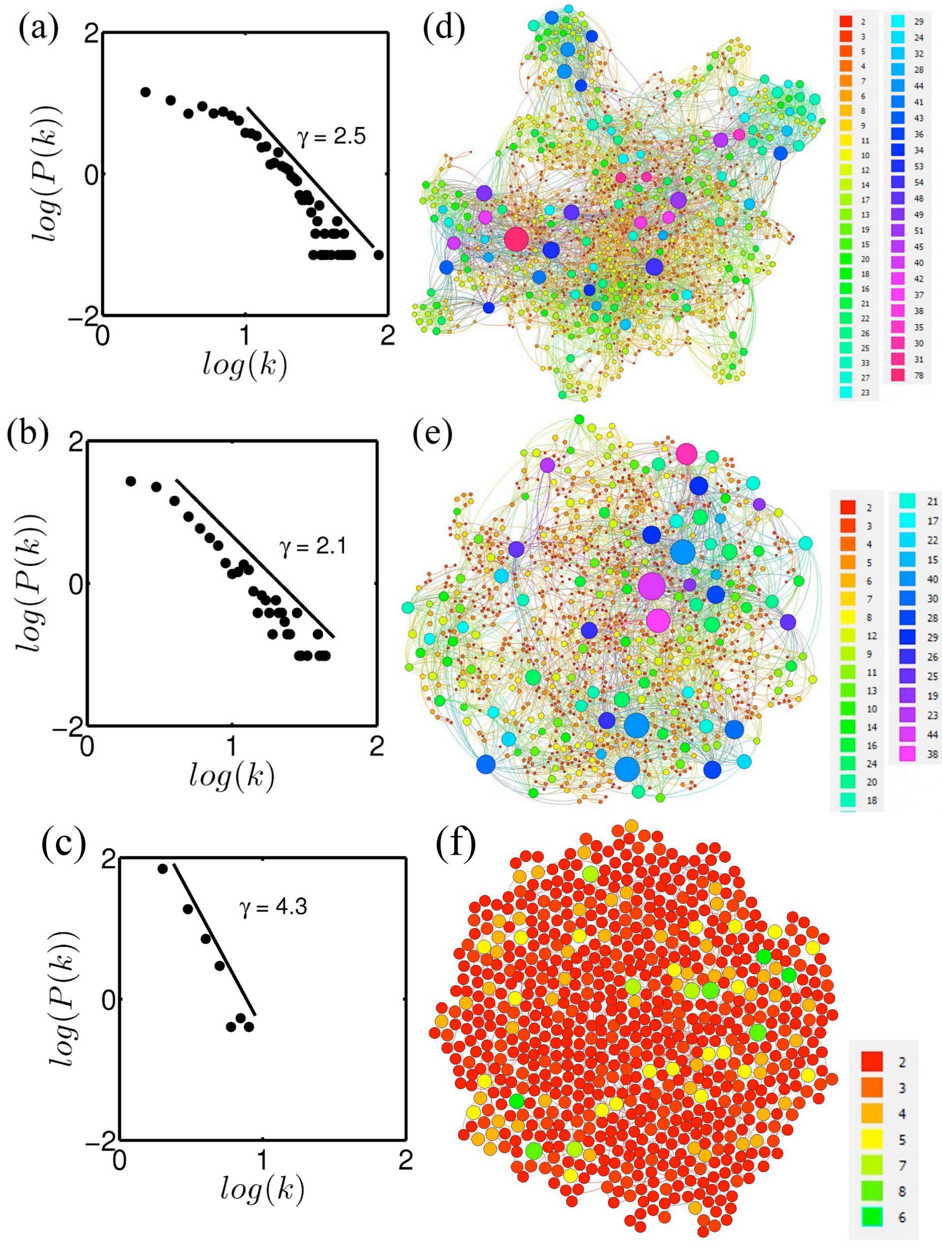

Figure 3.5: Degree distributions of complex networks derived using visibility condition from time series of acoustic pressure during intermittency (Figures 3.4*b* and 3.4*c*) when *a*) $Re = 2.2 \times 10^4$ and *b*) $Re = 2.5 \times 10^4$. The degree distribution curves have power law trend showing that time series during intermittency are also converted into scale-free networks. The networks are plotted with the help of the Gephi software (Bastian *et al*., 2009). As one would expect, networks during intermittency (*d* and *e*) also have no characteristic degree. In contrast, *f*) network during combustion instability when $Re = 2.8 \times 10^4$, possess increased regularity in degrees of nodes. However, turbulence causes imperfection in periodicity. *c*) The degree distribution map during instability is characterized by a few discrete points.

In contrast to intermittency and combustion noise, complex networks during limit cycle oscillations (Fig. 3.5*f*) exhibit increased regularity in the degrees of the nodes. As can be seen in Fig. 3.5(*c*), the degree distribution map is characterized by a few discrete points. The slight non-uniformity in degrees of the nodes (Fig. 3.5*f*) is due to the cycle-to-cycle variability in limit cycle oscillations (see Fig. 3.5*d*) during combustion instability which arises from background turbulent fluctuations (Lieuwen, 2002). Through extensive investigation, Lieuwen (2002) showed that such cyclic variability does not reflect the presence of chaotic fluctuations. Rather, Lieuwen (2002) suggested that the cyclic variability in limit cycle oscillations arise from background disturbances with short correlation time relative to the period of limit cycle. The imperfect limit cycle oscillations in the dynamics of turbulent combustors are reported and characterized by Noiray and Schuermans (2012).

To view results in a better manner in such "noisy" situations, Nunez *et al*. (2012) introduced a threshold 'epsilon' to visibility condition.

$$
\begin{aligned}
&\text{if,} \quad p_k + \varepsilon < p_i + (p_j - p_i)\frac{t_k - t_i}{t_j - t_i}, && A_{i,j} = 1; \\
&\text{else,} && A_{i,j} = 0; \\
&\text{where,} && \varepsilon = e * mean(p)
\end{aligned}
\tag{3.2}
$$

Here, p is the vector that consists of data values belonging to the crest of each cycle in the time series. The time series data of acoustic pressure acquired from the combustor possess fluctuations of different scales. This causes, peaks (i.e., crest of each cycle in the time series) in the acoustic pressure time series to have both positive and negative values varying in a wide range. As an example, for time series data during combustion noise (when $Re = 1.8 \times 10^4$), the maximum value of the peaks is 516.5 Pa, the minimum value of the peaks is - 441.4 Pa and the mean value of the peaks is 58.3 Pa. Therefore, the threshold $\varepsilon = 0.24 * mean(p)$ is 13.992 Pa which is 2.7% of maximum value of the peaks. Since the value of ε is very small with respect to the peak amplitude; we consider that the information in the time series is preserved with the addition of epsilon into the visibility algorithm.

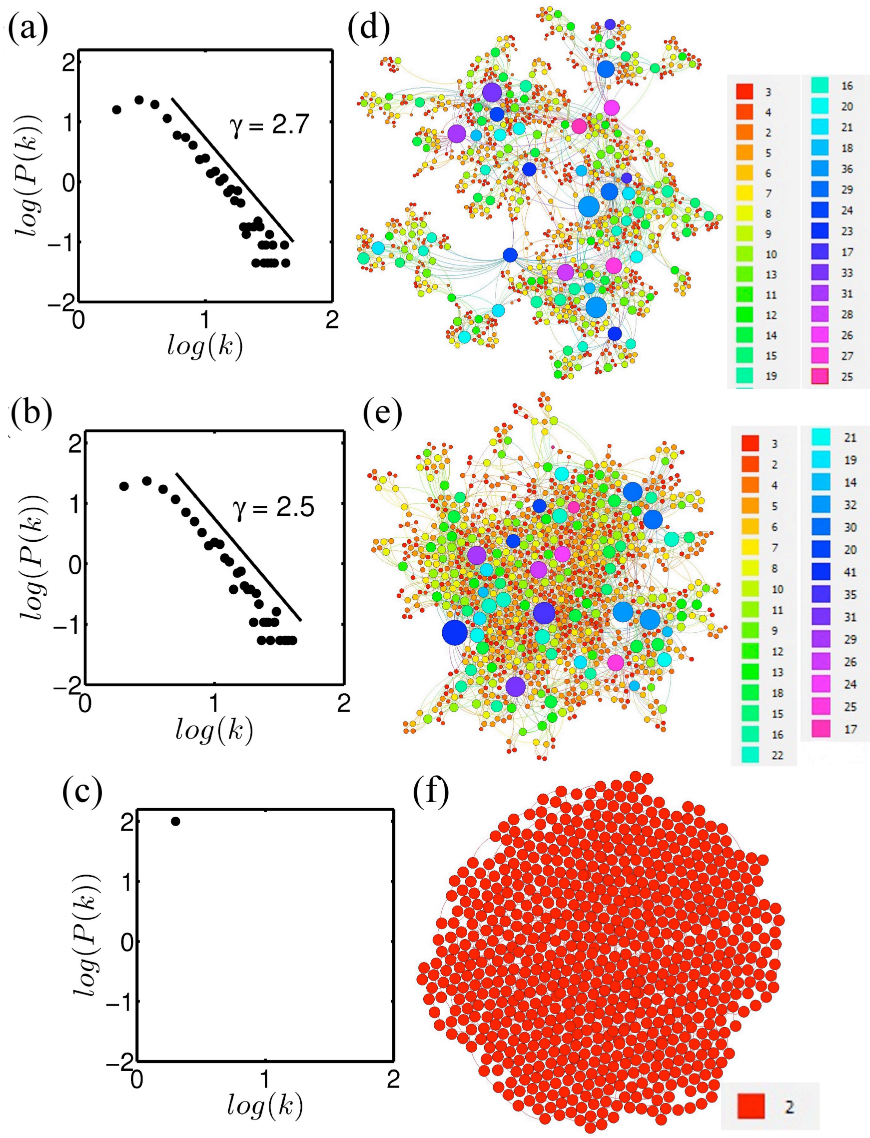

Figure 3.6: Degree distributions and networks derived using visibility graph with threshold (e = 0.24) during the occurrence of *a*) and *d*) combustion noise ($Re = 1.8 \times 10^4$), *b*) and *e*) Intermittency ($Re = 2.2 \times 10^4$) and *c*) and *f*) combustion instability ($Re = 2.8 \times 10^4$). The power law exponent of degree distributions during the occurrence of (a) combustion noise and *b*) intermittency remains the same as that of networks without using a threshold. The use of ε in the visibility condition helped in detecting the periodicity hidden in the noisy limit cycle oscillations during combustion instability. At the onset of combustion instability, the scale-free behavior disappears and the network transitions into a regular network. The regular network corresponding to the combustion instability is characterized by a single characteristic degree. All the nodes have the same number of links with other nodes in the network and a discrete point appears in the plot of $P(k)$ Vs k (Fig. 3.6*c*).

The degree distributions of complex networks derived using the visibility condition with epsilon during the occurrence of combustion noise (Fig. 3.6*a*) and intermittency (Fig. 3.6*b*) remain qualitatively same as that of degree distributions of complex networks derived without using epsilon in visibility condition during combustion noise (Fig. 3.3*a*) and intermittency (Fig. 3.5*a*). The power law exponents of complex networks during combustion noise and intermittency do not change with the inclusion of epsilon into the visibility condition, implying that the corresponding networks are indeed scale-free (The degree distributions of complex networks for different values of threshold are provided in Appendix A). However, the main advantage of incorporating epsilon into the visibility algorithm is the detection of periodicity in the time series which is masked by the presence of irregular fluctuations in experiments.

In contrast to combustion noise and intermittency, degree distribution of complex network during combustion instability is characterized by a single discrete point (Fig. 3.6*c*). Discrete points appear in the degree distribution of a regular network. A network is called 'regular' if all the nodes in the network have the same number of connections (Quenell, 1994). The period-1 time series (limit cycle) is converted into a regular network with a single point in the degree distribution map (Quenell, 1994). The situation is illustrated using Fig. 3.7.

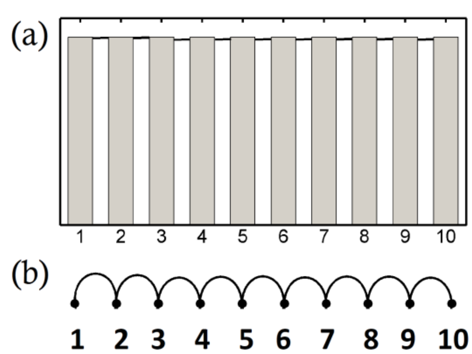

Figure 3.7: Illustration of complex network derived using visibility graph from a periodic time series. Peaks in the periodic time series are considered as nodes. All the nodes are of the same height and have visibility only with their neighbors. Therefore, all the nodes are connected only with their neighbors.

In an example illustrated in Fig. 3.7, nodes are connected only with two of their neighbors. Therefore, the degree (number of nodes that are connected with a given node) of all the nodes become two. During the occurrence of combustion instability, all the nodes are connected only to their neighbors. Thus, in the degree distribution (Fig. 3.6*c*) of a complex network that correspond to combustion instability, the percentage of nodes ($P(k)$) having degree $k = 2$ is 100%, implying that the network at combustion instability is 'regular'.

The complex networks during *d*) combustion noise, *e*) intermittency and *f*) combustion instability with the use of epsilon in the visibility graph are shown in Fig. 3.6. Nodes of different degrees (degree of a node is the number of nodes that are connected with that node) are shown in different colors. The color code with respect to degree is provided near the corresponding complex networks in figure 6. Further, sizes for nodes are assigned based on their degree.

The network of combustion noise and intermittency are composed of nodes of various degrees and various sizes. Nodes are filled with various colors and the network has no single characteristic degree. At combustion instability, all the nodes in the complex network have a degree of two (colored in red) due to the periodic oscillations and hence the entire network is colored in pink.

The transition from combustion noise to combustion instability is shown as transition from scale-free to regularity in complex networks topology. The physical mechanism underlying this transition is linked with the mechanisms that cause order to emerge in turbulent systems.

In the transition from turbulence to order, fully developed turbulent flow is shown to be self-organizing into an ordered state through the mechanism of spectral condensation and inverse energy cascade (Shats *et al*., 2005). The turbulent energy in a broadband spectrum is redistributed to form an ordered state at high energy level (Kraichnan, 1967; Dubos *et al*., 2001; Shats *et al*., 2005). In this spectral redistribution, the turbulent energy is shown to be accumulated in the lowest accessible mode (Sommeria, 1986; Paret and Tabling, 1998; Shats *et al*., 2005). In thermoacoustic systems, during the transition to thermoacoustic instability from combustion noise, the growth in the acoustic pressure amplitude close to the acoustic modes of the combustor can be seen in the acoustic amplitude spectrum (Figures 3.4*f*, 3.4*g* and 3.4*h*). Finally, at full blown combustion instability the acoustic pressure amplitude reaches a maximum value near the duct acoustic modes. Moreover, it is well known in the literature that combustion instability is associated with the formation of organized coherent vortices in the flow indicating an increase in order of the thermoacoustic system. Hence, we conjecture that the transition from combustion noise to combustion instability may be due to the self-organization of multiple scales in turbulence to an ordered state with a single scale.

Further, self-organization of turbulent fluids to high energy ordered state is identified to be due to the mechanism of inverse energy cascade (Sommeria, 1986; Paret and Tabling, 1998; Dubos *et al*., 2001; Shats *et al*., 2005; Xiao *et al*., 2009). However, this inverse energy cascading is in contrast to conventional thought of energy being transferred from large to smaller scales till the scales of dissipation. Inverse energy cascade was first conjectured by Kraichanan (1967) who proposed that that energy in a forced turbulent fluid can cascade to larger scales. In turbulent reacting flows, heat release rate fluctuations from combustion supply energy into acoustics. The interaction of the generated acoustic waves with shear layer induces the formation of vortices of different sizes. The size of vortices depends on the hydrodynamic instability frequency matching with the acoustic instability frequency (Schadow and Gutmark, 1992). The occurrence of large-amplitude pressure fluctuations during combustion instability is driven by periodic heat release rate fluctuations, when heat release rate fluctuations are in proper phase with acoustic pressure fluctuations, which is a necessary condition known as Rayleigh criteria (Rayleigh, 1878) for self-sustained pressure oscillations. Therefore, the process of combustion instability could possibly be expected to be driven by the inverse cascading of energy from combustion to large scales which are in turn decided by the matching of hydrodynamic frequency and acoustic mode. This is in agreement with the observation of development of large scale vortices driving combustion instability (Rogers, 1956; Smith and Zukoski, 1985; Poinsot *et al*., 1987; Schadow *et al*., 1989; Yu *et al*., 1991; Coats, 1996). Further, Zank and Matthaeus (1990) indicated the possibility of inverse energy cascade, wherein energy is cascaded to long-wavelength acoustic modes from smaller scales in the theoretical analysis of nearly incompressible flows with heat addition.

From a complex networks perspective, with a single scalar pressure measurement, the patterns emerging during this transition are visualized as the structural changes happening in the topology of complex networks. Further, these structural changes can be quantified in terms of network properties. The network properties are used to distinguish different dynamical regimes in turbulent jet flows (Charakopoulos *et al*., 2014) and three dimensional fully developed turbulence (Liu *et al*., 2010). We have utilized the properties of complex networks to provide early warning for the onset of instabilities in many types of combustors and an aeroacoustic system operated in a turbulent environment (Murugesan *et al*., 2014).

3.7.3 Network properties as precursors to thermoacoustic instability

The network properties such as clustering coefficient, characteristic path length, network diameter and global efficiency are useful in characterizing the structure or topology of complex networks and can be calculated from the adjacency matrix. The network properties are calculated for each operating conditions of the combustor. For each operating condition, the vector $p(t)$ (local maxima) is divided into a number of sets with each set having 100 data points. The network properties are computed for each set and averaged for all the sets. The network properties are then normalized with their maximum values (C_0, L_0, D_0 and E_0) respectively. The variation of the r. m. s. value of the pressure and normalized values of the network properties such as clustering co-efficient, characteristic path length, global efficiency, and network diameter are shown in Fig. 3.8.

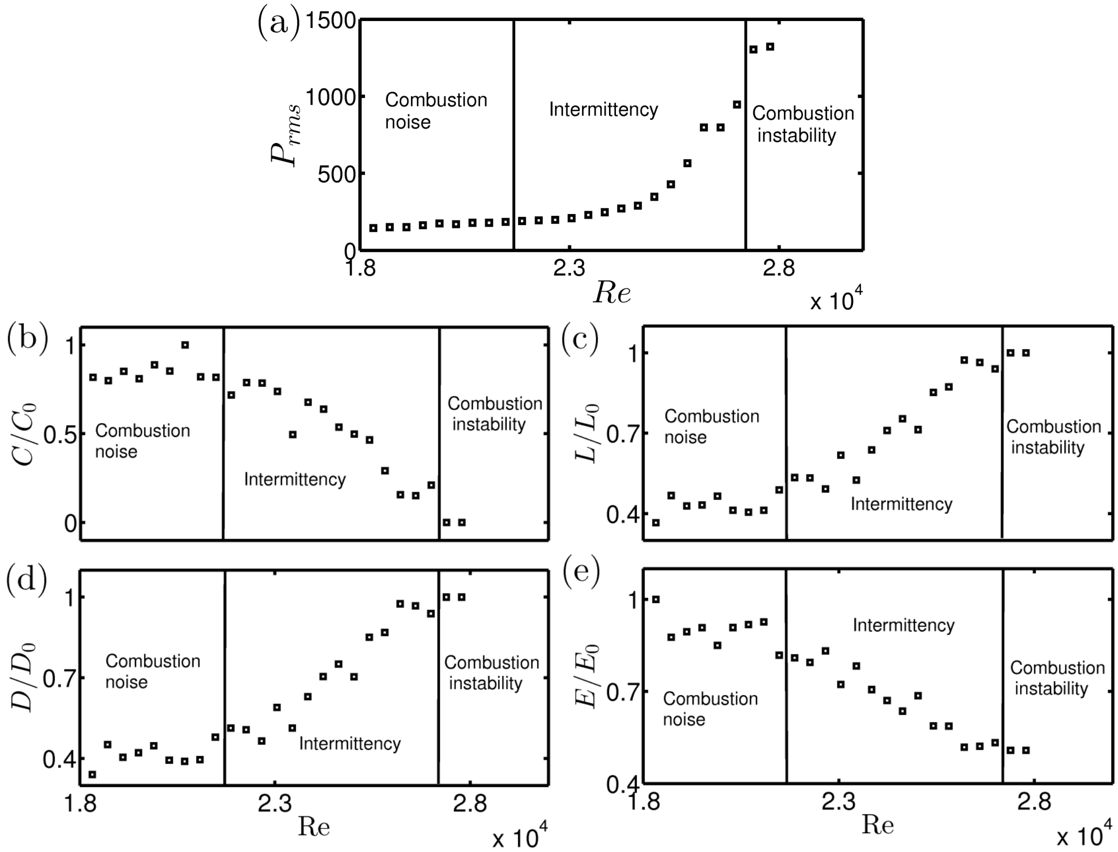

Figure 3.8: Variation of *a*) r.m.s. value of the pressure signal, normalized values of *b*) the clustering co-efficient, *c*) the characteristic path length, *d*) the network diameter and *e*) the global efficiency.

The variation of r.m.s. values of the acoustic pressure for different values of the Reynolds number is shown in Fig. 3.8(*a*). This measure corresponds to a typical measure one uses to assess the stability of the combustion system. In the regimes of combustion noise, the amplitude levels are low. The rise in the amplitude occurs at a Reynolds around $Re = 2.6 \times 10^4$. However, since the amplitude at combustion instability is unknown, unlike the frequency which can be estimated reasonable well, this would not be a suitable precursor for instability detection, since the higher values may just be the result of higher amplitude levels during combustion noise. Also, it could be possible that the value of the r.m.s. rises significantly only after the instability has set in, which means it is difficult to detect an impending instability.

The experimental setup and the unsteady pressure data used in the current analysis is same as that of the data used by Nair *et al*. (2014) and Nair and Sujith (2014). Nair *et al*. (2014) have shown the variation of damping rate calculated from the autocorrelation analysis of the unsteady pressure data acquired from bluff-body stabilized and swirler stabilized turbulent combustors. The transition to thermoacoustic instability from combustion noise is identified as the operating condition at which the damping rate approaches zero. Although the occurrence of thermoacoustic instability has been identified by the correlation analysis, the damping rate attains the value of zero only after the instability has set in, which is not desirable. Further, the variation of damping rate is not monotonous due to the presence of intermittency during the transition to thermoacoustic instability. As we have already mentioned, these methods may not be effective for combustors exhibiting noise induced transition to instability. The existence of several frequencies in the spectrum makes the estimation of damping rate difficult.

Recently, Nair and Sujith (2014) proposed Hurst exponent calculated from the multifractal analysis as a precursor to thermoacoustic instability. In this method, one has to rely on a single measure to obtain early warning about thermoacoustic instability which can lead to false positives and negatives. Alternatively, Nair *et al*. (2014) proposed recurrence quantities as the precursors. In addition to these instability detection methods, we consider that early warning from a number of network properties could enables us to eliminate false positives and negatives, thereby making the warning system more robust. This is the motivation to propose network properties as precursors.

Therefore, in the present work, we propose the network properties as the precursors to the onset of impending combustion instability. Here, we discuss the variation of network properties namely normalized clustering coefficient, normalized characteristic path length, normalized network diameter and normalized global efficiency for the change in system dynamics. However, once the adjacency matrix is obtained, any of the other network properties can be calculated as well.

Variation of normalized clustering coefficient

The clustering coefficient is a measure of cliquishness of the nodes. The term cliquishness was introduced by Watts and Strogatz (1998) to quantify whether the nodes in the neighborhood of any node are also neighbors (i.e connected) or not. For example, consider a node connected to two other nodes. The maximum possible number of connections in the neighborhood of a given node is 1. If two other nodes are connected with each other, then the clustering coefficient attains its maximum value of 1. The value of 1 for the clustering coefficient for any node implies that all the nodes in the neighborhood of a given node are connected to each other. The average clustering coefficient (C) of a network is defined as the average of clustering coefficients for all the nodes. The value of the normalized clustering coefficient computed at each operating condition from the acoustic pressure signal is shown in Fig. 3.8*b*.

Note that the value of clustering coefficient is minimum as the Reynolds number is around $Re = 2.8 \times 10^4$. The lowest value of clustering coefficient implies that in the network derived from the time series data during the occurrence of combustion instability, the nodes are more independent than that of the network during combustion noise. This reflects the underlying physics during the combustion instability. The periodic oscillations occur due to the large coherent vortices in the flow. As already discussed, nodes in a network that is derived from a periodic time series are connected only with their neighbors according to the visibility graph. So, the average clustering coefficient of the complex network during the occurrence of combustion instability is a minimum.

However, during the occurrence of combustion noise, nodes of various degrees are present in the complex network (Fig. 3.3*a*). Neighbors of the nodes are more connected and the network is highly clustered. Therefore, during the occurrence of combustion noise, the value of the normalized clustering coefficient (C/C_0) is closer to the maximum (maximum value of C is 1). Therefore, as one would expect that during the transition from combustion noise to combustion instability, the value of clustering coefficient begins to drop (at the onset of intermittent bursting states). The drop in the normalized clustering coefficient (C/C_0) happens well before the rise in the amplitude of the unsteady pressure in the combustor.

Variation of normalized characteristic path length

Node i and node j can be connected in a number of ways. Shortest path length ($L_{i,j}$) is the number of connections required in the shortest path between i and j. As an example, if node i and node j are directly connected, then $L_{i,j}$= 1. For a disconnected node, $L_{i,j} = \infty$. The characteristic path length (L) is the sum of all the shortest path lengths divided by the maximum possible number of links in a network. The variation of normalized characteristic path length of the networks computed at each operating condition is shown in Fig. 3.8(c).

$L_{i,j}$ measures how fast the information can be spread in a network. Since all the nodes are highly connected (high clustering coefficient) in the scale-free networks derived from the time series data of combustion noise, the nodes can be reached in a smaller number of steps from other nodes in the network. Therefore, the average value of $L_{i,j}$ called characteristic path length (L) for the entire network is small for the case of the network corresponding to combustion noise. At combustion instability, the nodes are connected only with their neighbors and it takes more number of steps to reach any node from any other nodes in the network. The characteristic path length has the maximum value at the condition of combustion instability. Hence, during the transition from combustion noise to combustion instability (scale-free to regular), the value of normalized L/L_0 increases (shown in Fig. 3.8c) and it happens well before the rise in P_{rms} (Fig. 3.8a).

Variation of normalized network diameter

The variation of normalized diameter of the networks computed at each flow condition is shown in Fig. 3.8(d). The network diameter is just the maximum value of the characteristic path length and follows a similar trend as that of variation of L/L_0. As we have discussed in the previous section, the values of L/L_0 and D/D_0 is minimum at the condition of combustion noise (Figures 3.8c and 3.8d). The lowest values of L/L_0 and D/D_0 indicate that network derived from the time series data measured during the occurrence of combustion noise have more number of links between the nodes. In the case of combustion noise, the flow is characterized by large and small scale vortices. These small, short-living, high-frequency vortices lead to the fast disturbances of small-magnitudes in the time series data. Consequently, the nodes in the network that correspond to these small-magnitudes have a fewer connections with other nodes. However, if we consider the nodes that correspond to the intermediate and large scale vortices, these nodes are connected to more number of other nodes. This reflects as the lowest values of the characteristic path length and the network diameter at the condition of combustion noise. Similar to L/L_0, the value of D/D_0 rises during the transition and provides early warning signal for the onset of combustion instability.

Variation of normalized global efficiency

The global efficiency is an indicator of how efficiently a node can be reached from other nodes in the network. The variation of the normalized global efficiency is shown in Fig. 3.8(*e*). The global efficiency is calculated from the sum of inverse of short path lengths. If the short path length is small, the global efficiency becomes high, indicating that nodes are highly connected. This quantity is very useful for networks with disconnected nodes. E/E_0 has a high value for the network corresponding to combustion noise (nodes are highly connected). At combustion instability, the nodes are linked only to their neighbors, the value of global efficiency drops to a minimum value. The drop in value of E/E_0 to lower values occurs well before the onset of combustion instability.

In a nutshell, the network properties, normalized global efficiency (E/E_0), normalized characteristic path length (L/L_0), normalized network diameter (D/D_0) and normalized clustering coefficient (C/C_0) change significantly before the rise in P_{rms}. We have discussed the sensitivity of the network properties to the length and sampling rate of the temporal signal in Appendix B). The variation of network properties do not change for different values the length and sampling rate of the temporal signal.

We therefore can use the smooth variation of these quantities (properties of the complex network) as a measure of proximity to an impending instability in the thermoacoustic systems. These changes in the network properties are related to the change in system dynamics during the transition from combustion noise to combustion instability. We have utilized the properties of complex networks to predict the onset of instabilities in many types of combustors and an aero-acoustic system that are operated in a turbulent environment (Murugesan *et al.*, 2014).

3. 8 Interim Summary

We investigated the scale invariance of combustion noise generated from confined turbulent flames using complex networks. We showed that acoustic pressure fluctuations, which reflect the dynamics of combustion noise, can be represented as a scale-free network. The power law exponent in the degree distribution of scale-free network is related to the scale invariance of combustion noise. Scale-free network indicates that there is no single characteristic scale in the dynamics of combustion noise. This scale-free behavior of combustion noise is hard to discern from the frequency spectrum, due to the domination of duct acoustic modes. The scale-free behavior of combustion noise is due to the presence of turbulence. The spatial/temporal fluctuations of scales that range from large scales of the order of characteristic dimension of the flow to small Kolmogorov scales in turbulent reacting flows give rise to the complex topology and heterogeneous structure in network during combustion noise.

This scale-free behavior is shown to transition into regular topology during the transition from combustion noise to combustion instability. The presence of scale-free behavior in combustion noise and the emergence of order from scale-freeness at the onset of combustion instability draw attention to the possibility of spectral condensation and inverse energy cascade which can possibly explain the emergence of order. Complex network representation helped visualize and formulate quantities to quantitatively describe the topological changes during this transition. The variation of network properties can be used to detect the onset of combustion instability.

The network properties, normalized clustering coefficient (C/C_0), normalized characteristic path length (L/L_0), normalized network diameter (D/D_0) and normalized global efficiency (E/E_0) with respect to the operating conditions are presented. The changes in these properties happen significantly prior to the onset of an impending thermoacoustic instability. The network properties capture the change in physical state of the system dynamics during the transition from combustion noise to combustion instability. The method was also successfully used in detecting the onset of thermoacoustic instability in other systems such as a lifted turbulent jet flame combustor, a combustor with swirler as the flame holding device and even aero-acoustic systems. Further, the presented results are not specific to a visibility algorithm. Similar results are obtained when we employed other methods, for example, horizontal visibility graphs, to extract complex networks from time series. Further, any other network properties can also be employed to detect the onset of instability. Instead of relying on a single precursor measure, early warning from the variation of a number of network properties enables us to eliminate the false positives and negatives, thereby making the warning system more robust.

3.9 Onset of blowout

The blowout of flame is a major challenges for the development of practical combustion systems. In this section, the dynamical behaviour of transition to flame blowout in a bluff-body stabilized turbulent combustor is investigated in the framework of complex networks. As the equivalence ratio is decreased, the dynamics of thermoacoustic systems transitions from operation of the combustor to self-sustained limit cycle oscillations during thermoacoustic instabilities through intermittency. The self-excited thermoacoustic instability transition to intermittency again and finally, the flame blows out of the combustor as the equivalence ratio is further reduced.

The complex network approach unravels the hidden dynamical features in the temporal variations of the dynamic pressure which is a reflection of the underlying physics during the transition to blowout of flame. The use of complex networks reveals that the dynamical states close to blowout conditions involve power law behaviour in the degree distributions and scale-free topological structures in the complex networks. Further, the changes in combustion dynamics during the transition to flame blowout are clearly reflected as topological changes in network structures. As a quantitative analysis, the network topological measures are computed and demonstrated that these measures vary well before the onset of an impending flame blowout and are the robust precursors for the detection of flame blowout.

3.9.1 Transition to blowout of flame from combustion noise

The system dynamics bifurcates from combustion noise state to thermoacoustic instability as we decrease the equivalence ratio ($\varphi = 0.95$ to 0.29) by increasing the air flow rate. We measure the unsteady pressure as an important physical quantity to understand the dynamical changes in the complex phenomena of combustion dynamics. The pressure data was acquired at a sampling rate of 10 *kHz* for a period of 3 seconds. We present the time series data of pressure oscillations corresponding to different equivalence ratio conditions to indicate the presence of rich dynamical states in the combustion system dynamics in Fig. 3.9. These data are same as the data reported by Unni and Sujith (2015).

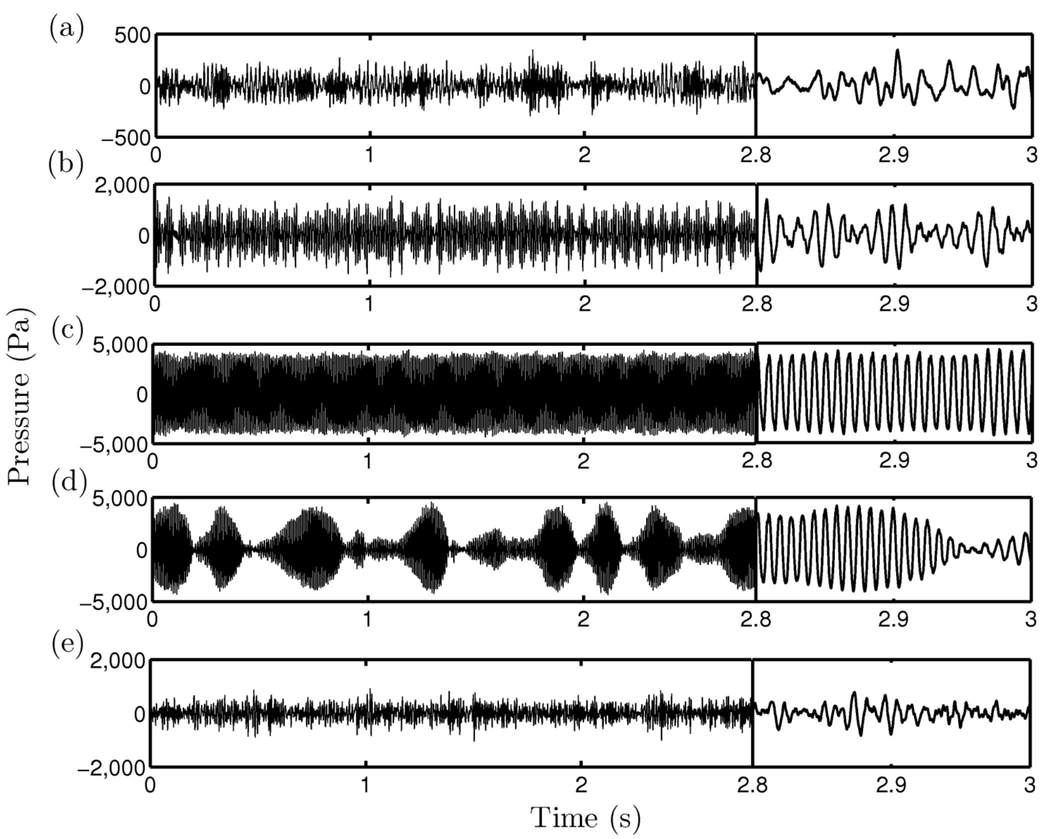

Figure 3.9: Time signals of unsteady pressure correspond to various oscillating states observed in the system (Unni and Sujith, 2015). *a*) combustion noise ($\varphi = 0.95$), *b*) intermittency that presages thermoacoustic instability ($\varphi = 0.79$), *c*) self-excited thermoacoustic oscillations ($\varphi = 0.5$), *d*) intermittency that presages blowout ($\varphi = 0.47$) and *e*) a dynamical state prior to blowout ($\varphi = 0.29$).

The system dynamics exhibit chaotic oscillations during the stable operation of the combustor under turbulent flow conditions, as shown in Fig. 3.9(*a*). Such chaotic oscillations during the stable operation are termed 'combustion noise' by the thermoacoustic community. Traditionally, combustion noise was considered as the stochastic oscillations arising from the background turbulent fluctuations. Recently, Nair *et al*., (2013) showed through a number of deterministic tests that combustion noise has deterministic chaotic nature with a phase space embedding dimension of 8-10.

These moderately high-dimensional chaotic oscillations transition into self-excited thermoacoustic oscillations through intermittency. The self-excited thermoacoustic oscillations most often exist as high-amplitude ordered 'limit cycle' oscillations, as shown in Fig. 3.9(*c*). Here, the frequency of limit cycle oscillations was measured to be 120 *Hz*. The time series data corresponding to the intermittent bursting of periodic oscillations during the onset of self-excited oscillations was shown in Fig. 3.9(*b*). These intermittent bursting phenomena in a combustor under turbulent flow conditions was found to be of type II intermittency through recurrence plots (Nair and Sujith, 2013).

The system undergoes another bifurcation from self-excited oscillations to intermittency again as we further decrease the equivalence ratio by increasing the air flow rate, as shown in Fig. 3.9(*d*). As we further decrease the equivalence ratio, the amplitude levels of intermittent bursts of periodic oscillations drops down and finally, the flame has blown out of the combustion system. In the next section, as we have mentioned already, we provide a novel approach for understanding the complex nonlinear phenomena of transition to flame blowout in the framework of complex networks that could possibly lead to a paradigm shift in the field of blowout and combustion science.

3.9.2 Complex network representation of near blowout dynamics

We used the visibility algorithm, as discussed in Sec. 3.2, to map the combustion dynamics onto complex networks. The limit cycle oscillations of the pressure, as shown in Fig. 3.9(*c*), measured from the combustor operated in a turbulent environment are not perfectly periodic. To deal with the variability in the limit cycle amplitude, we used the visibility algorithm as specified in equation 3.2 to obtain complex networks. We used the threshold as, $\varepsilon = 0.24 * mean(p)$.

The time series $p(t)$ in equation 3.2 contains the data values that correspond to local peaks in the unsteady pressure data. The chaotic oscillations arising from the combustion dynamics gives rise to local peaks to have both positive and negative values. For example, the lowest value of the local peaks is -282.7 Pa and the highest value of the local peaks is 349.9 Pa for the time series data of the unsteady pressure acquired during combustion noise. The average value of the local peaks is 8.1 Pa and the threshold 'epsilon' ($\varepsilon = 0.24 * mean(p)$) is 1.95 Pa. The threshold ε is less than 1% of the highest value of the local peaks in the unsteady pressure data and hence, we consider that the inclusion of epsilon in the visibility condition has not filtered any useful information present in the time series.

Fig. 3.10 illustrates the time series, degree distribution and complex networks during the transition from combustion noise ($\varphi = 0.95$) to blowout of flame ($\varphi = 0.29$) via self-excited thermoacoustic oscillations ($\varphi = 0.5$).

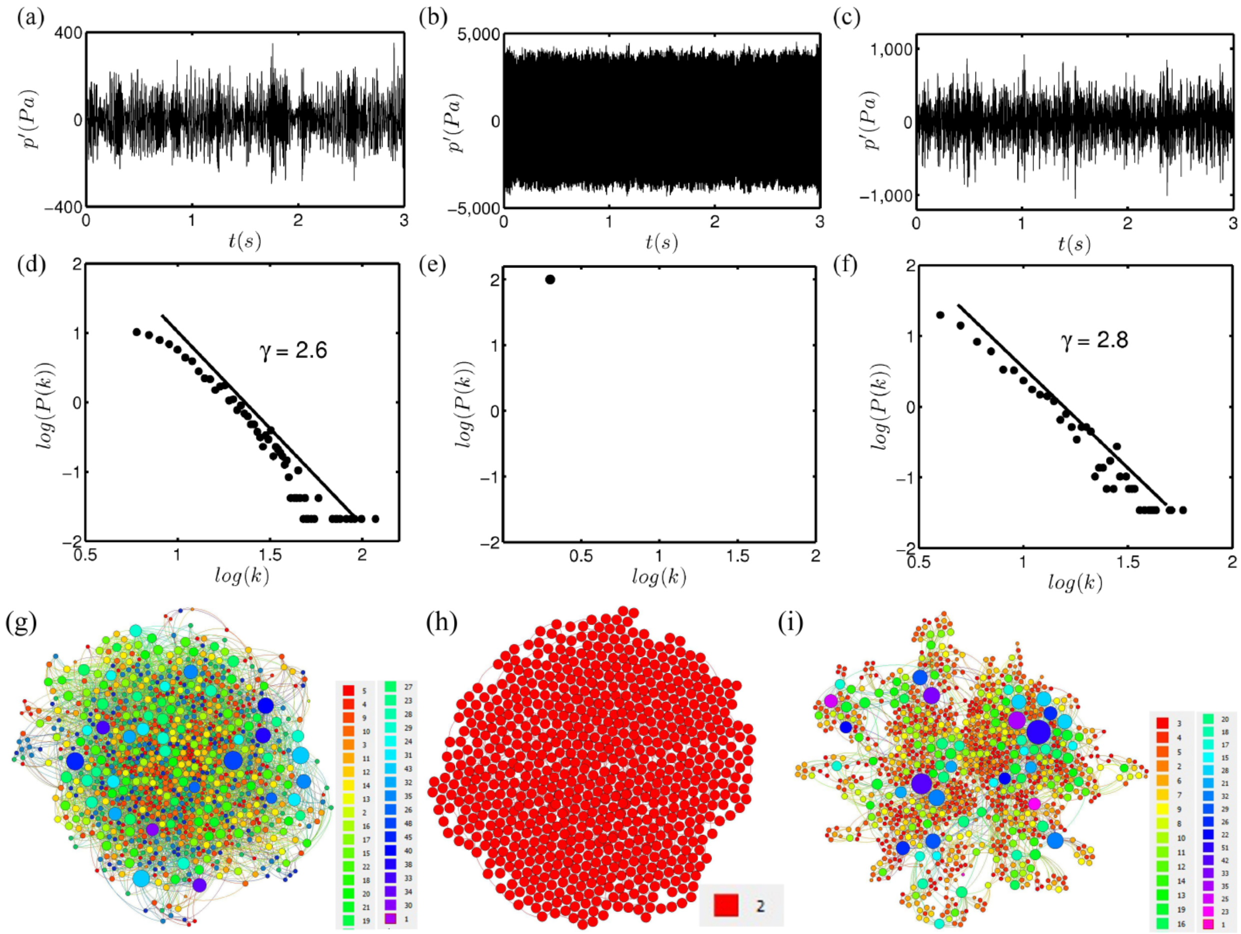

Figure 3.10: (from top to bottom) Temporal signal, degree distribution and complex network generated using the visibility algorithm, respectively for oscillating pressure correspond to *a*), *d*) and *g*) combustion noise, *b*), *e*) and *h*) thermoacoustic instability and *c*), *f*) and *i*) a dynamical state prior to blowout of flame.

The degree distribution of a complex network that corresponds to a dynamical state prior to flame blowout is shown in Fig. 3.10(*f*). It is clear that the degree distribution displays a power law behaviour.

$$P(k) \sim k^{-\gamma}$$

The exponent in the power law is estimated to be $\gamma = 2.8$ with an uncertainty of ± 0.1. The signature of power law behaviour means that the network corresponding to a dynamical state prior to flame blowout is scale-free. This is the first time that near blowout dynamics is represented as scale-free network.

Recently, Unni and Sujith (2015) showed that a dynamical state prior to blowout display multifractal characteristics. Fig. 3.10(*f*) shows that multifractal nature of near blowout dynamics convert into scale-free topological structure in the network. The power law behaviour in the degree distribution of the networks are related to the fractal nature of the original time series (Lacasa *et al.*, 2009; Zhang and Small, 2006). For non-stationary time series, a linear correlation is developed between the Hurst exponent and the power law exponent ($\gamma = 3.1 - 2H$) by Lacasa *et al.*, (2009). We obtain the Hurst exponent as $H = 0.15$ for time series data correspond to a dynamical state prior to blowout as we used the power law exponent in the relation ($\gamma = 3.1 - 2H$) that connects the power law exponent and the Hurst exponent (Lacasa *et al.*, 2009).

The obtained value of the Hurst exponent ($H = 0.15$) is less than 0.5 which shows that time signals correspond to near blowout dynamics is anti-persistent. If the signal has anti-persistent behaviour, a small value is likely to be followed a large value and a large value is likely to be followed by a small value. The value of the Hurst exponent obtained from the power law exponent is consistent with the Hurst exponent calculated using the multifractal detrended fluctuation analysis (Unni and Sujith, 2015).

The network corresponding to near blowout dynamics is shown in Fig. 3.10(*i*). The networks are plotted using the Gephi software (Bastian *et al.*, 2009). The advantage of analysing the blowout dynamics in a framework of complex networks is that different dynamical features in the time series can be mapped and investigated as distinct structures in the complex networks topology. In the network, circles represent nodes and are presented in different sizes and colours based on the degree of the corresponding nodes. Fig. 3.11(*i*) shows that network correspond to a dynamical state prior to flame blowout involves nodes possessing heterogeneous degrees. There is no single characteristic degree associated with this network. The absence of characteristic scale is the reason why it is called a scale-free network.

The scale-freeness of the network is related to the physical state and underlying mechanisms of the near blowout dynamics. The dynamics prior to blowout involves a large number of scales that arises from the aperiodic flame extinction and re-ignition events. The aperiodic fluctuations in the dynamic pressure due to such flame extinction and re-ignition events are reported by Nair and Lieuwen (2005) and Muruganandam et al. (2005). They reported that the bursts of oscillations in the time series data of dynamic pressure are associated with the flame re-ignition events.

According to the visibility condition, the nodes that are mapped from the data values of higher magnitudes are connected with a large number of nodes having lower data values. These most connected nodes in the network are most often called hubs. In contrast, the nodes that correspond to data points having intermediate and small data values in the time series are connected with a small number of other nodes in the network. The spatial-temporal changes resulting from the aperiodic flame extinction and re-ignition events are the reason for scale-free structure of the network that corresponds to near blowout dynamics.

3.9.3 Network topological changes at the onset of flame blowout

As we have already mentioned, the transition to blowout of flame from the combustion noise happened via self-excited thermoacoustic oscillations. Fig. 3.10 illustrates the dynamical changes in time series, degree distribution and complex network during the transition to blowout of flame.

As can be seen from Fig. 3.10(d), the degree distribution of the network mapped from the time series corresponding to the stable operation (i.e. combustion noise) has a power law behaviour. It implies that the network corresponding to combustion noise is a scale-free network. The exponent in the power law is measured to be $\gamma = 2.6$ with an uncertainty of $\pm$ 0.1. Consequently, the Hurst exponent is calculated to be $H = 0.25$ using the relation between the Hurst exponent and the power law exponent ($\gamma = 3.1 - 2H$). These results on Hurst exponent is consistent with the results reported by Unni and Sujith (2015).

In contrast to combustion noise, the degree distribution of the network corresponding to self-excited thermoacoustic oscillations is characterized by a single discrete point (see Fig. 3.10e). This implies that limit cycle oscillations during thermoacoustic instability convert into a regular network. Figures 3.10(g) and 3.10(h) show the network mapped from time series data during combustion noise and self-excited thermoacoustic oscillations respectively. The network corresponding to combustion noise possess nodes of various sizes and colours, indicating the absence of characteristic degree associated with the network. In contrast to combustion noise, all the nodes in the network correspond to self-excited thermoacoustic oscillations have the same degree of two and are coloured in red. The networks (Figures 3.10(g) and 3.10(h)) illustrates that the transition from combustion noise to self-excited thermoacoustic oscillations is reflected as the transition from scale-free to regular topological structure in the complex network.

However, as the system dynamics transition to the onset of flame blowout (dynamical states prior to blowout) from self-excited thermoacoustic oscillations, the transition happen from a single discrete point to power law behaviour in the degree distribution and regular to scale-free topological structure in the complex networks. These physical mechanism and topological changes in the complex network during the transition to the onset of flame blowout from the stable operation are reflected in a clearer manner in the statistical measures of the complex network which will be discussed in the following section.

3.9.4 Detecting the occurrence of blowout using network properties

The statistical measures of complex networks quantitatively capture the hidden dynamical features in the time series during the transition in combustion dynamics near blowout conditions. Simple structural measures such as clustering coefficient (C), characteristic path length (L), network diameter (D) and global efficiency (E) are evaluated for each equivalence ratio condition and are normalized with their maximum values C_0, L_0, D_0 and E_0 respectively. The variation of these statistical measures during the transition from stable operation to flame blowout as we decrease the equivalence ratio ($\varphi = 0.95$ to $\varphi = 0.29$) is shown in Fig. 3.11. The Roman numerals (I to IV) has been used in Fig. 3.11 to indicate the presence of different dynamical states in combustion dynamics as we decrease the equivalence ratio.

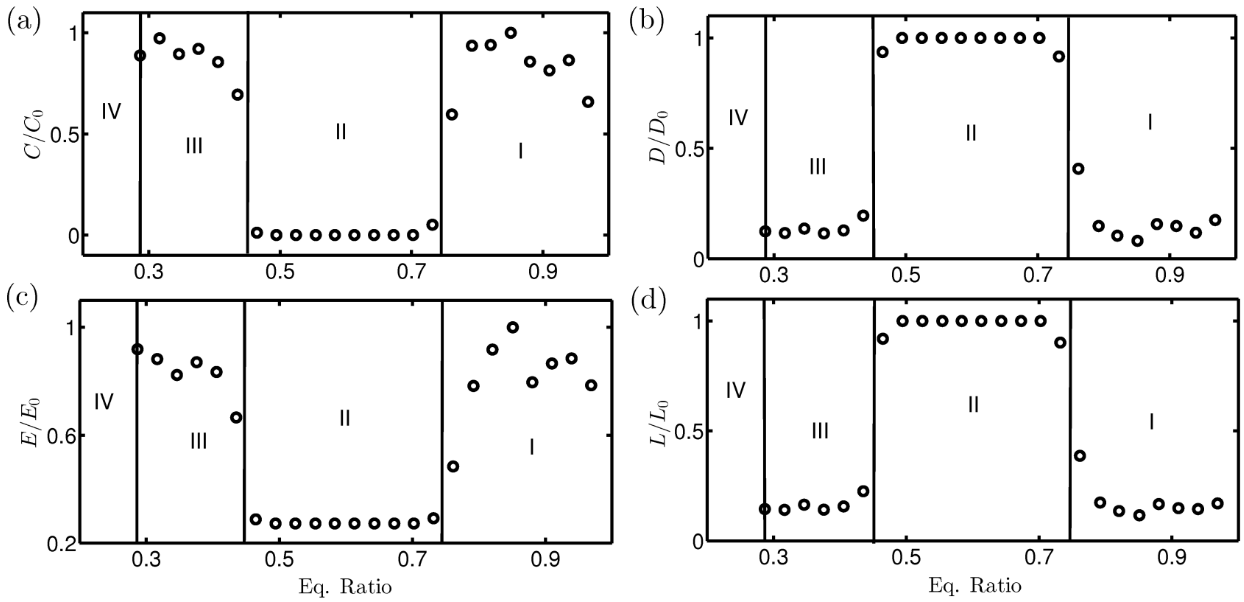

Figure 3.11: Variation of normalized values of *a*) clustering co-efficient, *b*) network diameter, *c*) global efficiency and *d*) characteristic path length of the networks during the transition to blowout of flame as we decrease the equivalence ratio. The Roman numerals (I - IV) are used to indicate the different oscillatory regions. Region I – stable operation, region II – thermoacoustic oscillations, region III – onset of flame blowout and region IV – the flame has blown out.

In Fig. 3.11(*a*), we show the variation of normalized clustering coefficient during the transition to the onset of blowout. It is clear that the clustering coefficient has the lowest value during self-excited thermoacoustic oscillations which is represented as region II in Fig. 3.11(*a*). In networks topology, the clustering coefficient quantifies the probability of neighbours of a node being neighbours or not. The clustering co-efficient measures the density of connections in the neighbourhood of a node. The lowest value of the clustering coefficient indicates that nodes in the network corresponding to self-excited thermoacoustic oscillations are more independent than that of the network corresponding to stable operation and dynamical states near blowout conditions.

This behaviour is related to the underlying physical state of the combustion dynamics. The self-sustained large coherent vortices dominate the flow during thermoacoustic oscillations, creating periodic oscillations in the flow and consequently, in the time series data of the unsteady pressure. In visibility graph, periodic time series convert into regular network with all the nodes being connected to only two of their neighbours. This reflect as neighbours of all the nodes being not connected and the average clustering coefficient attains a value very close to zero.

In contrast to self-excited thermoacoustic oscillations, the dynamical states during the onset of blowout, represented as region III in Fig. 3.11(*a*), are associated with the aperiodic fluctuations arising from the flame extinction and re-ignition events. These aperiodic fluctuations give rise to perturbations of various scales in the dynamics of the time series and results in more number of connections between the nodes in the networks that correspond to dynamical states during the onset of flame blowout. Finally, it can be understood that the change in system dynamics as the flame blows out of the combustion system is reflected as the rise in clustering coefficient of the complex networks.

Further, Figures 3.11(*b*) and 3.11(*d*) indicate the variation of network diameter and characteristic path length as the system dynamics transition to the onset of flame blowout. The network diameter and characteristic path length have their highest values during self-excited thermoacoustic oscillations (region II in Fig. 3.11). The path length implies the number of steps required to reach a node from any other node in the network. In other words, the path length refers to how fast a node can be reached from other nodes in the network. The network diameter is the highest value of the short path lengths of all the possible pairs in a network. The highest values of network diameter and characteristic path length implies that the network during self-excited thermoacoustic oscillations has lesser number of connections between the nodes than that of the networks corresponding to stable operation and dynamical states prior to blowout of flame.

As we have already mentioned, for the case of dynamical states prior to blowout, the flame extinction and re-ignition events contribute to fluctuations of multiple scales in the time series data of the unsteady pressure. Thus, according to the visibility condition, a large number of connections exists between the nodes in the networks that correspond to dynamical states near blowout conditions. The more number of connections reflect as lower values of the network diameter and the characteristic path length of the networks corresponding to dynamical states prior to blowout. In contrast, periodic oscillations from large scale coherent vortices during self-excited thermoacoustic oscillations translate to regular networks with highest values of network diameter and characteristic path length. The reason for the highest values of the network diameter and characteristic path length is that it takes a maximum possible number of steps to reach a node from any other node in the regular network mapped from 'limit cycle' using the visibility condition. These underlying physical mechanisms cause the values of the network diameter and the characteristic path length to drop during the onset of flame blowout.

In Fig. 3.11(*c*), we show the estimated values of global efficiency for each network during the transition to blowout of flame from the stable operation of the combustion system. From a networks perspective, global efficiency means the efficiency of how fast a node can be reached from any other node in the network. Global efficiency is defined as the average of the inverse of the short path lengths and the purpose of defining global efficiency is to avoid infinity in the calculations of the topological measures of the networks involving disconnected nodes. One can observe that the lowest value in global efficiency occurs during self-excited thermoacoustic oscillations (region II). This reflects that the transfer of information in the network corresponding to self-excited thermoacoustic oscillations happens less efficiently compared to that of the networks corresponding to the stable operation and the dynamical states near flame blowout.

In contrast to self-excited thermoacoustic oscillations, networks resulting from the dynamical states close to flame blowout (region III) have higher values of global efficiency. The underlying physics near blowout conditions is the reason for such higher values of global efficiency. The flame extinction and re-ignition events close to flame blowout condition creates fluctuations of various scales in the system dynamics. Consequently, the networks corresponding to the dynamical states close to flame blowout attain more connectivity between the nodes. As a result of such increase in connectivity between the nodes in the networks, the global efficiency rises significantly during the transition to flame blowout.

We have investigated the transition to blowout in the turbulent lifted jet flame combustor. In the case of lower fuel flow rate, the system does not exhibit instability and from stable operation of the combustor it directly transitions to blowout as the airflow rate is increased.

The experiments were conducted at low fuel flow rate ($\dot{m}_f = 2.2\,SLPM$) and as the co-flowing air flow rate was increased from a value of $45.5\,SLPM$ to $66.5\,SLPM$ in steps of $1\,SLPM$, the system dynamics transition from stable operation (i.e. combustion noise) to flame blowout without thermoacoustic instability.

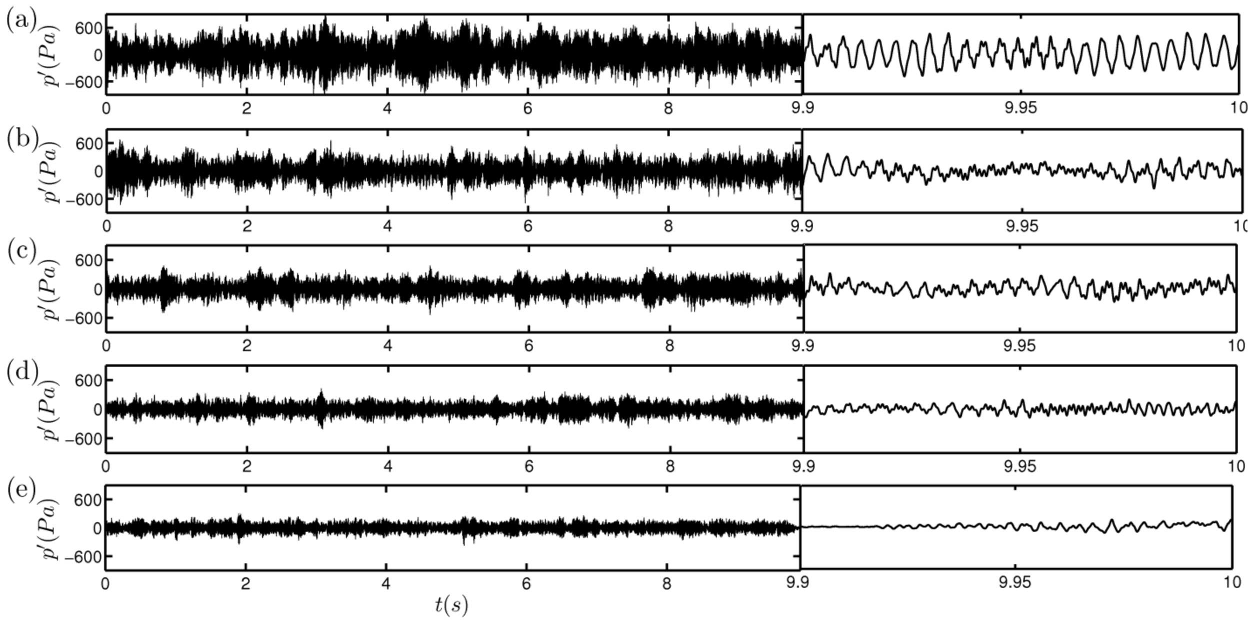

Figure 3.12: Unsteady pressure time series acquired when the volumetric flow rate of air is (a) $\dot{Q}_a = 45.5\,SLPM$, (b) $\dot{Q}_a = 51.5\,SLPM$, (c) $\dot{Q}_a = 56.5\,SLPM$, (d) $\dot{Q}_a = 61.5\,SLPM$ and (e) $\dot{Q}_a = 66.5\,SLPM$.

As the airflow rate is increased, the amplitude of pressure fluctuations decreases. Further, no periodic oscillations are observed. In other words, the system does not exhibit thermoacoustic instability. The complex networks corresponding to the time series during the transition to blowout are shown in Fig. 3.13.

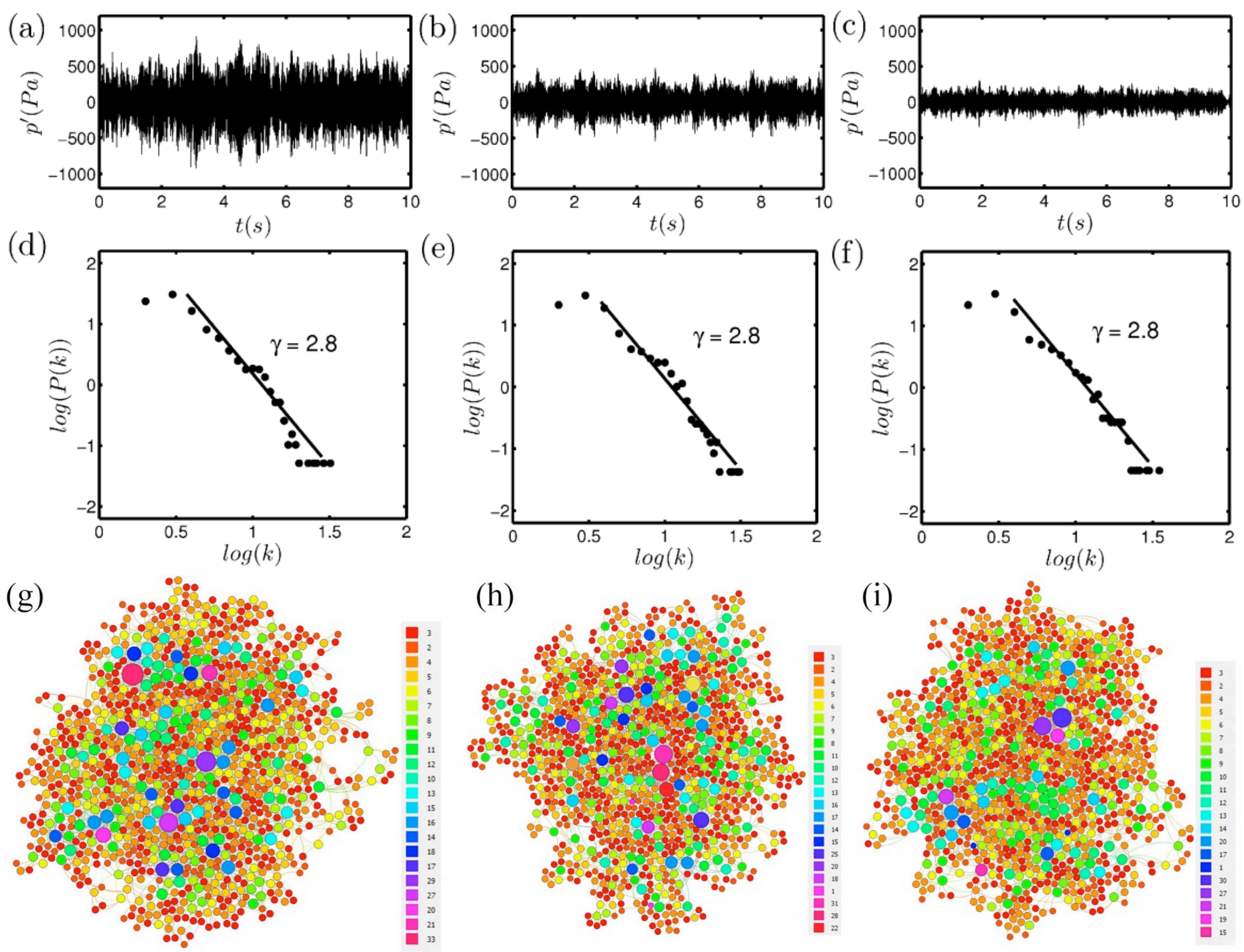

Figure 3.13: (from top to bottom) Temporal signal, degree distribution and complex network generated using the visibility algorithm, respectively for oscillating pressure when the volumetric flow rate of air is a), d) and g) $\dot{Q}_a = 45.5\ SLPM$, b), e) and h) $\dot{Q}_a = 56.5\ SLPM$ and c), f) and i) $\dot{Q}_a = 66.5\ SLPM$.

As can be seen from Fig. 3.13, the power law exponent in the degree distribution corresponding to the stable operation (Fig. 3.13*d*) and a dynamical state near blowout condition (Fig. 3.13*f*) remain the same. The value of power law exponent is not sufficient to differentiate the near and far from blowout condition.

For each network, the corresponding network properties such as clustering coefficient (C), network diameter (D), global efficiency (E) and characteristic path length (L) are evaluated. Figure 3 depicts the variation of normalized network properties with the parameter (airflow rate).

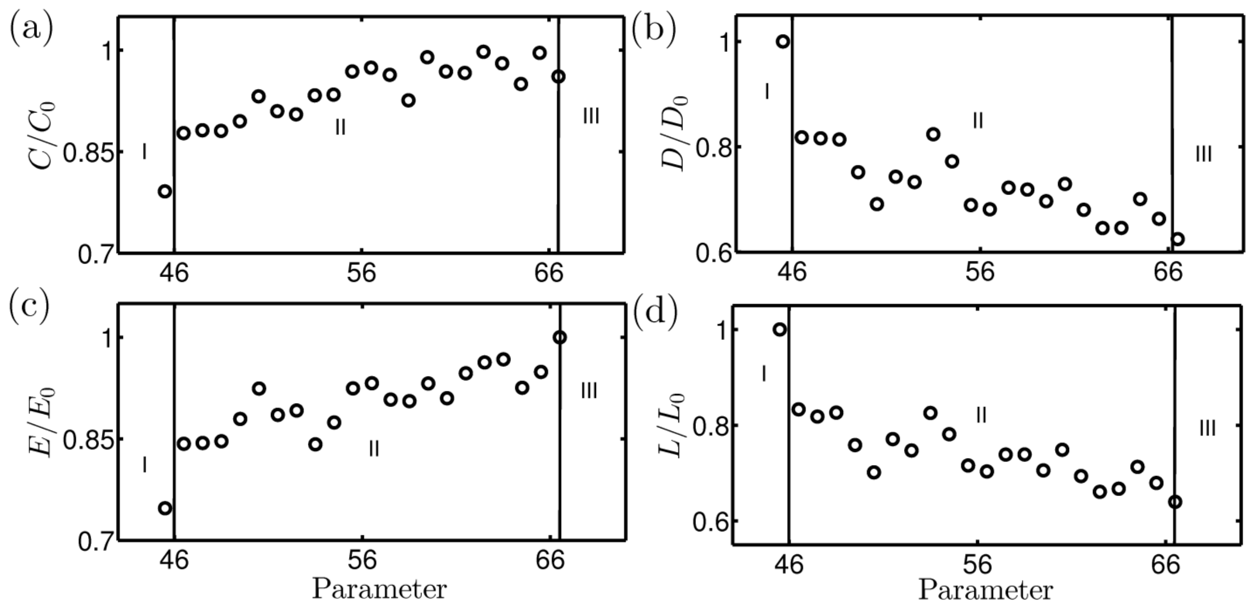

Figure 3.14: Variation of normalized values of a) clustering co-efficient, b) network diameter, c) global efficiency and d) characteristic path length of the networks during the transition to blowout of flame as we increase the air flow rate.

Note that the clustering coefficient (*C*) increases near to blowout. Also the diameter of the network (*D*) reduces as we transition from stable combustion to blowout. The normalized characteristic path length (*L*) reduces close to blowout and the global efficiency (*E*) increases.

We have used the variation of these network measures to identify the transition from stable operation of the combustor to near blowout condition that happen without thermoacoustic instability (Murugesan *et al*., 2014).

In summary, we have shown that the rise in the values of clustering coefficient and global efficiency and the drop in the values of the network diameter and the characteristic path length occur during the onset of flame blowout. The changes in these structural measures arises from the underlying physical mechanism in combustion dynamics during the onset of flame blowout. It is interesting to note that the statistical measures from the complex networks approach helps to identify the onset of flame blowout well before the flame actually blows out of the combustion system.

Although we have obtained the networks using visibility condition, the networks constructed using other different algorithms also show the same qualitative behaviour for the time series data obtained from the turbulent systems35. Further, the novel idea of obtaining early warning signals for blowout using network properties is not limited to the four network properties that we presented in the current work. Any other statistical measures from complex networks approach, quantifying the underlying physics in combustion dynamics can also be treated as precursors to flame blowout.

3. 10 Concluding remarks

We investigated the dynamical behaviours of a thermoacoustic system during the transition to flame blowout using complex networks. We showed that the dynamical states near flame blowout conditions exhibit scale-free topological structure. The power law behaviour in the degree distribution is related to the fractal nature of underlying system dynamics close to flame blowout. The physical reason for this scale-free nature of the combustion dynamics is the presence of multiple spatial/temporal scales associated with the turbulent reacting flows. The approach of complex networks enabled us to visualize and understand the underlying combustion dynamics close to flame blowout.

We also represented the dynamical states during the transition to flame blowout from stable operation via self-excited thermoacoustic oscillations as complex networks. We showed that the transition to blowout from self-excited thermoacoustic oscillations can be represented as the transition from regular to scale-free structure in networks topology.

We calculated the topological measures such as clustering coefficient, network diameter, characteristic path length and global efficiency for each equivalence ratio conditions, during the transition to flame blowout. These structural quantities change well ahead of the onset of an impending blowout in combustion systems. The early indication from a number of network measures is the reason for treating network properties as the robust blowout detection precursors.

CHAPTER 4

PHYSICAL REASONS FOR TRANSITIONS IN THERMOACOUSTIC SYSTEMS

In the previous chapter, the dynamical features or pattern formation during the transition to thermoacoustic instability and blowout in a combustion system operated under turbulent flow conditions are discussed. It is clear that the transition to thermoacoustic instability and blowout occur via intermittent dynamics. In the present chapter, the flow physics during intermittency that presages thermoacoustic instability and blowout are investigated in order to unravel the physical reasons that cause such transitions to thermoacoustic instability and blowout in thermoacoustic systems.

The experiments are performed in a turbulent lifted jet flame combustor. The complete optical access over the entire length of the combustor with transparent quartz duct was the priority in deciding to choose such a combustor. We vary the relative location of the burner inside a confinement as a bifurcation parameter. The transition occur from combustion noise to thermoacoustic instability and blowout via intermittency which is similar to that of the transitions observed in large-scale gas turbine model combustors (Nair and Sujith, 2014; Nair *et al*., 2014; Gotoda *et al*., 2014).

We show that the alternating positively and negatively correlated interaction of flow, flame dynamics and combustion chamber acoustics is the physical reason for intermittency that presages thermoacoustic instability. In contrast, intermittent dynamics that presages blowout occurs due to the interplay between flame blowout precursor events and the driving of high-amplitude oscillations as the flame propagates towards the fuel tube.

Alternatively, from a dynamical systems perspective, the type of intermittency before the onset of both thermoacoustic instability and blowout are identified as type II using return maps and recurrence plots.

4.1 Background

The intermittency route to thermoacoustic instability in turbulent combustors is first reported by Nair *et al*., (2014). The bursts of periodic oscillations in the intermittent regime become more frequent as the combustion systems approach the condition of thermoacoustic instability. Nair *et al*., (2014) used the recurrence quantities to quantify the dynamical changes during the intermittent oscillations. In a spray combustion system, Pawar *et al*. (2015) reported intermittency route to thermoacoustic instability.

Intermittency is seen prior to the onset of blowout as well (Kabiraj and Sujith, 2012; Unni and Sujith, 2015; Thampi and Sujith, 2015; Gotoda *et al*., 2014). From a dynamical systems perspective, intermittency prior to combustion instability (Nair and Sujith, 2013) and blowout (Nair, 2014) are shown to arise from the formation of homoclinic orbits in the reconstructed phase space. Homoclinic orbit is a phase space trajectory in which an unstable manifold of a fixed point of the system merges with its own stable manifold (Strogatz, 2014). This results in switching of the system dynamics back and forth between the stable and unstable orbits in the phase space. In time series, such dynamics manifest as the alternative appearance of bursts of high-amplitude periodic oscillations and low-amplitude chaotic fluctuations in the unsteady pressure. Further, from the high-speed flame images, Nair and Sujith (2015) explained that the aperiodic detachments of the flame from the flame-holding device correspond to the intermittent fluctuations in the unsteady pressure prior to blowout.

However, the role of flow-flame-acoustic interaction during the occurrence of intermittency is still not clear, and needs further investigation. From a reacting flow perspective, thermoacoustic instability and blowout are two different phenomena. Intermittency presages both these phenomena, and we need to investigate the flow physics during its occurrence. On the other hand, from a dynamical systems perspective, we need to investigate if there are any commonalities between the intermittency that presages thermoacoustic instability and the intermittency that presages blowout.

In order to answer these intriguing questions, we investigate the interactions between the flow, flame and the acoustic field during the intermittency that presages the onset of thermoacoustic instability and the intermittency that presages blowout. The simultaneous measurement of acoustic pressure, CH^* chemiluminescence images and Mie scattering images are acquired to study the coupling of duct acoustics, flame and flow during the occurrence of intermittency, before both thermoacoustic instability and blowout. We present the behavior of the flow, flame and duct acoustics during high-amplitude periodic oscillations, low-amplitude chaotic fluctuations and in the regime where the system transitions between high-amplitude and low-amplitude pressure fluctuations during the intermittent dynamics prior to both thermoacoustic instability and blowout.

4.2 Description of the experimental setup

The experiments are conducted on a turbulent lifted jet flame combustor to understand the physical reason for transition to thermoacoustic instability and blowout. The transparent quartz duct provides complete optical access over the entire length of the combustor. Having a simple configuration with ease of visualization was the priority in deciding to choose such a burner. Further, the experiments can be performed for a longer duration without any necessity for cooling. The transition undergone by the thermoacoustic oscillations in this turbulent lifted jet flame combustor is very similar to the transitions observed in the large-scale gas turbine model combustors (Nair and Sujith, 2014; Nair *et al.*, 2014; Gotoda *et al.*, 2014).

A schematic of the experimental setup and instrumentation is shown in Fig. 4.1. A turbulent jet flame lifted from a burner (referred to as A in Fig. 4.1) is established inside a quartz confinement (referred to as B in Fig. 4.1). The coupling of the jet flow, turbulent flame and acoustic field in the duct gives rise to nonlinear thermoacoustic oscillations.

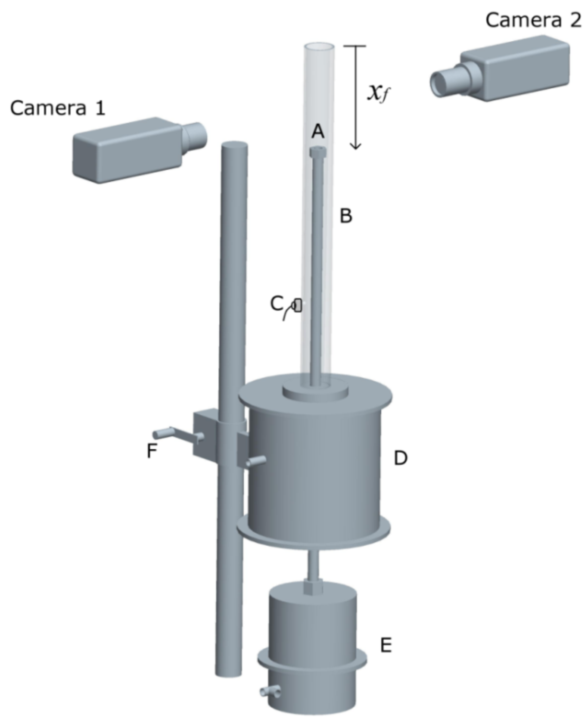

Figure 4.1 : Schematic of the experimental configuration. The turbulent jet flame lifted from the burner (A) is established inside a confinement (B). The fuel (LPG) and air are supplied to the burner through a settling chamber (E). The co-flowing air is supplied to the quartz duct (B) through another settling chamber (D). The position of the burner inside the confinement is varied with a traverse mechanism (F). The acoustic pressure, CH^* chemiluminescence and Mie scattering images are simultaneously acquired to understand the interaction of acoustics, flame and flow-field in the dynamics of intermittency. The acoustic pressure is measured 25 *cm* from the bottom end of the quartz tube using a pressure transducer (C) (PCB Peizotronics, Model no. PCB 103B02). The CH* chemiluminescence is recorded using camera 1 (Phantom v12.1) with a band pass filter having a central wavelength of 430 *nm* and a bandwidth of 5 *nm*. For Mie scattering experiments, the flow through the burner is seeded with olive oil particles and the plane of interest is illuminated with a monochromatic light sheet of wavelength 527 *nm* (green) from a Nd: YLF laser. The scattered light depicting the flow-field of unburnt reactants is recorded in camera 2 (Photron FASTCAM) with a band pass filter having a central wavelength of 527 *nm* and a bandwidth of 10 *nm*.

The setup consists mainly of a burner confined within a quartz duct having a length of 1 *m*, an inner diameter of 45 *mm* and a thickness of 2.5 *mm*. The quartz duct acts as an acoustic resonator. The burner is made of a copper tube of 1.3 *m* long with an inner diameter of 12.5 *mm* and a thickness of 1.5 *mm*. Liquefied petroleum gas (60% butane & 40% propane by volume) is used as the fuel. Fuel is partially premixed with air in a plenum chamber (referred to as E in Fig. 4.1) before being supplied into the burner. The partial premixing of fuel with air is performed in order to establish a shorter flame. Otherwise, the flame becomes very long for the flow rates provided in the present work. Further, a hexagonal shaped nut having a thickness of 5.5 *mm* and a height of 4 *mm* is mounted at the tip of the burner. This hexagonal nut acts as a bluff-body and creates a low-velocity regime for the stabilization of the flame. The co-flowing air is provided through another settling chamber. Air is supplied from a high pressure chamber through a moisture separator. The position of the burner within the quartz confinement can be changed mechanically with the help of a rack and pinion traverse mechanism. The relative location of the burner can be read from a ruler attached on the traverse, with a least count of 1 *mm*.

4.3 Simultaneous measurement of unsteady pressure, chemiluminescence images and Mie scattering images

In the study of intermittent dynamics in the turbulent lifted jet flame combustor, the volumetric flow rates of the fuel and air are maintained constant. The flow rates are measured using mass flow controllers (Alicat Scientific, MCR Series) in terms of standard litres per minute (SLPM is standardized for air at a temperature of 25 °C & pressure of 14.696 psi with an uncertainty of ± 0.8% of reading + 2% of full scale). The Reynolds number of the fuel/air mixture (Re = 7060 ± 56) and the co-flowing air (Re = 1350 ± 11) are maintained constant. The pipe flow inside the burner can be considered as a fully developed turbulent flow because Re = 7060 ± 56 is greater than 2000 (Ben-Dov and Cohen, 2007). Further, the flame is established at a location away from the exit of the flow where the spreading of flow introduces increased levels of turbulence (Schlichting and Gersten, 2000). The procedure to calculate the Reynolds number of the gas mixture can be found in Nair and Sujith (2014). The equivalence ratio is also maintained constant (φ = 0.87 ± 0.011) throughout the experiments.

For all the experiments, the ambient temperature was measured to be (27 ± 1°C) using a dry bulb thermometer and the relative humidity was measured to be (60 ± 2 %) using a hygrometer.

In order to ensure that all the experiments are performed under identical acoustic losses in the system, the decay rates of acoustic pressure was measured multiple times before starting the combustion experiments. The combustor under cold conditions was forced at a fundamental acoustic frequency of 140 *Hz* with a loudspeaker (Ahuja AU60) that is mounted on the fuel plenum chamber, and the amplitude decay rate is measured when the forcing was switched off. The decay rate was measured to be -13 s^{-1} with ± 4% variation. The detailed procedure for calculating the decay rate is provided by Mariappan (2011).

We start the experiments by igniting the flame manually using a butane torch. In the present investigation, the relative location of the burner within the quartz confinement is chosen as the control parameter. The change in relative location of the burner inside the quartz confinement results in a change in the local acoustic admittance at the flame. The position of the burner is varied systematically from 30 *cm* to 77 *cm* in steps of 1 cm from the top end of the quartz tube. The state of the thermoacoustic system at every burner location is captured by recording the acoustic pressure, CH^* chemiluminescence and Mie scattering images. The acoustic pressure is measured using a pressure transducer (PCB piezotronics, Model Number 103B02, sensitivity 217.5 *mV*/*kPa*, 0.14 *Pa* uncertainty). To avoid the exposure of hot gases, the pressure sensor is mounted at a location 25 cm from the bottom end of the quartz tube using a Teflon pressure port at the quartz tube wall. The measured pressure signal is digitally recorded in a computer using a 16 bit analog to digital conversion card (NI-6143) through a signal conditioner.

The flame dynamics is captured by recording the CH^* chemiluminescence intensity using a high speed camera (Phantom v12.1) with a band pass filter of central wavelength of 430 *nm* and a bandwidth of 5 *nm* at a frame rate of 2 *kHz* for 10 seconds. The global heat release rate from the flame is calculated by integrating the CH^* chemiluminescence intensities at each frame.

In order to study the flow-field dynamics, planar Mie scattering technique is employed (Roehle *et al*., 2000). Olive oil droplets generated using Laskin nozzles of diameter less than 1 μm (Kumara Gurubaran, 2005) are seeded to the air flowing through the inner tube. The plane of interest is illuminated using a monochromatic light sheet of wavelength 527 *nm* (green) from a Nd: YLF laser. The light scattered by the oil particles are recorded using another high speed camera (Photron FASTCAM) with a band pass filter having a central wavelength of 527 *nm* and a bandwidth of 10 *nm* at a frame rate of 2 *kHz* for 10 seconds.

Both cameras, Phantom v12.1 (camera 1) and Photron FASTCAM (camera 2), are focused at the same plane of interest and synchronized with the data acquisition system for measuring the acoustic pressure. The acoustic pressure, Mie scattering images and CH^* chemiluminescence images are acquired simultaneously. Measurements are performed at each burner location after waiting for at least 2 minutes for the system to settle in that state. Changes in system dynamics happen almost instantly for the change in control parameter and the settling time of 2 minutes is adequate to capture the asymptotic state of the system.

4.4 Transitions in thermoacoustic systems

The change in system dynamics is presented for varying values of the relative location of the inner tube inside the quartz duct as the control parameter. The nonlinear interaction of the flow-flame-duct acoustics results in different dynamical states. The plot is divided into different regimes to show the different dynamical states observed in the system dynamics (shown in Fig. 4.2).

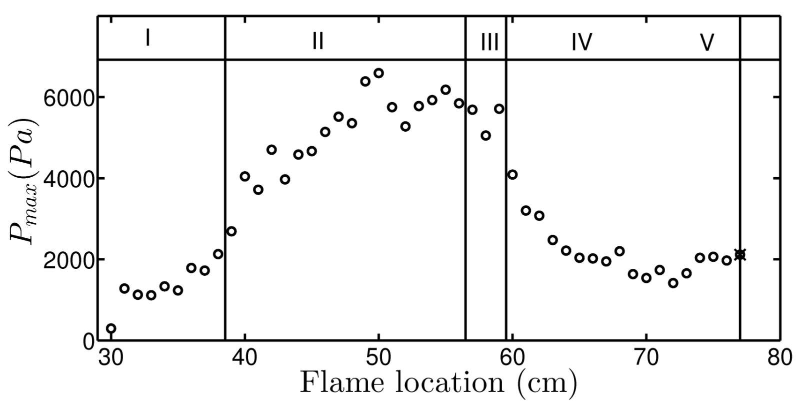

Figure 4.2: The variation of the maximum value of the unsteady pressure ($P_{\max}$) with respect to change in inner tube location. The bifurcation diagram is divided into five regimes; (I) combustion noise, (II) intermittency, (III) combustion instability, (IV) intermittency and the condition of blowout is marked as ×. In region V, the flame has blown out of the combustor.

In regime I (x_f = 30 *cm* to 39 *cm*), the system exhibits low-amplitude pressure fluctuations. The acoustic pressure (x_f = 32 *cm*) acquired in regime I is shown in Fig. 4.3(*a*). The fluctuations are seemingly irregular. These irregular fluctuations during the stable operation of the combustor are traditionally referred to as combustion noise (Strahle, 1978). On increasing the distance of the inner tube from the top end of the duct, the thermoacoustic system exhibits a transition from combustion noise (region I) to combustion instability (region III).

Traditionally, the stable state of combustion operation (combustion noise) is treated as a stable fixed point and combustion instability as an unstable limit cycle oscillations (Lieuwen, 2002). The transition to combustion instability from combustion noise has been traditionally considered as a sudden switching from stable to unstable state (Lieuwen, 2002). However, in a turbulent environment, the transition to combustion instability happens via intermittency (region II). In our experiments, for change in the burner location further past the condition of combustion instability, intermittency is observed again (regime IV) and finally the flame blows out at x_f = 77 *cm*.

4.5 Physical mechanisms that cause intermittency prior to thermoacoustic instability

The onset of intermittency that presages thermoacoustic instability occurs with the seemingly random appearance of bursts of high-amplitude periodic oscillations amidst regions of low-amplitude aperiodic pressure fluctuations as the burner is located at x_f = 40 *cm* (see Fig. 4.3*b*).

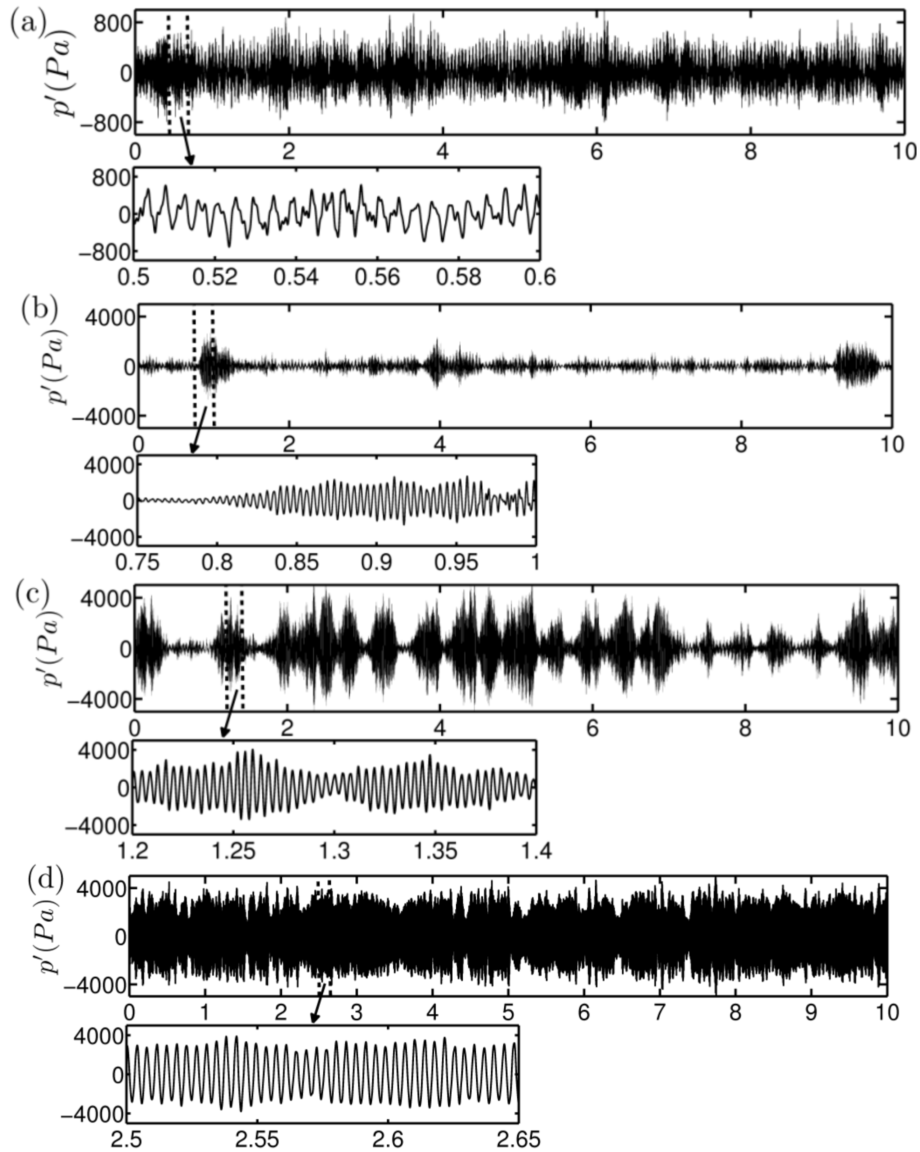

Figure 4.3: Time series data of unsteady pressure as the inner tube is at *a*) 32 *cm*, *b*) 40 *cm*, *c*) 47 *cm* and *d*) 57 *cm* from the top end of the quartz tube respectively. In the parameter range of 40 *cm* to 56 *cm*, the acoustic pressure oscillations are characterized by intermittent appearance of bursts of periodic oscillations amidst regions of low-amplitude aperiodic fluctuations. The occurrence of bursts become more frequent for further change in the burner location and finally the limit cycle oscillations are observed at $x_f = 57$ *cm*.

The appearance of intermittent periodic oscillations become more frequent as we further change the burner location (see Fig. 4.3*c*). Also, the amplitude of these intermittent bursts of periodic oscillations increases with change in burner location. Following these intermittent states, limit cycle oscillations are observed at x_f = 57 *cm* (shown in Fig. 4.3*d*). The intermittent state is also associated with the flame travelling repeatedly towards and away from the inner tube. This is discussed in Sections 4.5 and 4.7.

An inner tube location of 48 *cm* from the top end of the quartz tube is chosen to investigate the flow-flame-acoustics dynamics during the intermittency that presages the onset of thermoacoustic instability. The time series data of the acoustic pressure and the normalized CH^* chemiluminescence intensity during this intermittent state are shown in Fig. 4.4.

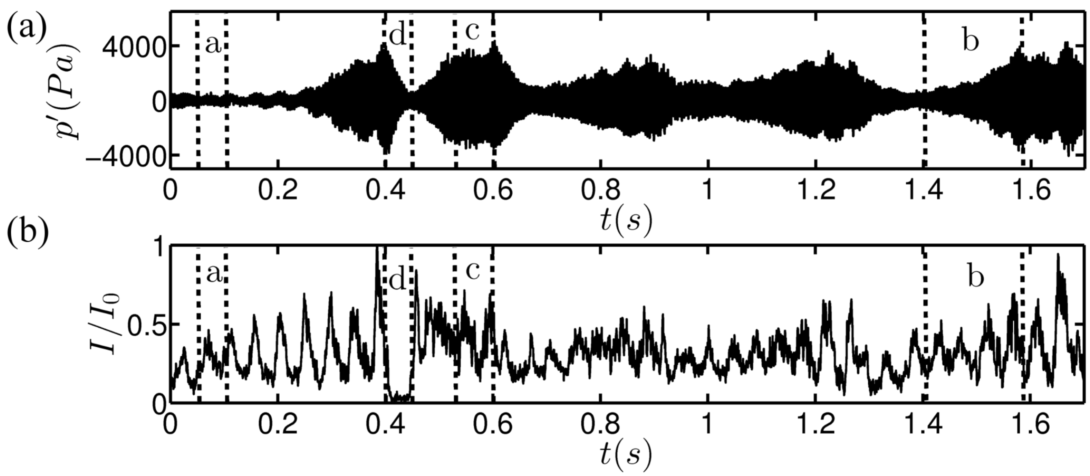

Figure 4.4: Time series data of *a*) the acoustic pressure and *b*) the normalized CH^* chemiluminescence intensity acquired during the occurrence of intermittency as the inner tube is located at 48 *cm* from the top end of the quartz tube. The time series is divided into four regions; (a) low-amplitude regime, (b) transition from low-amplitude to high-amplitude regime, (c) high-amplitude regime and (d) transition from high-amplitude to low-amplitude regime.

We decompose the time series data of intermittency into four regimes; *a*) low-amplitude regime, *b*) transition from low-amplitude to high-amplitude regime, *c*) high-amplitude regime and *d*) transition from high-amplitude to low-amplitude regime. The flame and flow images are mapped in a single image for illustration. The Mie scattering images are colored in green and the CH^* chemiluminescence images are colored in blue. The presented images of the flame and the flow are instantaneous. However, the dynamics of the flame and the flow was qualitatively the same every time during the occurrence of intermittency.

4.5.1 Low-amplitude regime

The time series of acoustic pressure and chemiluminescence intensity during the low-amplitude regime in intermittency (shown in Fig. 4.4) are zoomed in for a smaller time interval for illustration in Fig. 4.5(*I*).

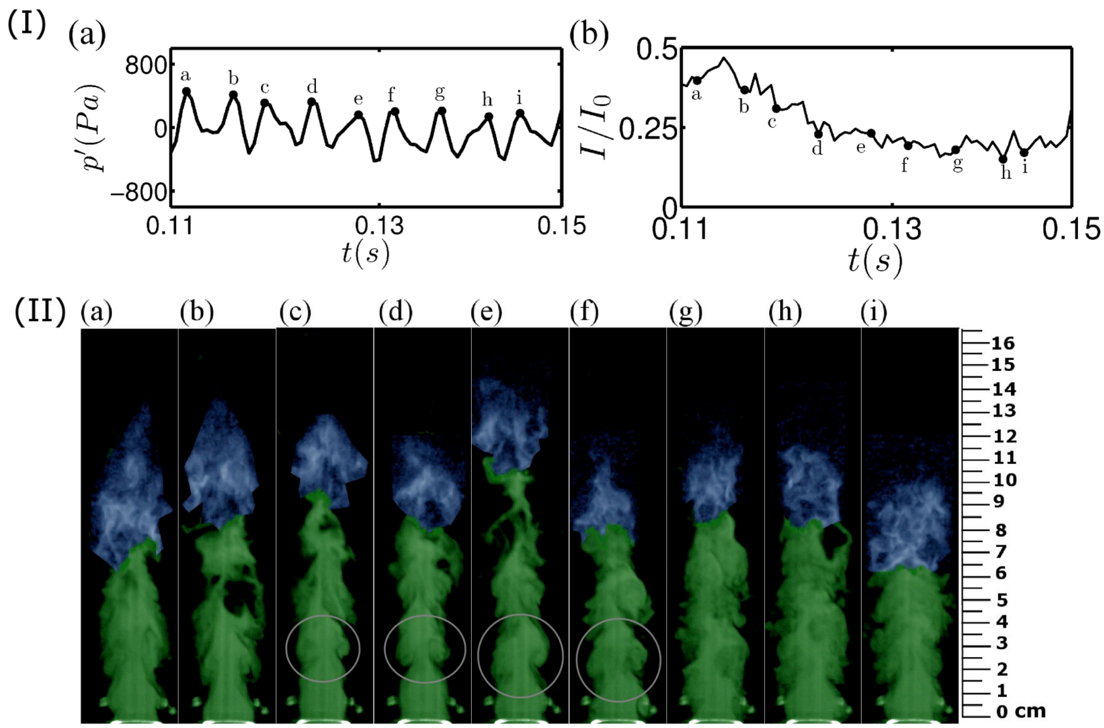

Figure 4.5: *I*) Low-amplitude fluctuations during intermittency are aperiodic. *a*) Time series of acoustic pressure that correspond to Fig. 4.4(*a*) and *b*) time series data of normalized CH^* chemiluminescence intensity that correspond to Fig. 4.4(*b*) are zoomed for a smaller time interval. *II*) Instantaneous Mie scattering (green) and CH^* chemiluminescence (blue) images correspond to the points marked in Fig. 4.5(*I*). The circles in Fig. 4.5(II), mark the small vortices and elongation at their braids. In low-amplitude regime during intermittency, incoherent fluctuations in the flow lead to unsteady fluctuations in the flame, which in turn produce aperiodic fluctuations in the acoustic pressure. As can be seen, peaks (marked as points *a* to *j* in Fig. 4.5*Ia*) in the acoustic pressure are associated with local minimum values (marked as points *a* to *j* in Fig. 4.5*Ib*) in the heat release rate fluctuations. This negative correlation of pressure and heat release rate may be the reason for the thermoacoustic system to be in a low-amplitude state.

The low-amplitude regime is characterized by aperiodic fluctuations in the acoustic pressure. The sequence of instantaneous images of the flame (CH^* chemiluminescence) and the flow-field (Mie scattering images of unburnt jet from the burner) corresponding to the points marked in Fig. 4.5(*I*) are shown in Fig. 4.5(*II*).

The shear layer rolls up near the exit of the burner to form small vortical structures in the flow. These small vortices do not grow or merge to become self-sustained, organized, large, coherent vortices. Instead, these small eddies undergo elongation at their braids as they travel downstream of the flow and breakdown into fine scale turbulence. The circles in Fig. 4.5(*II*) mark the elongation of small vortices at their braids. The convection velocity of these vortices is approximately half of the exit velocity of the reactants from the inner copper tube.

The flame base is directly influenced by the oscillations in the shear layer. Notice that the shear layer changes the base of the flame instantaneously, influencing the overall flame surface area (see that the base of the flame changes due to the shear layer in images from *a* to *i* of Fig. 4.5*II*). Further, the flame waist undergoes aperiodic oscillations. As an example, the flame waist is the maximum in the image (*b*) in Fig. 4.5(*II*) and changes to the minimum at image (*f*) in Fig. 4.5(*II*). In addition, the flame length exhibits aperiodic oscillations (see flame images (blue) from *a* to *i* in Fig. 4.5*II*).

The lift-off distance of the flame fluctuates approximately around a location of 8 *cm* from the exit of the jet. This fluctuation of the jet flame base around the lift-off distance produces low frequency modulations of around 24 *Hz* in the heat release rate and hence in the acoustic pressure as well.

Strouhal number (St) is calculated based on this frequency from the expression $St = fL/U$, where L (L = 5.5 *mm*) is the thickness of the hexagonal nut and U is the velocity of the co-flowing air (U = 0.63 ms^{-1}). Strouhal number (St) is calculated to be approximately 0.21, which belongs to the Benard/Von Karman (BVK) hydrodynamic instability for the Reynolds number range of 1000 to 200,000. The co-flowing air approaches the hexagonal nut and the flow undergoes the BVK instability with a characteristic frequency of 24 *Hz*.

The unsteady flame surface area as can be seen from the CH^* chemiluminescence intensity acts as a major source of low-amplitude aperiodic pressure fluctuations during intermittency. Such unsteady heat release rate fluctuations in the flame are reported as the source of combustion noise as well (Bragg, 1963; Strahle, 1978).

These unsteady pressure fluctuations, in turn, disturb the flow-field. This interlinked nonlinear interaction of flow, flame and duct acoustics in the low-amplitude regime during intermittency is manifested as incoherent fluctuations in the flow-field and aperiodic fluctuations in the acoustic pressure. Further, as can be seen in Fig. 4.5(*I*), the peaks in the acoustic pressure (marked as points from *a* to *j* in Fig. 4.5*Ia*) are associated with the local minimum values (marked as points from *a* to *j* in Fig. 4.5*Ib*) in the heat release rate fluctuations. The acoustic energy does not grow as a consequence of this negative correlation (out of phase) between the heat release rate and the unsteady pressure fluctuations and the dynamics of the system tends to be in a low-amplitude aperiodic state.

4.5.2 Transition from low to high-amplitude regime

The transition from low-amplitude aperiodic fluctuations to high-amplitude pressure oscillations begins with the organization of the flow into coherent vortex structures in the shear layer (see images *c* and *d* in Fig. 4.6*II*). The coherent structures developing for some of the acoustic cycles during period when the acoustic pressure amplitude is growing are occasionally interrupted by incoherent flow fluctuations (see images *e* and *f* in Fig. 4.6*II*).The organization of the vortex structures, once again continues to happen (see images *g* and *h* in Fig. 4.6*II*).

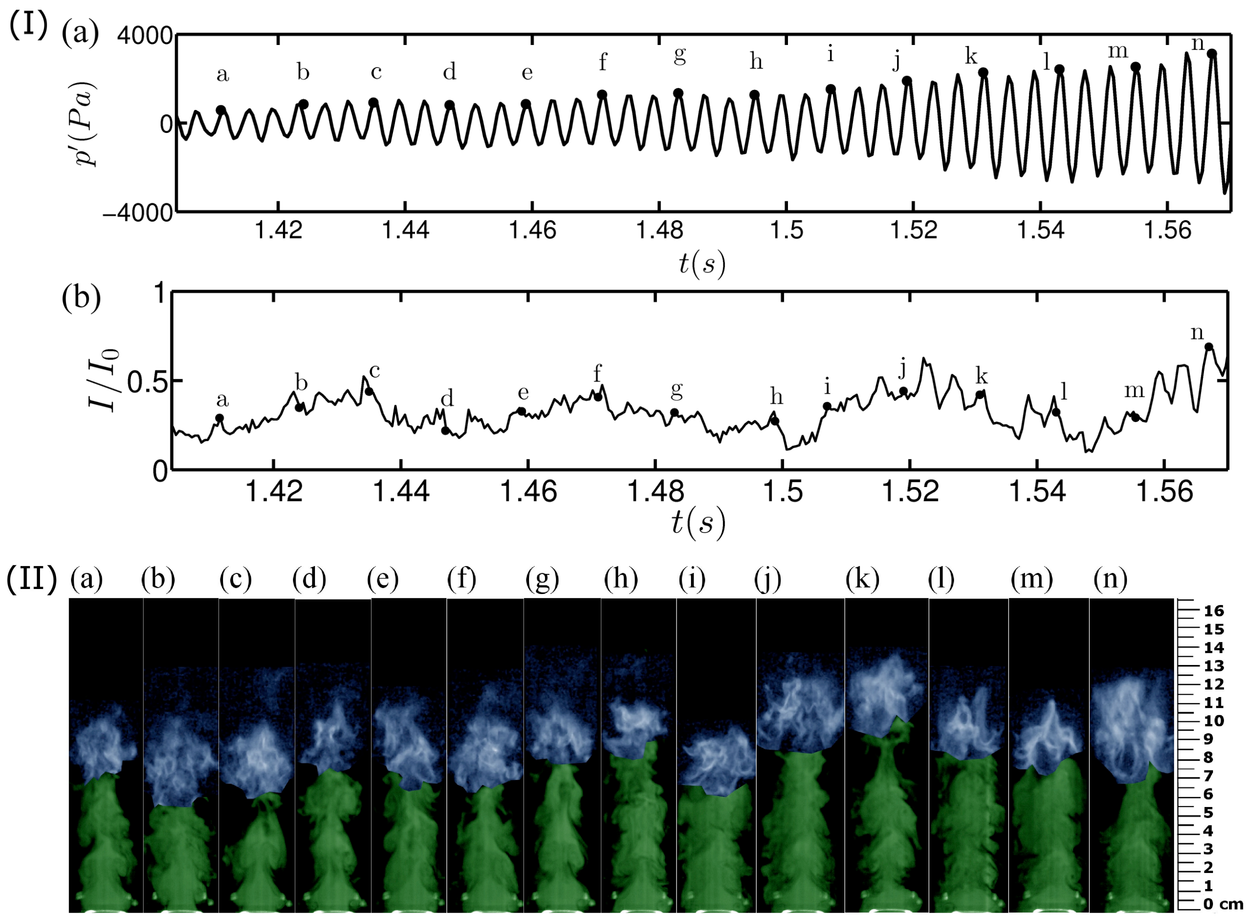

Figure 4.6: *I*) Time series data of *a*) unsteady pressure and *b*) normalized CH* chemiluminescence intensity during the transition from low-amplitude to high-amplitude oscillations during intermittency. *II*) Instantaneous flame (blue) and flow (green) images correspond to the points marked in Fig. 4.6(*I*). During the transition from low-amplitude to high-amplitude oscillations in intermittency, coherent vortices begin to form in the shear layer (see images *c* and *d* in Fig. 4.6*II*). The formation of coherent vortices is interrupted by incoherent flow fluctuations (images *e* and *f* in Fig. 4.6*II*). The formation of coherent vortices happens again in images (*g*) and (*h*) in Fig. 4.6(*II*).

Meanwhile, the lift-off distance of the flame oscillates aperiodically and such aperiodic oscillations in the flame lift-off distance are modulated by periodic oscillations having a frequency around 24 *Hz*. This can be evident from Fig. 4.6(*Ib*) where the fluctuations in the chemiluminescence intensity are modulated by low frequency oscillations. These oscillations in the flame produce low-amplitude periodic oscillations in the acoustic pressure. We observed a low-amplitude peak in the amplitude spectrum of the acoustic pressure at a frequency around 24 *Hz* (The amplitude spectrum is not shown here.). Similar low frequency oscillations of the flame base are also observed during the low-amplitude regime of intermittency. As discussed in the previous section, these oscillations with a frequency around 24 *Hz* in the chemiluminescence intensity and the acoustic pressure occur due to the Benard/Von Karman (BVK) hydrodynamic instability in the flow.

However, the length of the flame exhibits periodic oscillations of frequency around 260 *Hz*. The periodic changes in the flame surface area due to such flame length oscillations gives rise to unsteady pressure oscillations. Therefore, the transition from low to high-amplitude pressure oscillations happens in the form of ordered pressure oscillations. Meanwhile, the flow-field also exhibits periodic oscillations due to the presence of coherent vortices in the shear layer. Further, the heat release rate fluctuations (Fig. 4.6*Ib*) and the acoustic pressure fluctuations (Fig. 4.6*Ia*) are observed to be positively correlated with each other (i.e., peaks in chemiluminescence intensity are associated with peaks in acoustic pressure). This positive coupling initiates the growth in the acoustic energy. In a nutshell, the self-organization of the coherent vortices in the flow, along with the in-phase interaction of the flame and duct acoustics appears to be the mechanism behind the growth of periodic oscillations during intermittency prior to thermoacoustic instability.

4.5.3 High-amplitude regime

In contrast with the low-amplitude regime during intermittency, the high-amplitude regime is characterized by ordered periodic oscillations (Fig. 4.7*Ia*). The sequence of instantaneous images depicting the dynamics of the flame and the flow-field during one cycle of periodic high-amplitude pressure fluctuations are shown in Fig. 4.7(*II*).

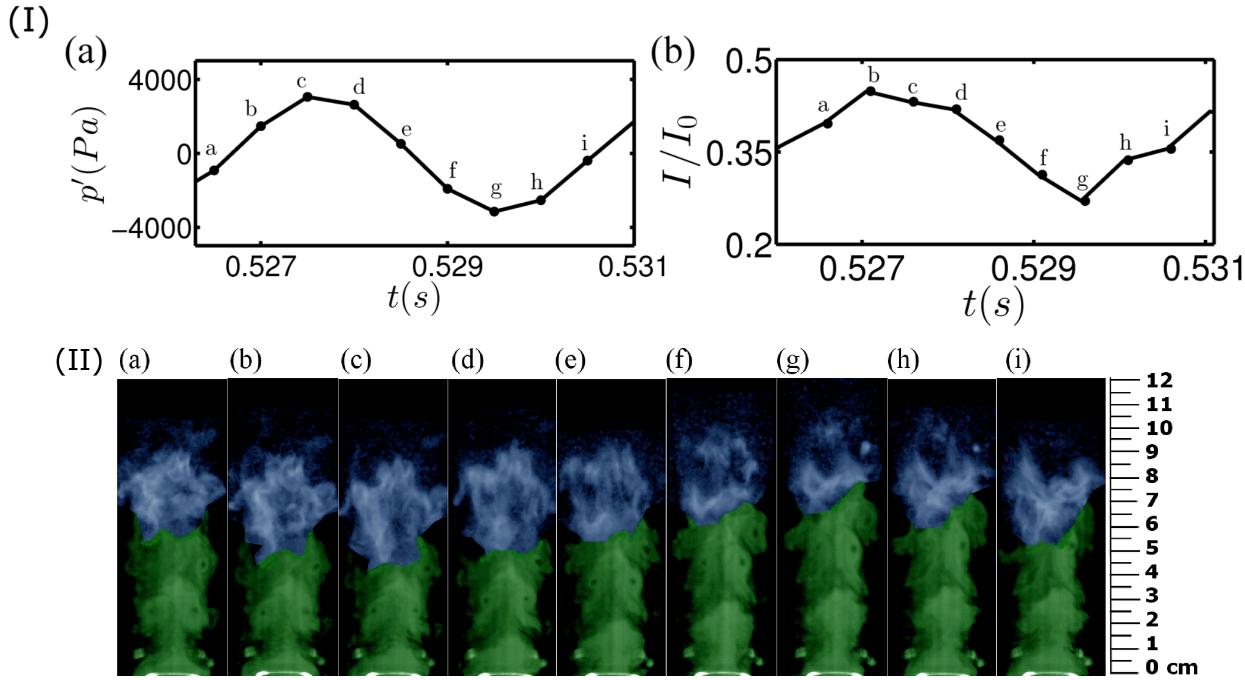

Figure 4.7: *I*) High-amplitude regime during intermittency is associated with periodic oscillations in *a*) acoustic pressure and *b*) CH^* chemiluminescence intensity and are shown for one cycle for illustration. *II*) The instantaneous images showing the flow-field (green) and flame (blue) that correspond to the points marked in Fig. 4.7(*I*). Self-organized coherent vortex structures are formed and convect downstream in the shear layer between the high and low speed streams. The influence of the coherent structures on the flame leads to periodic heat release rate oscillations. Oscillatory heat release rate supplies energy to the acoustic pressure, which in turn controls the formation of coherent structures. This positive correlation between the flow, flame and acoustics sustains the driving of high-amplitude pressure oscillations during intermittency that presages thermoacoustic instability.

The unburnt, partially premixed, stream of fuel and air rolls up into a pair of symmetric vortices rotating in opposite directions, as can be seen in the images of Fig. 4.7(*II*). In the initial stage of vortex formation, large scale mixing of fuel and air happen at the braids of vortices due to high straining rate of the flow at the braids (Thiffeault and Finn, 2006). These pair of vortices travels downstream in the shear layer between the high speed and the low speed streams and the burning happens at a distance of approximately 5 *cm* from the tip of the inner tube. The flame is stabilized perpendicular to the direction of flow and is not established in the shear layer between the high speed and the low speed jets. Consequently, changes in the surface area of the flame during high-amplitude oscillations are not directly influenced by straining of the shear layer. However, the surface area of the flame changes because of the stretching and straining of the flame base that occurs due to the influence of the shear layer which can be seen in the flame (blue) images (*a*) to (*d*) in Fig. 4.7(*II*). The increased surface area of the flame causes a rise in the heat release rate which is followed by shrinking of the flame as can be seen from images (*e*) to (*i*) in Fig. 4.7(*II*).

The periodic formation and the convection of the coherent vortex structures is closely related to this stretching and shrinking of the flame surface area, which further gives rise to periodic oscillations in the heat release rate that can be understood from the fluctuations in CH^* chemiluminescence intensity as shown in Fig. 4.7(*Ib*). The turbulent flame almost becomes flat at certain instances (see images *f*, *g*, *h* and *i* in Fig. 4.7*II*). Also, as can be seen from Fig. 4.7(*II*), the intensity of CH^* chemiluminescence during the high-amplitude regime is more compared to that during the low-amplitude regime. Consequently, due to the increased heat transfer from the hot products to the cold reactants, burning happens at a closer distance from the exit of the jet for high-amplitude oscillations as compared to that of the low-amplitude oscillations.

Oscillatory heat release rate supplies energy into the acoustic pressure oscillations. The generated acoustic waves control and sustain the formation of coherent vortices in the shear layer. As can be inferred from Fig. 4.7(*II*), during one cycle of acoustic pressure oscillations, a vortex pair forms in the shear layer and travels downstream and is then followed by the formation of the next vortex pair. The frequency of coherent vortex formation is equal to the frequency of acoustic pressure oscillations (~ 260 *Hz*). Also, the frequency of high-amplitude periodic oscillations during intermittency is the same as the frequency of limit cycle oscillations during thermoacoustic instability. Schadow and Gutmark (1992) reported that the matching of acoustic frequency and vortex formation frequency produces coherent vortices of minimum size.

Smith and Zukoski (1985) showed that the frequency of vortex formation does not change with respect to changing flow velocity, and strongly depends on the frequency of combustion instability. This gives a hint that the coherent vortices that are formed in the flow during high-amplitude (of the order of 3000 *Pa*) periodic oscillations in intermittency may not be due to the

Strouhal type hydrodynamic instability. However, a low-amplitude (of the order of 40 *Pa*) peak is observed in the amplitude spectrum of acoustic pressure (not shown in the paper) at a frequency around 24 *Hz*. This frequency is due to the BVK type hydrodynamic instability in the flow.

Further, Yu *et al*. (1991) systematically varied the inlet velocity and combustor length to assess the role of vortices and duct acoustics on the frequency of combustion instability. The frequency of combustion instability does not lock on to any particular natural frequency of the resonators in the combustion system. This shows that combustion instability is not purely acoustic in nature. Further, they showed that combustion instability is controlled by both vortex kinematics and the acoustic response of the system. Therefore, they suggested that combustion instability can be considered as a mixed acoustic-convective mode. The fluid mechanical behavior during the bursts of high-amplitude, periodic oscillations during intermittency seems to be the same as that during the occurrence of full blown combustion instability. The fluid physics during combustion instability is well established in the literature (Smith and Zukoski, 1985; Poinsot *et al*., 1987; Yu *et al*., 1991; Schadow and Gutmark, 1992).

Further, it can be seen from Figures 4.7(*Ia*) and 4.7(*Ib*), the acoustic pressure oscillations and heat release rate fluctuations happen in phase with each other. Also, the frequency of oscillations in the acoustic pressure and the frequency of vortex formation and its convection is the same during the high-amplitude oscillations in intermittency. This shows that a strong coupling is established with acoustic pressure, fluid dynamics, and heat release rate fluctuations from the flame. Such strong coupling is the cause for the driving of high-amplitude periodic pressure oscillations during intermittency that presages thermoacoustic instability.

4.5.4 Transition from high to low-amplitude regime

The switching from high-amplitude to low-amplitude regime during intermittency that presages thermoacoustic instability is initiated by a sharp reduction in the heat release rate. The flame is standing closer to the tip of the copper tube in image (*a*) in Fig. 4.8(*II*) (at time $t = 0.401$ *s*). In the subsequent time instants, the flame moves away from the burner along with a considerable reduction in the flame surface area and the intensity of the chemiluminescence. The chemiluminescence intensity is extremely low such that the flame is not even visible in the following frames (images *c* to *k* in Fig. 4.8*II*). This leads to the reduction in the heat release rate. The acoustic pressure closely follows the heat release rate history, and decay of unsteady pressure from high-amplitude to low-amplitude is observed. The pressure amplitude was 3942 *Pa* at time $t = 0.401$ *s* and it drops down to a value of 323 *Pa* at time $t = 0.448$ *s* (i.e., from image *a* to image *l* in Fig. 4.8*II*).

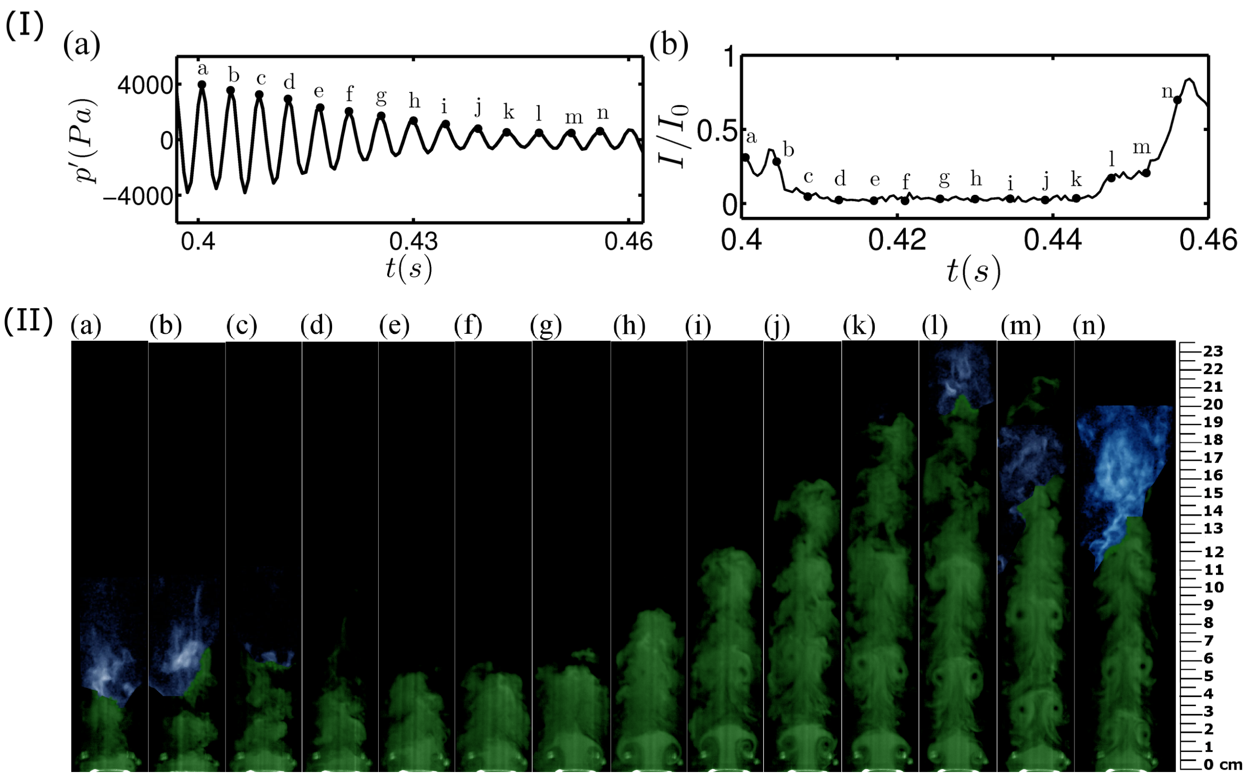

Figure 4.8: *I*) Time series data of *a*) unsteady pressure and *b*) normalized CH^* chemiluminescence intensity during the transition from high-amplitude to low-amplitude oscillations. *II*) Sequence of flame and flow images correspond to the points marked in Fig. 4.8(*I*). The intensity of CH^* chemiluminescence sharply reduces during the transition from high-amplitude to low-amplitude pressure oscillations. The intensity of chemiluminescence is very low such that the flame is not even visible in the images (*c*) to (*k*). The reduction in the heat release rate causes the sharp drop in acoustic pressure. Meanwhile, the jet of unburnt mixture of the fuel and the air travel without burning far downstream of the exit of the burner.

As discussed in the previous section, the flow-field during the high-amplitude fluctuations in intermittency is manifested as coherent vortex structures. Consequently, during the transition from high-amplitude to low-amplitude oscillations, the flow was developed as pairs of well organized vortices. The visualization of the flow is due to the illumination of olive oil particles that are seeded in the mixture of fuel/air at the inlet. Therefore, the Mie scattering images, in turn, reflect the presence of unburnt fuel in the flow. During the switching from high-amplitude to low-amplitude oscillations, the unburnt fuel is transported far downstream of the exit of the inner tube without burning (see the flow structures from the images (*a*) to (*l*) in Fig. 4.8*II*).

After the thermoacoustic system transitioned from high-amplitude to low-amplitude fluctuations, the flame begin to travel towards the tip of the burner with high heat release rate fluctuations (correspond to the images *m* and *n* in Fig. 4.8*II*). This flame propagation towards and away from the burner is observed repeatedly every time during the switching from high-amplitude to low-amplitude pressure fluctuations.

4. 6 Interim Summary

From the analysis of the different regimes during intermittency, we conjecture that the cause for intermittency before the onset of thermoacoustic instability is the concurrent presence of the dynamics of both combustion noise and thermoacoustic instability. The flame and the flow dynamics in low-amplitude fluctuations during intermittency that presages thermoacoustic instability are observed to be similar to that of the combustion noise. The state of combustion noise is dominated by incoherent, seemingly random, fluctuations in the flow, acoustic pressure and flame (Bragg, 1963; Strahle, 1978). The coupled interaction of fluid dynamics, combustion and duct acoustics is not positively correlated so that the dynamics of the system is manifested as irregular, low-amplitude fluctuations.

In contrast to combustion noise, thermoacoustic instability is well known to be associated with self-organized coherent vortex structures (Smith and Zukoski, 1985; Poinsot *et al*., 1987; Yu *et al*., 1991). The behavior of the flame and the flow-field in the occurrence of high-amplitude oscillations during the intermittency that presages thermoacoustic instability is also dominated by the presence of self-organized coherent vortices. In the high-amplitude regime during intermittency before thermoacoustic instability, fluid dynamics, flame and acoustic pressure are positively correlated. Coherent vortices influence the flame and cause periodic oscillations in the heat release rate, which in turn affect the acoustic pressure. The acoustic field affects the shear layer and sustains the formation of coherent vortices. Such self-organized interaction sustains the high-amplitude ordered acoustic pressure oscillations.

Though combustion noise and thermoacoustic instability are dynamically two different states, intermittency that appears during the transition from combustion noise (irregular) to thermoacoustic instability (order) interestingly has characteristics of both combustion noise and combustion instability. Intermittency has regions of coherence amidst regions of incoherent fluctuations in the flow. As the control parameter is varied towards the condition of onset of thermoacoustic instability, coherent vortex structures in the flow (periodic oscillations in acoustic pressure) exist for longer time. Finally, the flow-field becomes fully coherent at the occurrence of full blown thermoacoustic instability.

4.7 Physical mechanisms that cause intermittency prior to flame blowout

As we change the location of inner tube inside the confinement further past the condition of thermoacoustic instability, intermittency is once again observed before the flame blows out. Various qualitatively different states that are observed in the acoustic pressure before the flame blows out are shown in Fig. 4.9.

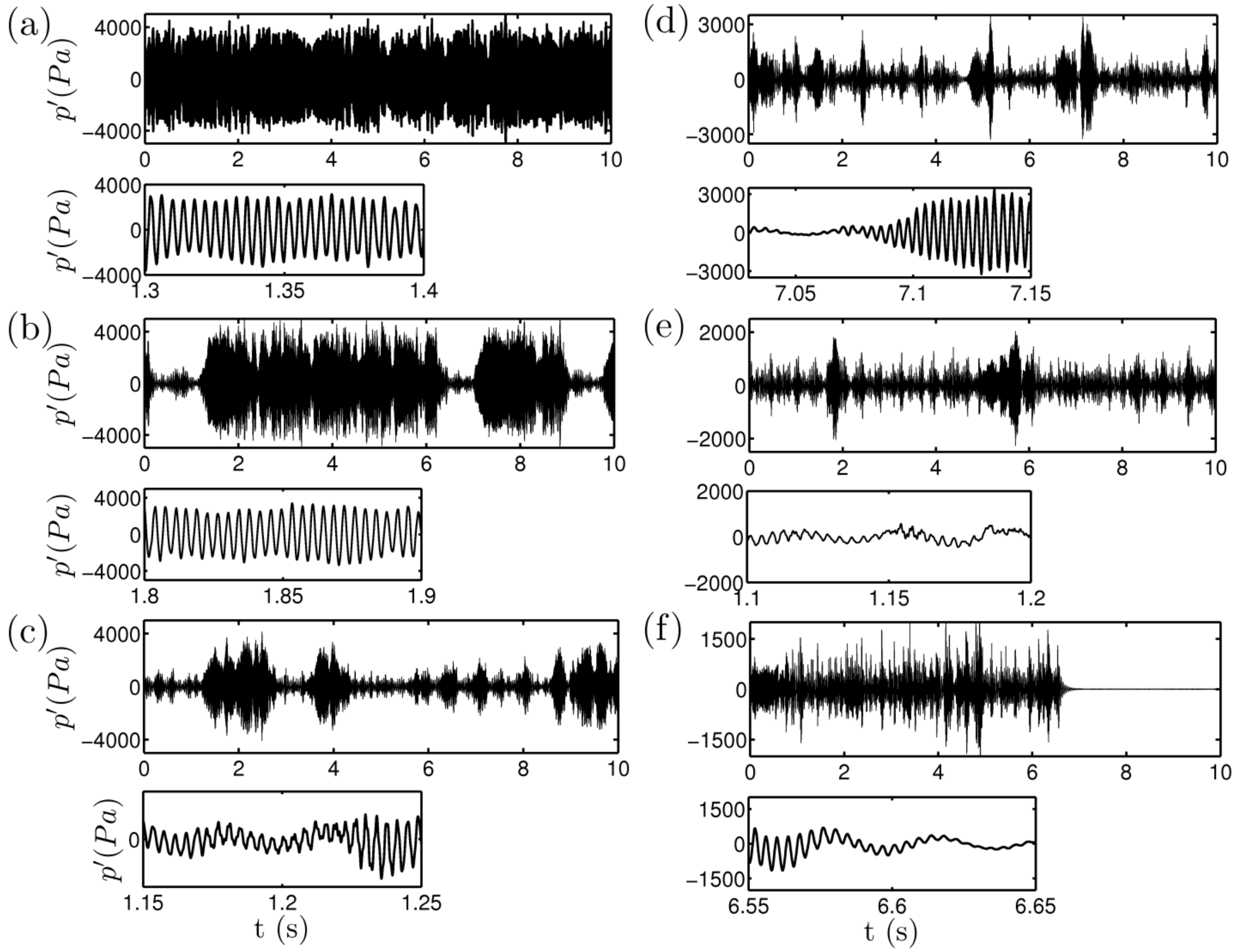

Figure 4.9: Time series data of unsteady pressure acquired during the occurrence of intermittency before the onset of blowout as the inner tube is located at *a*) 57 *cm*, *b*) 61 *cm*, *c*) 63 *cm*, *d*) 66 *cm* *e*) 70 *cm* and *f*) 77 *cm* from the top end of the quartz tube. The amplitude and duration of the intermittent high-amplitude periodic oscillations reduces as we approach the blowout limit. In situation closer to blowout, the amplitude of unsteady pressure dies and sudden growth is observed (see Fig. 4.9*d*).

Self-sustained thermoacoustic oscillations are observed as the inner tube was located at 57 *cm* from the top end of the combustor (see Fig. 4.9*a*). As the inner tube location is varied to 61 *cm* from the top end of the duct, low-amplitude aperiodic oscillations are intermittently observed amidst regimes of large-amplitude periodic oscillations. The amplitude and duration of the high-amplitude periodic oscillations in this intermittent regime reduces for further change in control parameter. Further, the oscillations in acoustic pressure become more and more aperiodic during the transition to blowout. At certain instances closer to the blowout (Fig 4.9*d*), the amplitude of pressure oscillations nearly dies out and then grows suddenly.

Blowout usually occurs as the equivalence ratio is decreased and is usually referred to as lean blowout. However, in the present work, while the equivalence ratio is not altered, we observed the transition to blowout occur via thermoacoustic oscillation as we varied the burner location (local admittance) inside a confinement. This observation suggests that the observed blowout could be a thermoacoustically induced blowout.

The intermittent dynamics as the inner tube is located at 66 *cm* from the top end of the confinement is chosen to study the interaction of flame-flow-duct acoustics during the intermittency that presages blowout. The time series data of acoustic pressure and normalized CH^* chemiluminescence intensity measured during this situation are shown in Fig. 4.10.

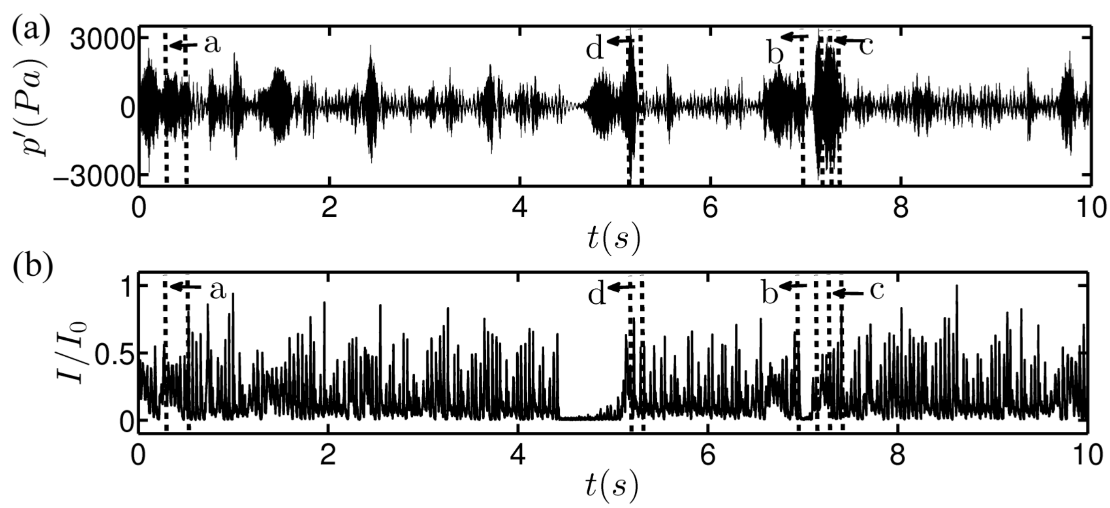

Figure 4.10: Time series data of *a*) acoustic pressure and *b*) normalized CH^* chemiluminescence intensity acquired during the intermittency prior to blowout.

Similar to the intermittency prior to combustion instability, we observed a low-amplitude peak at a frequency around 24 *Hz* in the amplitude spectra of the chemiluminescence intensity and the acoustic pressure (The amplitude spectrum is not shown here) acquired during intermittency that presages blowout. These fluctuations occur because the co-flowing air underwent a Strouhal type

BVK hydrodynamic instability in the flow as the flow approaches the hexagonal nut. Consequently, the fluctuations in the flow result in oscillations in the heat release rate and in the unsteady pressure. Further, the time series data is divided into four regimes for analysis; *a*) low-amplitude regime, *b*) transition from low-amplitude to high-amplitude regime, *c*) high-amplitude regime and *d*) transition from high-amplitude to low-amplitude regime.

4.7.1 Low-amplitude regime

The low-amplitude pressure fluctuations during the intermittency before blowout are also aperiodic. The corresponding flame and flow images are presented in Fig. 4.11(II).

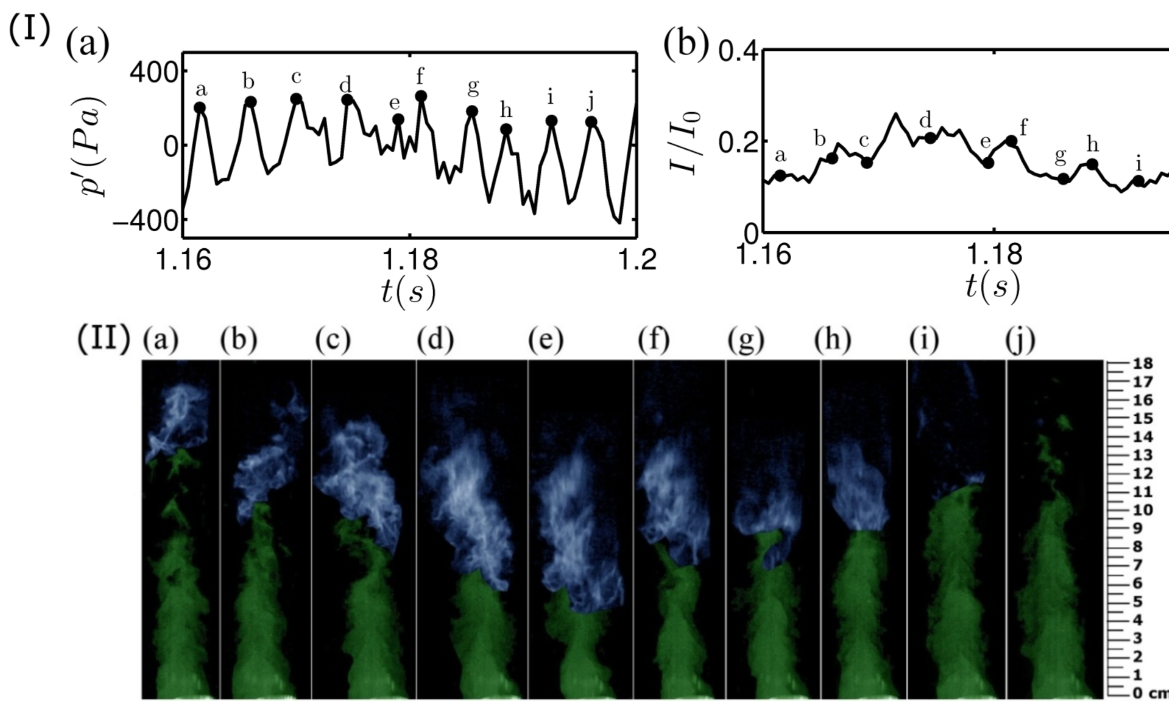

Figure 4.11: *I*) Time series data of *a*) unsteady pressure and *b*) chemiluminescence intensity fluctuations during the low-amplitude regime in intermittency before blowout. *II*) Flame (CH^* chemiluminescence images are colored in blue) and flow (Mie scattering images of unburnt jet from the burner are colored in green) corresponding to the points marked in Fig. 4.11(I). The flame propagates towards and away from the burner. The flame stretching (images *c*, *d*, *e* and *f*) and shrinking (images *g* and *h*) is observed. The local extinction of the flame sheet is observed (see images *i* and

j in Fig. 4.11*II*) during the low-amplitude oscillations occurring during intermittency that presages blowout.

The jet from the burner is characterized by incoherent fluctuations. Around 10 *cm* from the tip of the inner tube, the flame is formed at the shear layer. The portion of the flame closer to the edge of the shear layer is feeble as can be seen from image (*a*) in figure 4.11(*II*).

Further, the luminosity of the flame is significantly weaker during the low-amplitude regime of intermittency prior to blowout, as an example, see images (*a*), (*b*), (*g*), (*h*), (*i*) and (*j*) in Fig. 4.11(*II*), compared to that of the low-amplitude regime in intermittency prior to combustion instability. Such progressive weakening of the flame is identified as an initiating event in the sequence of blowout precursor events (Biswas *et al*., 2013). At certain instances, the base of the flame is locally extinguished (see images *i* and *j* of Fig. 4.11*IIb*). The localized extinction events occurring on the flame surface area are related to the unsteady fluctuations in the flame prior to blowout (Shanbhougue *et al*., 2009). This local extinction occurs at the points of high flame strain rate resulting from the turbulent fluctuations (Driscoll, 2008). The reduced levels of the luminosity indicate that the heat release rate from the flame is significantly low. This causes the reduction in temperature of the mixture of products and reactants (Rasmussen and Driscoll, 2008). Further, it is known that the sufficient heat transfer from the products to reactants is required for the flame to propagate into the unburnt mixture. This results in change in the flame speed. Meanwhile, the jet velocity of the mixture is intact, since the flow rates of the mixture are not altered. Thus, the imbalance of the flame speed and the flow speed causes the flame to propagate repeatedly towards and away from the burner.

In frames (*d*), (*e*) and (*f*) of Fig. 4.11(*II*), the flame length evolves to a larger extent in the stream wise direction. Such stretching of flame length is reported in the study of flame dynamics close to blowout (Biswas *et al*., 2013). The shrinking of the flame happens in frames (*g*) and (*h*) in Fig. 4.11(*II*). The heat released from the flame decreases due to the reduction in the surface area of the flame during events such as local extinction, weakening of the flame and flame shrinking.

Moreover, as can be seen in Fig. 4.11(*I*), the peaks in the acoustic pressure (marked as points from *a* to *j* in Fig. 4.11*Ia*) are neither positively correlated nor negatively correlated with the local minimum values (marked as points from *a* to *j* in Fig. 4.11*Ib*) of the heat release rate fluctuations. Further, oscillations in the flow-field do not seem to be correlated either with the acoustic pressure or with the flame dynamics.

However, the reduction in the heat release rate due to flame stretching and local extinction can be the possible reason for the low-amplitude pressure oscillations during intermittency before blowout. Further, the stretching and the local extinction of the flame are the noticeable features in the low-amplitude regime during intermittency before blowout that is distinct from the low-amplitude regime during intermittency prior to combustion instability.

4.7.2 Transition from low to high-amplitude regime

The flow, flame and acoustic pressure data acquired during the transition from low-amplitude to high-amplitude oscillations during intermittency prior to blowout are shown in Fig. 4.12. During intermittency prior to blowout, at certain instances, the flame propagates far away from the lift-off location that corresponds to the stable operation of the combustor, till the end of the quartz duct. The event of flame propagating away from the fuel tube occurs when the local flame speed of the mixture of the products and the reactants is lesser than the jet velocity. This lowering of the flame speed happens due to the reduced temperature of the gaseous mixture (Rasmussen and Driscoll, 2008). Sufficient heat transfer between products and reactants must take place to sustain the flame. However, the weakening of the flame in the low-amplitude regime during the occurrence of intermittency prior to blowout created the low temperature regime.

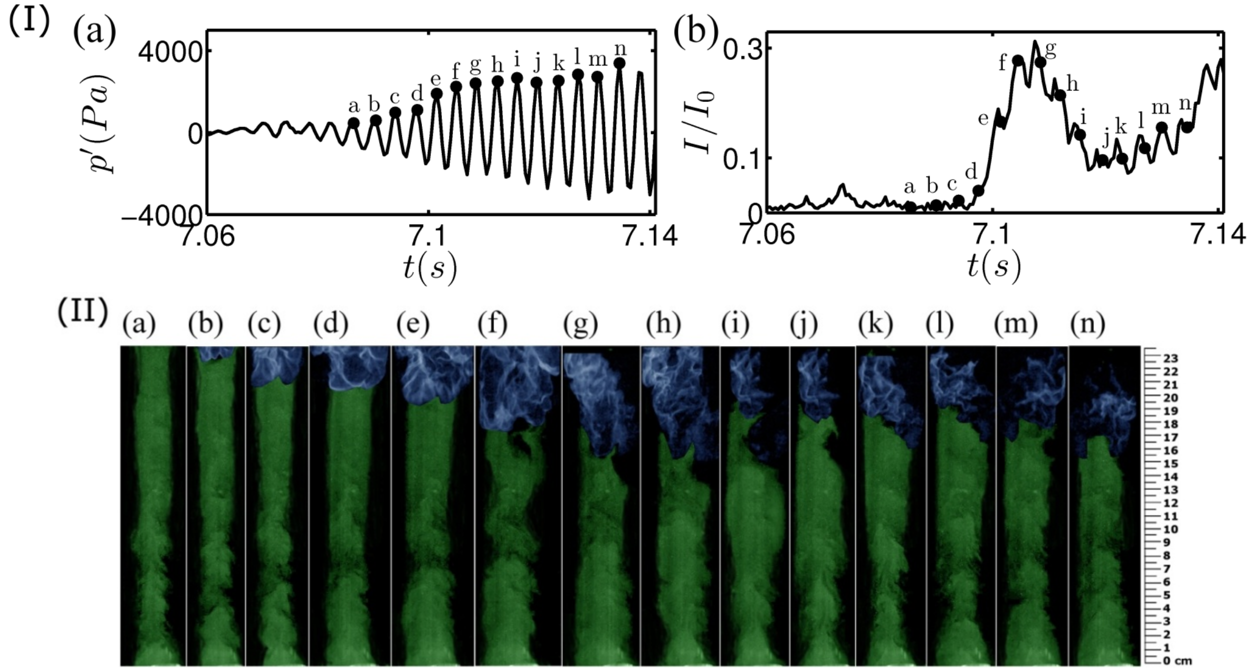

Figure 4.12: *I*) Time series data of *a*) acoustic pressure and *b*) chemiluminescence corresponding to the region of transition from low-amplitude to high-amplitude fluctuations during intermittency prior to blowout. *II*) Sequence of instantaneous images of the flame (blue) and the flow (green) correspond to the points marked in Fig. 4.12(*I*). At certain instances, the flame moves completely far away from the lift-off location that corresponds to the stable operation of the combustor (image *a*) and travels back towards the burner (images *b* to *h*) along with a rise in amplitude of the acoustic pressure.

As an example, the flame moved far away from the lift-off distance that corresponds to the stable operation of the combustor during the time t = 7.05 s (image *a* in Fig. 4.12*II*). This causes the acoustic pressure oscillations to die out due to the absence of driving from combustion. It is evident from Figures 4.12(*Ia*) and 4.12(*Ib*) that there are hardly any oscillations in the acoustic pressure and the intensity of the chemiluminescence is very low during the time instant of t = 7.06 s.

As the mixture of the products and the reactants again attains sufficient temperature for sustaining the combustion, the enhanced heat transfer, in turn, leads to the increase in flame speed. Consequently, the flame travels towards the burner. As the flame propagates towards the burner, the acoustic pressure raises suddenly (corresponds to the images *b* to *h* in Fig. 4.12*II*). Experimental observation of the amplification of acoustic pressure due to the propagation of flame towards the fuel tube is reported in the literature (Searby, 1992; Searby and Rochwerger, 1991). Wu *et al*. (2003) explained that the weak coupling of the instability mode of the flame and the acoustic field in the duct is the main reason for the amplification of acoustic pressure levels. Therefore, we postulate that the flame propagation towards the fuel tube is the reason for the switching from low-amplitude to high-amplitude regime during intermittency that presages blowout.

Further, the luminosity of the flame is weaker in frames (*i*) to (*n*) in Fig. 4.12(*II*). Meanwhile, the flow-field is characterized by incoherent fluctuations (see images *a* to *n* in Fig. 4.12*II*). The physical mechanism for the transition from low-amplitude to high-amplitude regime during intermittency that presages blowout appears to the propgation of flame towards the burner. This is in contrast with the transition from low-amplitude to high-amplitude regime during intermittency that presages thermoacoustic instability, which in fact happen due to the self-organization of coherent vortices in the flow.

4.7.3 High-amplitude regime

Similar to the high-amplitude fluctuations during intermittency before thermoacoustic instability, the high-amplitude oscillations during intermittency prior to blowout are also associated with ordered periodic oscillations in the acoustic pressure (shown in Fig. 4.13*Ia*).

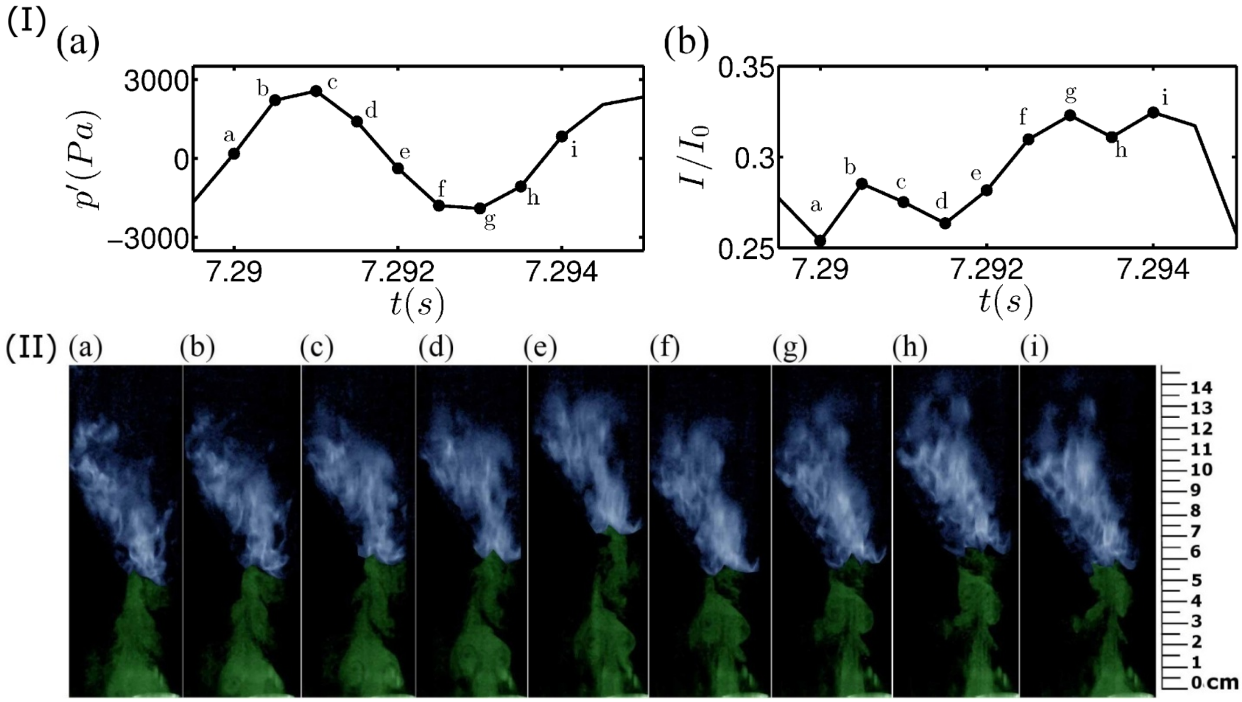

Figure 4.13: *I*) Time series of *a*) acoustic pressure and *b*) chemiluminescence intensity during the occurrence of high-amplitude pressure oscillations before blowout. *II*) Sequence of instantaneous CH^* chemiluminescence (flame images are colored in blue) and Mie scattering images (flow images are colored in green) corresponding to the points marked in Fig. 4.13(*I*). The acoustic pressure and chemiluminescence intensity undergo ordered periodic oscillations. Coherent vortices are formed and convected downstream of the flow with the time scales that are approximately equal to the characteristic time scales of the acoustic pressure.

During these high-amplitude periodic oscillations in the acoustic pressure, the flame also undergoes an oscillation cycle, which is reflected as the periodic oscillations in the chemiluminescence intensity (Fig. 4.13*Ib*). The lift-off distance of the flame fluctuates with the frequency of the acoustic pressure oscillations. The intensity of the chemiluminescence during the high-amplitude regime in intermittency prior to blowout is higher than that of the low-amplitude regime (Fig. 4.11*Ib*), transition from low-amplitude to high-amplitude regime (Fig. 4.12*Ib*) and transition from high-amplitude to low-amplitude regime (Fig. 4.14*Ib*). The dynamics of the shear layer greatly affects the flame dynamics, particularly at the base of the flame. As an example, the shear layer influencing the base of the flame can be seen in images (*b*) to (*i*) of Fig. 4.13(*II*).

As the jet of fuel-air mixture from the burner enters the shear layer region between high speed and low speed jets, the shear layer rotates to form a pair of symmetric, counter-rotating vortices. This pair of coherent vortices travels downstream of the flow followed by the generation of the next vortex pair in the flow (see Fig. 4.13*II*). The time of generation of one vortex pair and its convection downstream of the flow followed by the generation of the next vortex pair is approximately equal to the characteristic time scale of the acoustic pressure oscillations. The vortex generation and convection repeats periodically and combustion takes place approximately at a location of 6 *cm* from the tip of the burner.

The periodic oscillations developed in the flow due to the presence of these coherent vortices have a great effect on the flame dynamics. As the coherent vortices develop and travel downstream of the flow, they can interact with the flame in a periodic manner during the thermoacoustic cycle. These periodic oscillations cause the heat release rate oscillations, which are in phase with the acoustic pressure. Further, the amplitude of the acoustic pressure oscillations and intensity of the chemiluminescence from the flame have a larger magnitude and indicates that the system is in a high energy state.

Even though, the high-amplitude regime during intermittency prior to blowout is associated with coherent vortices in the shear layer, the transition from low-amplitude to high-amplitude oscillations during intermittency prior to blowout does not happen due to the self-organization of coherent vortices (which is discussed in the previous section). The travelling of the flame towards the fuel tube gave rise to the growth in amplitude of the acoustic pressure. Once the amplitude of the acoustic pressure oscillations is increased, the high-amplitude acoustic wave triggered the formation of coherent vortices in the flow and periodic oscillations in the heat release rate. After the formation of coherent vortices, in-phase interaction of the flame dynamics, vortex kinematics and chamber acoustics sustains the high-amplitude regime in intermittency that presages blowout.

This suggests us that the self-organization of coherent vortices may not be the cause for high-amplitude regime during the intermittency prior to blowout. But, the coherent vortices are formed as a consequence of the amplitude growth of acoustic pressure due to the flame-acoustic coupling, during the high-amplitude regime during the intermittency prior to blowout

4.7.4 Transition from high to low-amplitude regime

The acoustic pressure and chemiluminescence intensity corresponding to the regime of transition from high-amplitude to low-amplitude fluctuations during intermittency prior to blowout are shown in Fig. 4.14(I).

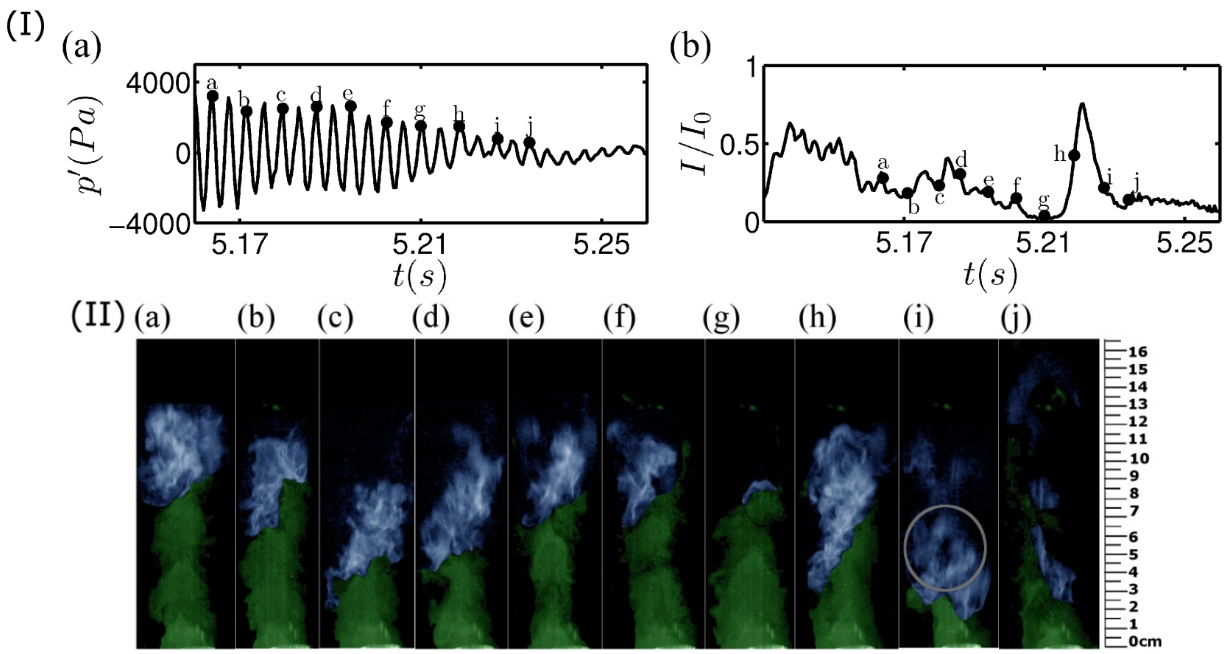

Figure 4.14: *I*) Time series of *a*) unsteady pressure and *b*) chemiluminescence intensity corresponding to the regime of transition from high-amplitude to low-amplitude fluctuations during intermittency before blowout. (*II*) Instantaneous flow and flame images correspond to the points marked in Fig. 4.14(*I*). The transition from high-amplitude to low-amplitude pressure oscillations is associated with the weakening and local extinction of the flame sheet (images *i* and *j*).

The aperiodic fluctuations in the flame surface area are observed during the transition from high-amplitude to low-amplitude regime during intermittency prior to blowout. These aperiodic oscillations in the chemiluminescence intensity are due to the localized extinction of the flame surface area. As an example, note that the flame undergoes a local extinction in the images (*g*) and (*j*) of Fig. 4.14(*II*). In situations close to blowout, images showing the holes in the flame surface area are presented in the literature (Nair and Lieuwen, 2005). Notice that the hole is formed in the flame sheet as can be seen in image (*i*) of Fig. 4.14(*II*). A circle is drawn to show the hole in flame in image (*i*) of Fig. 4.14(*II*). The holes in the flame surface area and local extinction of the flame are observed to happen at the points of high flame strain rate and are more relevant to the turbulent combustion (Shanbhougue *et al.*, 2009). The high intensity turbulent fluctuations in the flow are the cause for such high strain rate of the flame (Driscoll, 2008).

As the hole is formed in the flame sheet, cold unburnt reactants can penetrate through the flame and dilutes the mixture of the products and the reactants. This reduces the temperature of the mixture and also the flame speed. The imbalance created between the flame speed and the jet velocity causes the flame to propagate towards and away from the burner. As an example, the flame lift-off and travel towards the burner can be seen in Fig. 4.14(*II*). The lift-off height of the flame was 8 cm from the tip of the burner in image (*a*) in Fig. 4.14(*II*). The lift-off distance of the flame fluctuates aperiodically and the flame travels till a location of 2 *cm* from the tip of the burner. The flame travel towards and away from the fuel tube is reported as the flapping of the flame prior to blowout in the literature (Shanbhougue *et al*., 2009).

The instantaneous length of the flame is also observed to change in a near random manner. The structure of the flame is fragmented in image (*i*) in Fig. 4.14(*II*). In frame (*g*) of Fig. 4.14(*II*), the intensity of the chemiluminescence is very weak. Such a large drop in the acoustic and chemiluminescence emissions begins to occur in the situations closer to blowout. The frequency of such drops monotonically increases as the blowout limit is reached (Muruganandam *et al*., 2005; Nair and Lieuwen, 2005).

However, in frames (*a*) to (*f*) and (*h*) in Fig. 4.14(*II*), the length of the flame is high and holes are formed in the flame surface. As long as the holes are not formed in the flame, cold reactants do not pass through the flame. Moreover, the flow-field is observed to be dominated by incoherent fluctuations in the shear layer. There are no coherent vortices formed in the flow. The acoustic pressure exhibits transition from periodic to aperiodic oscillations during this transition from high-amplitude to low-amplitude regime. Moreover, the peaks in the acoustic pressure (points marked in Fig. 4.14*Ia*) are not correlated either positively or negatively with the peaks in the chemiluminescence intensity (points marked in Fig. 4.14*Ib*).

It is evident from the observation of flame dynamics during the transition from high-amplitude to low-amplitude regime during intermittency prior to blowout, that the reduction in the heat release rate happen due to the weakening and local extinction of the flame. This reduction in the heat release rate may be the main cause for switching from high-amplitude to low-amplitude regime during intermittency before blowout, similar to that of intermittency before instability.

4.8 Interim summary

In summary, the flame and the flow dynamics in low-amplitude fluctuations during intermittency that presages blowout are observed to be similar to that of the blowout precursor events. The blowout is presaged by the precursor events such as formation of holes in the flame, local extinction and re-ignition (Nair and Lieuwen, 2005; Muruganandam *et al*., 2005; Shanbhogue *et al*., 2009). The transition to high-amplitude periodic acoustic oscillations occurs as the flame propagates towards the fuel tube. The acoustic field affects the shear layer and sustains the formation of coherent vortices and the periodic oscillations in the heat release rate during high-amplitude regime of intermittency that presages blowout. The investigation of different regimes during intermittency that presages blowout led us to postulate that the physical reason for intermittency before the onset of blowout is the interplay of blowout precursor events and the driving of high-amplitude periodic oscillations as the flame propagate towards the fuel tube.

The different flow physics which lead to the occurrence of intermittency that presages the onset of thermoacoustic instability and blowout were discussed in the Sections 4.5 and 4.7. However, the commonalities between the intermittency that presages thermoacoustic instability and the intermittency that presages blowout are investigated from a dynamical systems perspective.

4.9 Type of intermittency prior to thermoacoustic instability and flame blowout

From a dynamical systems perspective, we investigate the type of intermittency that presages the onset of both thermoacoustic instability and blowout.

Pomeau and Manneville (1980) classified intermittency into three types, depending on the nature of the bifurcation. Type I corresponds to a saddle-node bifurcation. Type II is associated with a Hopf bifurcation. Type III is due to a reverse period doubling bifurcation. Some of the other types of intermittencies (type V, type X, chaos-chaos intermittency, on-off intermittency and in-out intermittency) and methods to distinguish different types of intermittencies using recurrence quantification analysis are described by Klimaszewska and Zebrowski (2009).

Nair *et al*. (2014) analyzed intermittency before thermoacoustic instability in combustors involving turbulent flow using recurrence plots. They used the recurring properties of intermittent bursts of periodic oscillations that are calculated using recurrence quantification analysis to detect the proximity to the onset of combustion instability (Nair *et al*., 2014). Pawar *et al*. (2015) used the nonlinear time series techniques such as phase space reconstruction, statistical distribution of lengths of aperiodic phases, first return map and recurrence plots to characterize the intermittency. They reported the presence of Type II intermittency prior to thermoacoustic instability in a spray combustion system.

From the recurrence plots, Kabiraj and Sujith (2012) identified the type of intermittency prior to blowout in a laminar flow system as Type II. Unni *et al*. (2013) used the measures such as recurrence rate, Shannon entropy, trapping time etc. derived from recurrence plots to detect the blowout in combustion systems. Gotoda *et al*. (2014) also used recurrence plots to characterize the state prior to lean blowout.

In the present work, the intermittent features of acoustic pressure time series data acquired before thermoacoustic instability and blowout are investigated using return maps and recurrence plots.

4.9.1 First return maps

First return map is a two-dimensional graph plotted between X_n and X_{n+1}, where X_n is a vector consists of local maxima of the time series and X_{n+1} is a vector containing the next local maxima (Sacher *et al*., 1989).

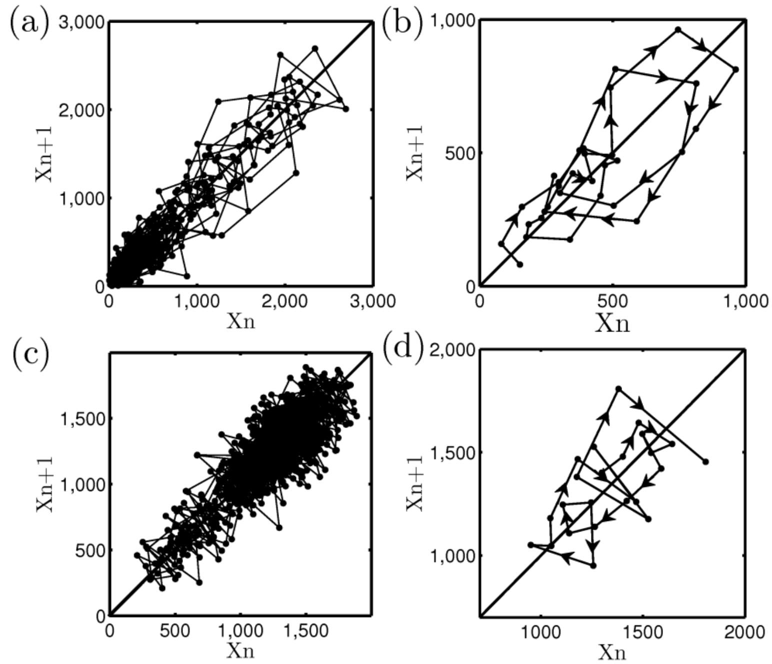

Figure 4.15: First return maps obtained from the time series data of acoustic pressure during the occurrence of intermittency prior to *a*) thermoacoustic instability and *c*) blowout. The spiral-like behavior of trajectories is observed in both the return maps that correspond to intermittency prior to instability and blowout. To show the spiraling behavior, the return maps of intermittency prior to *b*) thermoacoustic instability and *d*) blowout are shown for a smaller time interval. This is the typical characteristic of Type II intermittency, suggesting that the intermittency prior to both instability and blowout are of Type II.

Sacher *et al*. (1989) used the first return maps to identify the type of intermittency observed in an optical system. Fig. 4.15 shows the return maps obtained from the acoustic pressure time series during the occurrence of intermittency prior to thermoacoustic instability and blowout.

From the acoustic pressure time series, a vector consists of local maxima of the pressure time series is constructed. The first return maps are then plotted as a two-dimensional plot between local maxima and next local maxima. The points in the return map are scattered around a main diagonal line. Further, spiral-like behavior of trajectories is observed in the first return maps of intermittency prior to both instability and blowout. The scattering states around the main diagonal line and a spiral-like behavior are typical characteristic of Type II intermittency. This leads us to suggest from the first return maps that intermittency prior to combustion instability and blowout are of Type II.

4.9.2 Recurrence plots

Recurrence is a fundamental property of dynamical systems which can be used to characterize the system's behavior in phase space. The phase of the system during intermittent state is reconstructed by following the procedures given in Abarbanel (2012).

The pair-wise distance between the states in the reconstructed phase space is computed to calculate the binary recurrence matrix:

$$R_{i,j} = \Theta(\sigma - \|\mathrm{Z_u} - \mathrm{Z_v}\|),\ \mathrm{u, v} = 1, 2, \ldots, N - \mathrm{d_0}\tau_{\mathrm{opt}}$$

where Θ is the Heaviside step function and σ is the threshold for the maximum distance between a pair of states in the phase space to treat them as recurrent. The indices i and j are the time instants when the distance is calculated. The variable Z refers to the time delayed vectors indicating the state of the system in the phase space.

Recurrence plot is a plot of the symmetric matrix $R_{i,j}$ for various instants of time. All the elements in the recurrence matrix are either 0 or 1. A black dot appears in the recurrence plot if the element in the recurrence matrix is 1; otherwise, the element 0 in the recurrence matrix is marked as a white dot in the recurrence plot.

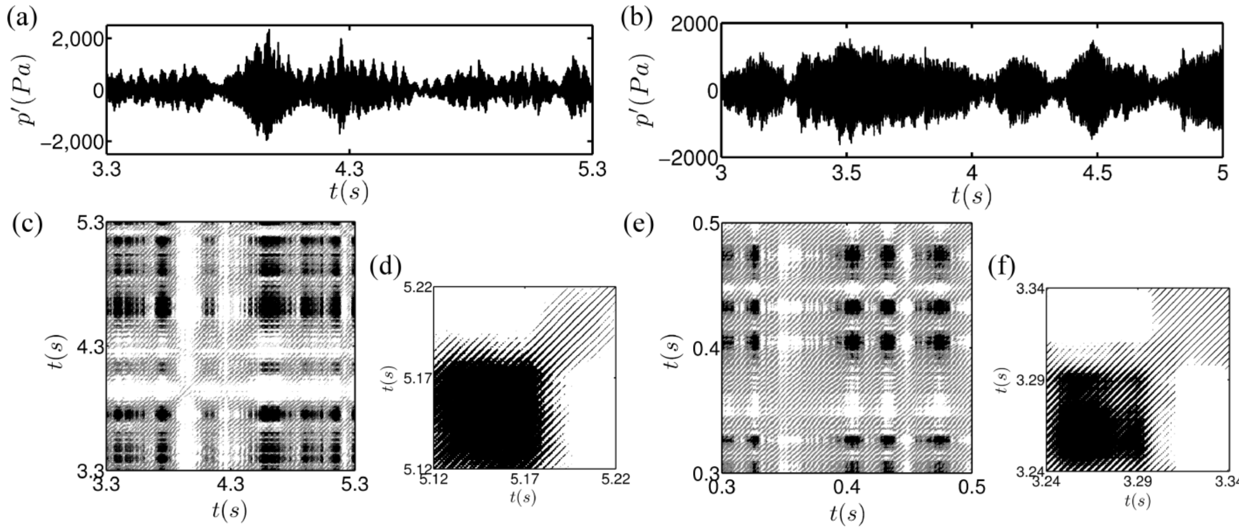

Figure 4.16: The time series data of acoustic pressure during *a*) intermittency before thermoacoustic instability and *b*) intermittency prior to blowout. The recurrence plot is drawn from the time series data for duration of 2 *s* as shown in Figures 4.16(*a*) and 4.16(*b*). The threshold value in the recurrence condition was chosen to be $\sigma = 0.2D$, where D is the diameter of the attractor in the phase space. In the recurrence plots of intermittent signals before *c*) instability and *e*) blowout, black squares indicate the low-amplitude regime and diagonal lines correspond to the periodic oscillations in the time series. The kite-like elongation in the recurrence plot is the characteristic of type II intermittency. To show the kite like elongation, recurrence plots are zoomed in for a smaller time interval in Figures 4.16(*d*) and 4.16(*f*). The pattern in the recurrence plot suggests that intermittent signals ahead of both combustion instability and blowout are of type II.

The recurrence plots for the portion of the time series of acoustic pressure acquired during intermittency prior to both combustion instability and blowout are shown in Fig. 4.16. The black squares in the recurrence plot correspond to the low-amplitude regimes during intermittency and the diagonal lines represent the periodic oscillations. The pattern in the recurrence plots are used to identify the type of intermittency (Klimaszewska and Zebrowski, 2009). In the recurrence plots, the kite-like elongation of the corner of the black square is the characteristic feature of type

II intermittency (Klimaszewska and Zebrowski, 2009). Fig. 4.16 suggests that intermittency before the onset of both combustion instability and blowout are of Type II.

4. 10 Concluding remarks

An experimental investigation is performed to understand the physical mechanism for the occurrence of intermittency that presages the onset of both thermoacoustic instability and blowout in a lifted partially premixed turbulent jet flame combustor. Intermittent dynamics is found to play a crucial role in the transition to both thermoacoustic instability and blowout.

Intermittency that is observed during the transition from combustion noise to instability have characteristics of both instability and combustion noise. The out of phase interaction (negative correlation) of the acoustic pressure and the heat release rate fluctuations causes the low-amplitude fluctuations during intermittency prior to combustion instability in a manner similar to the source of combustion noise. On the other hand, the positively coupled feedback of flow-flame-duct acoustics drives the high-amplitude ordered pressure oscillations during intermittency in a manner similar to the driving mechanism of combustion instability. This leads us to conclude that the coupled interaction (alternatively either positive or negative) of flow-flame-duct acoustics may be the physical reason for intermittent behavior that presages combustion instability.

In contrast, the low-amplitude regime during intermittency prior to blowout is found to be characterized by blowout precursor events such as progressive weakening of the flame, local extinction and stretching/shrinking of the flame. The driving of high-amplitude oscillations is accompanied by re-ignition and the flame propagating towards the burner. Therefore, the intermittent dynamics prior to blowout occurs due to the competition between blowout precursor events (flame extinction & re-ignition) and the driving of high-amplitude periodic oscillations as the flame propagates towards the burner.

Further, analysis from a dynamical systems perspective suggest that intermittency prior to both thermoacoustic instability and blowout belongs to Type II category using return maps and recurrence plots. An understanding of the flame-flow-acoustic interaction during the transition to both combustion instability and blowout can be used to identify the mechanism of transition to both and to avoid their occurrence.

CHAPTER 5

CONCLUSIONS AND FUTURE WORK

The present thesis is aimed at formulating a complex systems perspective on the dynamics of the thermoacoustic systems in the framework of complex networks. The unsteady pressure data, which is a reflection of spatio-temporal changes in the thermoacoustic system is mapped as complex networks. The pattern or complex dynamics of combustion noise, transition to thermoacoustic instability and blowout from combustion noise are investigated in this framework. Further, the physical mechanisms behind such transitions are also investigated. The key results from the present investigations are summarized as conclusions as follows.

5.1 Conclusions

As a first step, the unsteady pressure representing the dynamics of the stable operation of the combustor is mapped as a complex network. It was shown that the combustion noise generated in a confined environment during the stable operation can be represented as a scale-free network. This scale-free structure is related to the scale invariance of combustion noise inside a confinement. The scale invariance of the combustion noise generated inside a confinement is difficult to be identified with the use of the frequency spectra, due to the presence of the shallow peaks of the acoustic pressure that arises from the coupling of the confinement modes with the combustion noise.

The existence of power laws in the distribution of connections between the nodes is the indicative of the scale-free network. The absence of single characteristic scale in the distribution of connections in the network is the reason why it is called a scale-free network. The power-law exponent has been used to estimate the Hurst exponent which is a measure of the fractality of the time series. The scale invariance of combustion noise is due to the turbulence. The turbulent flow involves fluctuations of scales that span a range from the largest scale of the order of the characteristic dimension of the flow to the smallest Kolmogorov scales that dominate the viscous dissipation. The fluctuations of multiple scales due to the turbulence is reflected as heterogeneous scale-free structure in the networks topology during combustion noise.

Further, it was shown that the limit cycle oscillations during thermoacoustic instability can be represented as a regular network with ordered topological structure. The distribution of connections between the nodes in the network during thermoacoustic instability is characterized by a single characteristic scale which is in contrast to combustion noise. The transition from combustion noise to thermoacoustic instability via intermittency is illustrated as a change in topology from a heterogeneous scale-free structure to an ordered regular structure.

The structural changes in the networks topology during the transition from combustion noise to thermoacoustic instability (i.e., scale-free to order) has been quantified by calculating the topological measures such as clustering coefficient, characteristic path length, network diameter and global efficiency. These network measures that change significantly well before the onset of thermoacoustic instability are used as the precursors.

The transition to the onset of flame blowout from the stable operation of combustor with respect to the change in operating conditions (i.e., air flow rate is increased) are investigated using complex networks. The onset of blowout happened via the occurrence of thermoacoustic instability and intermittency from combustion noise. The dynamical states close to the blowout conditions of the flame are represented as scale-free networks. The transition to blowout from thermoacoustic instability is represented as a change from a single discrete point to a power-law behavior in the distribution of connections in the network. The network properties are calculated at each operating conditions during the onset of flame blowout and are used to detect the onset of blowout.

The transition to both thermoacoustic instability and blowout of flame occurred via intermittency. The flow, flame and acoustics interactions are investigated in order to understand the physical reasons for the transitions in the thermoacoustic systems. The investigation clearly indicated that the physical reason for the occurrence of intermittency prior to the onset of thermoacoustic instability from combustion noise is the alternating, positively and negatively, coupled interaction of the flame, flow and duct acoustics. In contrast, the physical mechanism underlying the intermittent dynamics that presages the onset of blowout is the interplay between the blowout precursor events (local extinction and re-ignition) and the driving of high-amplitude pressure oscillations as the flame propagate towards the fuel tube. Alternatively, it was shown that there exists a commonality between the intermittency that presages thermoacoustic instability and the intermittency that presages blowout using the tools from dynamical systems theory. The intermittency prior to both thermoacoustic instability and blowout are shown to be Type II intermittency from the features in the first return maps and the recurrence plots.

5.2 Scope of future work

The present thesis established the complex network framework to investigate the complexity or the dynamical features of the thermoacoustic systems by obtaining the complex networks from the time series data using visibility algorithm. However, the complex behaviour of the thermoacoustic systems arises from the spatio-temporal changes happening in the interactions of the turbulent flow with the combustion and the acoustics. Therefore, further research on the time varying spatial network analysis of thermoacoustic systems could provide an insight into the dynamical changes happening in both space and time.

The onset of thermoacoustic instability from combustion noise is shown as the emergence of order in the complex networks. The further research on self-organization or self-evolution of complex networks can help develop a complex network model for the thermoacoustic systems and explore the underpinning mechanisms.

APPENDIX A

Visibility algorithm with different values of threshold

The degree distribution maps of complex networks derived during combustion noise (Fig. A.1*a*), intermittency (Fig. A.1*b*) and combustion instability (Fig. A.1*c*) using different values of ε are shown in Fig. A.1.

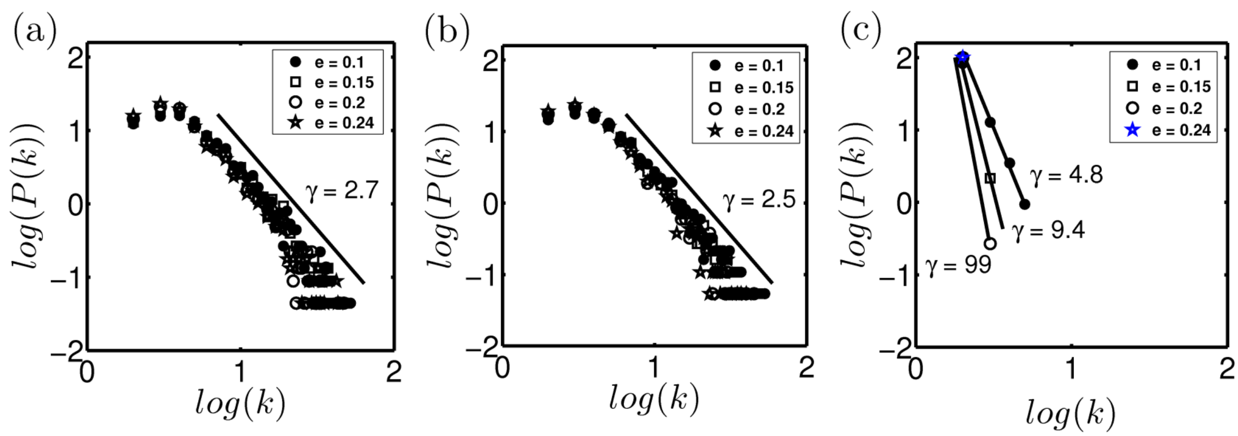

Figure A.1: Degree distribution maps of networks constructed from time series data of (*a*) combustion noise ($Re = 1.8 \times 10^4$), (b) Intermittency ($Re = 2.2 \times 10^4$) and (*c*) combustion instability ($Re = 2.8 \times 10^4$) for different values of *e*. For all *e*, combustion noise and intermittency remain to be scale-free. Use of ε helps us to detect periodicity in time series data during combustion instability. For all $e \geq 0.24$, network during combustion instability possess a discrete point in the degree distribution map, indicating that corresponding network is regular. The transition from combustion noise to combustion instability is reflected as transition from scale-free to regularity in complex networks topology.

The power law behavior of networks during the occurrence of combustion noise (Fig. A.1*a*) and intermittency (Fig. A.1*b*) remains the same and power law exponents do not change for different values of ε considered in the present work. This shows that combustion noise and intermittency remain scale-free with the use of ε. However, for increasing values of e from 0.1 to 0.24 (results are presented for values of $e = 0.1, 0.15, 0.2$ & 0.24 in Fig. A.1), number of points in the degree distribution map of complex network that correspond to combustion instability decreases along with an exponential increase in the value of power law exponent. For all $e \geq 0.24$, the network during combustion instability possesses a discrete point in the degree distribution map. Figure I confirms that use of epsilon helps in detecting the periodicity hidden in limit cycle oscillation during combustion instability and does not filter the information in the time series.

APPENDIX B

Sensitivity of network properties on length and sampling rate of the temporal signal

We illustrate the sensitivity of network properties to the length and sampling rate of the temporal signals in Fig. B.1 and Fig. B.2. Fig. B.1 and Fig. B.2 shows the variation of network properties during the transition from combustion noise to thermoacoustic instability via intermittency for different lengths (T = 1 *s*, 1.5 *s*, 2 *s*, 2.5 *s* and 3 *s*) and sampling rates (f = 2 *kHz*, 4 *kHz*, 6 *kHz*, 8 *kHz* and 10 *kHz*) of the time series respectively.

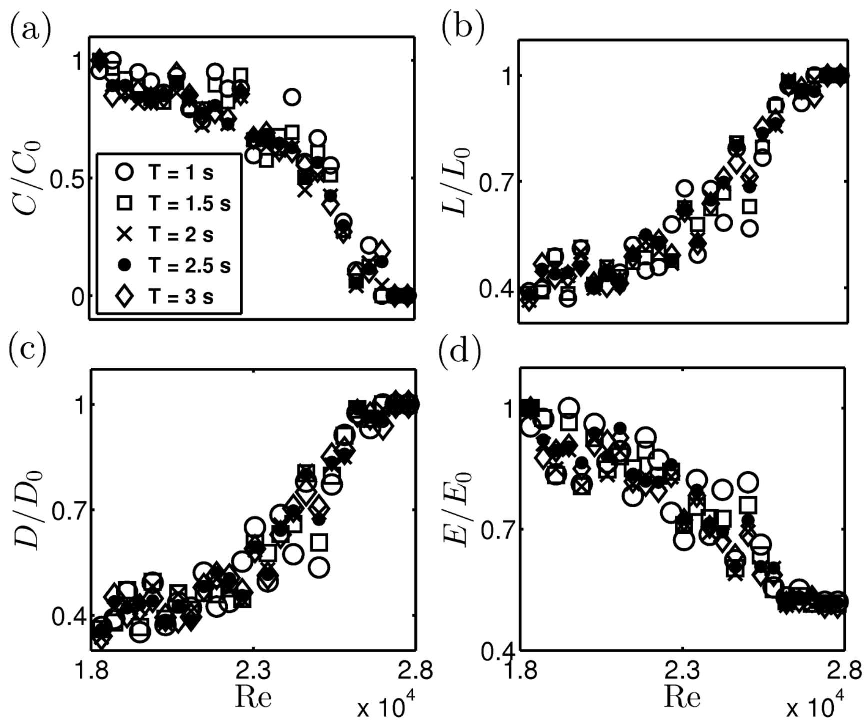

Figure B.1: Variation of normalized values of (*a*) clustering coefficient, (*b*) characteristic path length, (*c*) network diameter and (*d*) global efficiency for different values of lengths of the time series data. Here, the sampling rate of the time series is 10 *kHz*.

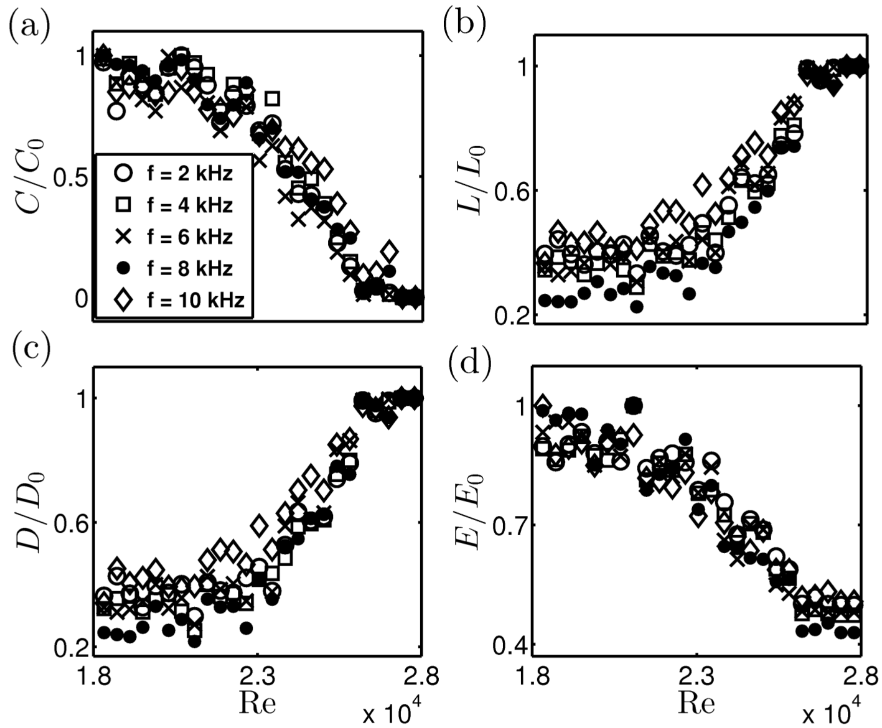

Figure B.2: Variation of normalized values of (*a*) clustering coefficient, (*b*) characteristic path length, (*c*) network diameter and (*d*) global efficiency for different values of sampling rates of the time series data. Here, the length of the time series is 3 seconds.

As can be seen from Fig. B.1 and Fig. B.2, the network properties do not change significantly for varying values of lengths and sampling rates of the temporal signal.

REFERENCES

Abarbanel, H. (2012). *Analysis of observed chaotic data*. Springer Science & Business Media.

Abugov, D. I. and **O. I. Obrezkov** (1978). Acoustic noise in turbulent flames. *Combustion, Explosion, and Shock Waves*, **14**, 606-612.

Albert, R., H. Jeong and **A. L. Barabasi** (2000). Error and attack tolerance of complex networks. *Nature*, **406**, 378-382.

Alm, E. and **A. P. Arkin** (2003). Biological networks. *Current opinion in structural biology*, **13**, 193-202.

Al-Shameri, W. F. H. (2012). Dynamical properties of the Hénon mapping. *Int J Math Anal*, **6**, 2419-2430.

Annaswamy, A. M., M. Fleifil, J. P. Hathout, and **A. F. Ghoneim** (1997). Impact of linear coupling on the design of active controllers for the thermoacoustic instability. *Combustion Science and Technology*, **128**, 131–180.

Arianos, S., E. Bompard, A. Carbone and **F. Xue** (2009). Power grid vulnerability: A complex network approach. *Chaos*, **19**, 013119.

Bastian, M., S. Heymann and **M. Jacomy** (2009). Gephi: an open source software for exploring and manipulating networks. *Proc.3rd International ICWSM Conf.*, 361-362.

Barabási, A. L. and **R. Albert** (1999). Emergence of scaling in random networks. *Science*, **286**, 509-512.

Barabasi, A. L., R. Albert and **H. Jeong** (1999). Diameter of the world wide web. *Nature*, **401**, 130-131.

Barabasi, A. L. and **E. Bonabeau** (2003). Scale-Free Networks, *Sci. American*, **288**, 60-69.

Barabasi, A. L. and **Z. N. Oltvai** (2004). Network biology: understanding the cell's functional organization. *Nature Rev. Genetics*, **5**, 101-113.

Barabasi, A. L. (2011). The network takeover. *Nature Physics*, **8**, 14-16.

Belliard, A. (1997). Etude expe´rimentale de l'e´mission sonore des flammes turbulentes, Ph.D. Dissertation, Universite´s d'Aix-Marseille, France.

Ben-Dov, G., and **J. Cohen** (2007). Critical Reynolds number for a natural transition to turbulence in pipe flows. *Phy. Rev. Lett.* **98**, 064503.

Biswas, S., K. Kopp-Vaughn, M. W. Renfro and **B. M. Cetegen** (2013). Phase resolved characterization of conical premixed flames near and far from blowoff. *Combustion and Flame* **160**, 2843.

Bragg, S. L. (1963). Combustion noise. *J. Inst. Fuel*, **36**, 12-16.

Candel, S. (2002). Combustion dynamics and control: progress and challenges. *Proc. Combust. Inst.* **29**, 1-28.

Chaparro, A.A. and **Cetegen, B.M.** (2006). Blowoff characteristics of bluff-body stabilized conical premixed flames under upstream velocity modulation. *Combustion and flame*, **144** (1), 318-335.

Chakravarthy, S. R., R. Sivakumar and **O. J. Shreenivasan** (2007*a*). Vortex-acoustic lock-on in bluff-body and backward-facing step combustors. *Sadhana*, **32**, 145-154.

Chakravarthy, S. R., O. J. Shreenivasan, B. Boehm, A. Dreizler and **J. Janicka** (2007*b*). Experimental characterization of onset of acoustic instability in a nonpremixed half-dump combustor. *The Journal of the Acoustical Society of America*, **122**, 120-127.

Charakopoulos, A. K., T. E. Karakasidis, P. N. Papanicolaou and **A. Liakopoulos** (2014). The application of complex network time series analysis in turbulent heated jets. *Chaos*, **24,** 024408.

Chaudhuri, S., and **Cetegen, B. M.** (2008). Blowoff characteristics of bluff-body stabilized conical premixed flames with upstream spatial mixture gradients and velocity oscillations. *Combustion and flame*, **153** (4), 616-633.

Chaudhuri, S., S. Kostka, S. G. Tuttle, M. W. Renfro and B. M. Cetegen (2010). Blowoff dynamics of V-shaped bluff body stabilized, turbulent premixed flames in a practical scale rig. *48th AIAA Aerospace Sciences Meeting including the new horizons Forum and Aerospace Exposition*, **AIAA-2010-1337**.

Chen, G., Z. Y. Dong, D. J. Hill, G. H. Zhang and **K. Q. Hua** (2010). Attack structural vulnerability of power grids: A hybrid approach based on complex networks. *Physica A* **389** (3), 595-603.

Chiu, H. H. and **M. Summerfield** (1974). Theory of combustion noise. *Acta Astronautica*, **1**, 967-984.

Clavin, P. and **E. D. Siggia** (1991). Turbulent premixed flames and sound generation. *Combustion Science and Technology*, **78**, 147-155.

Clavin, P. (2000). Dynamics of combustion fronts in premixed gases: from flames to detonations. *Proceedings of the Combustion Institute*, **28**, 569-585.

Coats, C. M. (1996). Coherent structures in combustion. *Prog. Energy & Combustion Sci.* **22** (5), 427-509.

Culick, F. E. C. (1970). Stability of longitudinal oscillations with pressure and velocity couping in a solid propellant rocket. *Combustion Science and Technology*, **2**, 179–201.

Culick, F. E. C. (1976). Nonlinear behavior of acoustic waves in combustion chambers. *ACTA Astronautica*, **3**, 715–734.

Culick, F. E. C. (1994). Some recent results for nonlinear acoustics in combustion chambers. *AIAA Journal*, **34**, 146–169.

Das, R. K. and **S. Pattanayak** (1993). Electrical impedance method for flow regime identification in vertical upward gas-liquid two-phase flow. *Meas. Sci. Tech*, **4**, 1457.

Davis, A., A. Marshak, W. Wiscombe and **R. Cahalan** (1996). Scale invariance of liquid water distributions in marine stratocumulus. Part I: Spectral properties and stationarity issues. *Journal of the atmospheric sciences*, **53**, 1538-1558.

Domen, S., H. Gotoda, T. Kuriyama, Y. Okuno and **S. Tachibana** (2015). Detection and prevention of blowout in a lean premixed gas-turbine model combustor using the concept of dynamical system theory. *Proceedings of the Combustion Institute*, **35**, 3245-3253.

Donner, R. V., Y. Zou, J. F. Donges, N. Marwan and **J. Kurths** (2010). Recurrence networks - A novel paradigm for nonlinear time series analysis. *New J. Phy.*, **12**, 033025.

Dowling, A. P. (1997). Nonlinear self-excited oscillations of a ducted flame. *Journal of Fluid Mechanics*, **346**, 271–290.

Dowling, A. P. and **S. R. Stow** (2003). Acoustic analysis of gas turbine combustors. *Journal of Propulsion and Power*, **19**, 751-764.

Dowling, A. P. and **Y. Mahmoudi** (2015). Combustion noise. *Proceedings of the Combustion Institute*, **35**, 65-100.

Driscoll, J. F. (2008). Turbulent premixed combustion: Flamelet structure and its effect on turbulent burning velocities. *Progress in Energy and Combustion Science* **34**, 91-134.

Dubos, T., A. Babiano, J. Paret and **P. Tabeling** (2001). Intermittency and coherent structures in the two-dimensional inverse energy cascade: Comparing numerical and laboratory experiments. *Physical Review E*, **64**, 036302.

Durox, D., T. Schuller, N. Noiray and **S. Candel** (2009). Experimental analysis of nonlinear flame transfer functions for different flame geometries. *Proceedings of the Combustion Institute*, **32**, 1391-1398.

Eser, J., Z. Pengsheng and **T. Jochen** (2014). Nonlinear dynamics analysis of a self-organizing recurrent neural network: chaos waning. PloS one, e86962.

Fichera, A., C. Losenno and **A. Pagano** (2001). Experimental analysis of thermoacoustic combustion instability. *Applied Energy*, **70**, 179–191.

Frisch, U. (1995). *Turbulence: the legacy of AN Kolmogorov*. Cambridge university press.

Gao, Z. and **N. Jin** (2009). Flow-pattern identification and nonlinear dynamics of gas-liquid two-phase flow in complex networks. *Physical Review E*, **79**,066303.

Gao, Z. K., N. D. Jin, W. X. Wang and **Y. C. Lai** (2010). Motif distributions in phase-space networks for characterizing experimental two-phase flow patterns with chaotic features. *Physical Review E*, **82**, 016210.

Gianni, G., G. Mariotti, E. Paganini and **S. Sello** (2003). Characterization and diagnostics of combustion thermoacoustic instabilities using nonlinear dynamics and topological methods. *Proc. Europ. Combust. Meeting*.

Gotoda, H., H. Nikimoto, T. Miyano and **S. Tachibana** (2011). Dynamic properties of combustion instability in a lean premixed gas-turbine combustor. *Chaos*, **21**, 013124.

Gotoda, H., M. Amano, T. Miyano, T. Ikawa, K. Maki and **S. Tachibana** (2012). Characterization of complexities in combustion instability in a lean premixed gas-turbine model combustor. *Chaos*, **22**, 043128.

Gotoda, H., Y. Shinoda, M. Kobayashi and **Y. Okuno** (2014). Detection and control of combustion instability based on the concept of dynamical system theory. *Phy. Rev. E*, **89**, 022910.

Griebel, P., E. Boschek and **P. Jansohn** (2007). Lean blowout limits and NOx emissions of turbulent, lean premixed, hydrogen-enriched methane/air flames at high pressure. *Journal of engineering for gas turbines and power*, **129**, 404-410.

Hegde, U. G., D. Reuter and **B. T. Zinn** (1988). Sound generation by ducted flames. *AIAA journal*, **26**, 532-537.

Jahnke, C. C. and **F. E. C. Culick** (1994). Application of dynamical systems theory to nonlinear combustion instabilities. *Journal of Propulsion and Power*, **10**, 508–517.

Kabiraj, L. and **R. I. Sujith** (2012). Nonlinear self-excited thermoacoustic oscillations: intermittency and flame blowout. *J. Fluid Mech.* **713**, 376-397.

Kalapala, V., V. Sanwalani, A. Clauset and **C. Moore** (2006). Scale invariance in road networks. *Physical Review E*, **73**, 026130.

Karimi, N., M. Brear, S. H. Jin and **J. P. Monty** (2009). Linear and nonlinear forced response of conical, ducted, laminar, premixed flames. *Combustion and Flame*, **156**, 2201–2212.

Kashinath, K., S. Hemchandra and **M. P. Juniper** (2013). Nonlinear thermoacoustics of ducted premixed flames: The influence of perturbation convection speed. *Combustion and Flame*, **160**, 2856-2865.

Kashinath, K., and **M. P. Juniper** (2013). Nonlinear phenomena in thermoacoustic systems with premixed flames. *Journal of Engineering for Gas Turbines and Power*, **135**, 061502-061502.

Kashinath, K., I. C. Waugh and **M. P. Juniper** (2015). Nonlinear self-excited thermoacoustic oscillations of a ducted premixed flame: bifurcations and routes to chaos. *Journal of Fluid Mechanics*, **761**, 399-430.

Klimaszewska, K., and J. J. Żebrowski (2009). Detection of the type of intermittency using characteristic patterns in recurrence plots. *Phy. Rev. E* **80**, 026214.

Kumar, R. N. (1975). Further experimental results on the structure and acoustics of turbulent jet flames. *AIAA 2nd Aero-Acoustics conference*, 24-26.

Kumara Gurubaran, R. (2005). *Experimental Investigation of Airblast Atomizer*. Master's thesis, IIT Madras, India.

Kraichnan, R. H. (1967). Inertial ranges in two-dimensional turbulence. *Phys. Fluids*, **10**, 1417–1423.

Lacasa, L., B. Luque, F. Ballesteros, J. Luque and **J. C. Nuno** (2008). From time series to complex networks: The visibility graph. *Proc. Nat. Acad. Sci.*, **105**, 4972-4975.

Lacasa, L., B. Luque, J. Luque and **J. C. Nuno** (2009). The visibility graph: A new method for estimating the Hurst exponent of fractional Brownian motion. *Euro physics Letters*, **86**, 1-5.

Lesne, A. and **M. Laguës** (2011). *Scale invariance: From phase transitions to turbulence*. Springer.

Lei, S. and **A. Turan** (2009). Nonlinear/chaotic behaviour in thermoacoustic instability. *Combustion Theory and Modelling*, **13**, 541–557.

Lewis, B. and **G. Von Elbe** (2012). *Combustion, flames and explosions of gases*. Elsevier.

Lieuwen, T. C. (2002). Experimental investigation of limit-cycle oscillations in an unstable gas turbine combustor. *J. Prop. Power*, **18**, 61-67.

Lieuwen, T. C. (2005). Online combustor stability margin assessment using dynamic pressure data. *Journal of engineering for gas turbines and power*, **127**, 478-482.

Lieuwen, T. C. (2012). *Unsteady combustor physics*. Cambridge University Press.

Liu, C., W. X. Zhou and **W. K. Yuan** (2010). Statistical properties of visibility graph of energy dissipation rates in three-dimensional fully developed turbulence. *Physica A.*, **389**, 2675-2681.

Longwell, J. P., J. E. Chenevey, W. W. Clark and **E. E. Frost** (1948). Flame stabilization by baffles in a high velocity gas stream. In Symposium on Combustion and Flame, and Explosion Phenomena, **3**, 40-44.

Lovejoy, S. and **D. Schertzer** (1986). Scale invariance, symmetries, fractals, and stochastic simulations of atmospheric phenomena. *Bulletin of the American meteorological society*, **67**, 21-32.

Luque, B., L. Lacasa, F. Ballesteros and **J. Luque** (2009). Horizontal visibility graphs: Exact results for random time series. *Physical Review E*, **80**, 046103.

Mariappan, S. (2011). *Theoretical and experimental investigation of the non-normal nature of thermoacoustic interactions*. Ph. D thesis, IIT Madras, India.

Mcmanus, K. R., T. Poinsot and **S. M. Candel** (1993). A review of active control of combustion instabilities. *Prog. Energy Combust. Sci.* **16**, 1-29.

Milgram, S. (1967). The small world problem. *Psychology today*, **2**, 60-67.

Mukhopadhyay, A., R. R. Chaudhari, T. Paul, S. Sen and **A. Ray** (2013). Lean blow-out prediction in gas turbine combustors using symbolic time series analysis. *Journal of Propulsion and Power*, **29**, 950-960.

Muruganandam, T. M., S. Nair, D. Scarborough, Y. Neumeier, J. Jagoda, I. C. Lieuwen, J. Seitzman and **B. T. Zinn** (2005). Active control of lean blowout for turbine engine combustors. *Journal of Propulsion and Power*, **21**, 807-814.

Muruganandam, T. (2006). *Sensing and dynamics of lean blowout in a swirl dump combustor*. Ph. D. thesis, Georgia Institute of Technology, Atlanda, United States.

Muruganandam, T. and **J. Seitzman** (2012). Fluid mechanics of lean blowout precursors in gas turbine combustors. *International Journal of Spray and Combustion Dynamics*, **4**, 29-60.

Murugesan, M., V. Nair and **R. I. Sujith** (2014). System and method for early detection of onset of instabilities using complex networks, Provisional Patent, Filed on April 29.

Murugesan, M. and **R. I. Sujith** (2014). Threshold grouping method to derive complex networks from time series. *Network and Complex Systems*, **4**, 17-23.

Nair, S., and **T. C. Lieuwen** (2005). Acoustic detection of blowout in premixed flames. *J. Prop. Power* **21**, 32-39.

Nair, S. (2006). *Acoustic characterization of flame blowout phenomenon*. Ph. D. thesis, Georgia Institute of Technology, Atlanda, United States.

Nair, S. and **T. C. Lieuwen** (2007). Near-blowoff dynamics of a bluff-body stabilized flame. *Journal of Propulsion and power*, **23**, 421-427.

Nair, V. (2014). *Role of intermittency in the onset of combustion instability*, Ph. D. thesis, IIT Madras, India.

Nair, V., G. Thampi, S. Karuppasamy, S. Gopalan and **R. I. Sujith** (2013). Loss of chaos in combustion noise as a precursor for impending instability. *Intl J. Spray Combus.Diag.*, **5**, 273-290.

Nair, V. and **R. I. Sujith** (2013). Identifying homoclinic orbits in the dynamics of intermittent signals through recurrence quantification. *Chaos: An Interdisciplinary Journal of Nonlinear Science*, **23**, 033136.

Nair, V. and **R. I. Sujith** (2014). Multifractality in combustion noise: Predicting an impending instability. *J. Fluid Mech.*, **747**, 635-655.

Nair, V., G. Thampi and **R. I. Sujith** (2014). Intermittency route to thermoacoustic instability in turbulent combustors. *J. Fluid Mech.*, **756**, 470-487.

Nair, V. and **R. I. Sujith** (2015). Intermittency as a transition state in combustor dynamics: An explanation for flame dynamics near lean blowout. *Combustion Science and Technology*, **187**, 1821-1835.

Ni, X. H., Z. Q. Jiang, and **W. X. Zhou (**2009). Degree distributions of the visibility graphs mapped from fractional Brownian motions and multifractal random walks. *Physics Letters A*, **373**, 3822-3826.

Nicholson, H. M. and **J. P. Field** (1948). Some experimental techniques for the investigation of the mechanism of flame stabilization in the wakes of bluff bodies. *In Symposium on combustion and flame, and explosion phenomena*, **3**, 44-68.

Noiray, N., D. Durox, T. Schuller and **S. Candel** (2006). Self-induced instabilities of premixed flames in a multiple injection configuration. *Combustion and Flame*, **145**, 435–446.

Noiray, N., D. Durox, T. Schuller and **S. Candel** (2008). A unified framework for nonlinear combustion instability analysis based on the flame describing function. *Journal of Fluid Mechanics*, **615**, 139-167.

Noiray, N. and **B. Schuermans** (2012). Theoretical and experimental investigations on damper performance for suppression of thermoacoustic oscillations. *J. Sound and Vibration*, **331**, 2753-2763.

Nunez, A. M., L. Lacasa, J. P. Gomez and **B. Luque** (2012). Visibility algorithms: A short review. *New Front. Graph Theory*, 119-152.

Okuno, Y., M. Small and **H. Gotoda** (2015). Dynamics of self-excited thermoacoustic instability in a combustion system: Pseudo-periodic and high-dimensional nature. *Chaos: An Interdisciplinary Journal of Nonlinear Science*, **25**, 043107.

Pagani, G. A. and **M. Aiello** (2014). Power grid complex network evolutions for the smart grid. *Physica A*, **396**, 248-266.

Paret, J. and **P. Tabeling** (1998) Intermittency in the two-dimensional inverse cascade of energy: Experimental observations. *Physics of Fluids (1994-present)*, **10**, 3126-3136.

Paschereit, C. O., B. Schuermans, W. Polifke and **O. Mattson** (2002). Measurement of transfer matrices and source terms of premixed flames. *Journal of Engineering for Gas Turbines and Power*, **124**, 239-247.

Pawar, S. A., R. Vishnu, M. Vadivukarasan, M. V. Panchagnula and **R. I. Sujith** (2015). Intermittency route to combustion instability in a laboratory spray combustor. *Journal of Engineering for Gas Turbine and Power*, **138**, 041505.

Pocheau, A. (1994). Scale invariance in turbulent front propagation. *Physical Review E*, **49**, 1109-1122.

Poinsot, T. J., A. C. Trouve, D. P. Veynante, S. M. Candel and **E. J. Esposito** (1987). Vortex-driven acoustically coupled combustion instabilities. *J. Fluid Mech.*, **177**, 265-292.

Pomeau, Y. and **P. Manneville** (1980). Intermittent transition to turbulence in dissipative dynamical systems. *Comm. Math. Phy.* **74**, 189-197.

Quenell, G. (1994). Spectral diameter estimates for *k*-regular. *Advances in Mathematics*, **106**, 122-148.

Rajaram, R. (2007). *Characteristics of sound radiation from turbulent premixed flames*, Ph. D thesis, Georgia Institute of Technology, USA.

Rajaram, R. and **T. C. Lieuwen** (2009). Acoustic radiation from turbulent premixed flames. *Journal of Fluid Mechanics*, **637**, 357-385.

Rasmussen, C. C. and **J. F. Driscoll** (2008). Blowout Limits of Flames in High-Speed Airflows: Critical Damkohler Number. In *44th AIAA/ASME/SAE/ASEE Joint Propulsion Conference & Exhibit,* **AIAA 2008-4571**.

Rayleigh, J. W. S. (1878). The explanation of certain acoustical phenomena. *Nature*, **18**, 319–321.

Renyi, A. and **P. Erdos** (1959). On random graphs. *Publicationes Mathematicae*, **6**, 290-297.

Roehle, I., R. Schodl, P. Voigt and **C. Willert** (2000). Recent developments and applications of quantitative laser light sheet measuring techniques in turbomachinery components. *Measurement Sci. Tech.* **11** (7), 1023.

Rogers, D. E. (1956). A mechanism for high-frequency oscillation in ramjet combustors and afterburners, *J. Jet Prop.*, **26**, 456-462.

Rouhani, S. Z. and **M. S. Sohal** (1983). Two-phase flow patterns: A review of research results. *Progress in Nuclear Energy*, **11**, 219-259.

Schadow, K. C., E. Gutmark, T. P. Parr, D. M. Parr, K. J. Wilson and **J. E. Crump** (1989). Large-scale coherent structures as drivers of combustion instability. *Combust. Sci tech.*, **64**, 167-186.

Schadow, K. C., and **E. Gutmark** (1992). Combustion instability related to vortex shedding in dump combustors and their passive control. *Prog. Energy and Combust. Sci.*, **18**, 117-132.

Schefer, R. W., D. M. Wicksall and **A. K. Agrawal** (2002). Combustion of hydrogen-enriched methane in a lean premixed swirl-stabilized burner. *Proceedings of the combustion institute*, **29**, 843-851.

Schlichting, H. and **K. Gersten** (2000). *Boundary-layer theory*. Springer Science & Business Media **8**, 1-800.

Schuller, T., D. Durox and **S. Candel** (2003). A unified model for the prediction of laminar flame transfer functions: comparisons between conical and V-flame dynamics. *Combustion and Flame*, **134**, 21-34.

Searby, G. and **D. Rochwerger** (1991). A parametric acoustic instability in premixed flames. *J. Fluid Mech.* **231**, 529-543.

Searby, G. (1992). Acoustic instability in premixed flames. *Comb. Sci. tech.* **81**, 221-231.

Shanbhogue, S. J., S. Husain and **T. C. Lieuwen** (2009). Lean blowoff of bluff body stabilized flames: Scaling and dynamics. *Progress in Energy and Combustion Science* **35**, 98-120.

Shats, M. G., H. Xia and **H. Punzmann** (2005). Spectral condensation of turbulence in plasmas and fluids and its role in low-to-high phase transitions in toroidal plasma. *Physical Review E*, **71**, 046409.

Smith, D. A. and **E. E. Zukoski** (1985). Combustion instability sustained by unsteady vortex combustion. *AIAA/SAE/ASME/ASEE 21st Joint propulsion conference*, **AIAA-85-1248**.

de Sola Pool, I. and **M. Kochen** (1979). Contacts and influence. *Social networks*, **1**, 5-51.

de Solla Price, D. J. (1965). Is technology historically independent of science? A study in statistical historiography. *Technology and Culture*, 553-568.

Solomonoff, R. and **A. Rapoport** (1951). Connectivity of random nets. The bulletin of mathematical biophysics, **13**, 107-117.

Sommeria, J. (1986). Experimental study of the two-dimensional inverse energy cascade in a square box. *Journal of fluid mechanics*, **170**, 139-168.

Spalding, D. B. (1955). *Some fundamentals of combustion*, **2**, Academic Press.

Sterling, J. D. (1993). Nonlinear analysis and modeling of combustion instabilities in a laboratory combustor. *Combustion Science and Technology*, **89**, 167–179.

Strahle, W. C. (1971). On combustion generated noise. *Journal of Fluid Mechanics*, **49**, 399-414.

Strahle, W. C. (1978). Combustion noise. *Progress in Energy and Combustion Science*, **4**, 157-176.

Strogatz, S. H. (2014). *Nonlinear dynamics and chaos: with applications to physics, biology, chemistry, and engineering*. Westview press.

Subramanian, P., S. Mariappan, R. I. Sujith and **P. Wahi** (2010). Bifurcation analysis of thermoacoustic instability in a horizontal Rijke tube. *International journal of spray and combustion dynamics*, **2**, 325-355.

Subramanian, P. and **R. I. Sujith** (2011). Non-normality and internal flame dynamics in premixed flame–acoustic interaction. *Journal of Fluid Mechanics*, **679**, 315-342.

Tan, C. O., M. A. Cohen, D. L. Eckberg and **J. A. Taylor** (2009). Fractal properties of human heart period variability: physiological and methodological implications. *The Journal of physiology*, **587**, 3929-3941.

Thampi, G. and **R. I. Sujith** (2015). Intermittent Burst Oscillations - The Signature Prior to Flame Blowout in a Swirl Stabilized Combustor. *J. Prop. Power* / In-Press.

Thiffeault, J. L. and **M. D. Finn** (2006). Topology, braids and mixing in fluids. *Philosophical Transactions of the Royal Society A: Mathematical, Physical and Engineering Sciences* **364**, 3251-3266.

Tyagi, M., S. R. Chakravarthy, and **R. I. Sujith** (2007). Unsteady response of a ducted non-premixed flame and acoustic coupling. *Combustion Theory and Modelling*, **11**, 205–226.

Unni, V. R., V. Nair and **R. I. Sujith** (2013). Early warning system and methods for online prediction of an impending blowout in combustion systems, Provisional Patent, Filed on 08 November.

Unni, V. R. and **R. I. Sujith** (2015). Multifractal characteristics of combustor dynamics close to lean blowout. (In press).

Waldrop, M. M. (1992). *Complexity: The Emerging Science at the Edge of Order and Chaos*. Simon and Schuster, New York.

Watts, D. J. and **S. H. Strogatz** (1998). Collective dynamics of 'small-world'networks. *Nature*, **393**, 440-442.

Watts, D. J. (1999). *Small worlds: the dynamics of networks between order and randomness*. Princeton university press.

Waugh, I. C., K. Kashinath and **M. P. Juniper** (2014). Matrix-free continuation of limit cycles and their bifurcations for a ducted premixed flame. *Journal of Fluid Mechanics*, **759**, 1-27.

Wu, X., M. Wang, P. Moin and **N. Peters** (2003). Combustion instability due to the nonlinear interaction between sound and flame. *J. Fluid Mech.* **497**, 23-53.

Wohl, K. (1953). *Quenching, flash-back, blow-off-theory and experiment*. In Symposium (International) on Combustion, **4**, 68-89.

Xiao, Z., M. Wan, S. Chen and **G. L. Eyink** (2009). Physical mechanism of the inverse energy cascade of two-dimensional turbulence: a numerical investigation. *Journal of Fluid Mechanics*, **619**, 1-44.

Yu, K. H., A. Trouve and **J. W. Daily** (1991). Low-frequency pressure oscillations in a model ramjet combustor. *J. Fluid Mech.*, **232**, 47-72.

Yi, T. and **E. J. Gutmark** (2008). Online prediction of the onset of combustion instability based on the computation of damping ratios. *Journal of Sound Vibration*, **310**, 442-447.

Yoshimura, T., V. McDonell and **S. Samuelsen** (2005). Evaluation of hydrogen addition to natural gas on the stability and emissions behavior of a model gas turbine combustor. *In ASME Turbo Expo 2005: Power for Land, Sea, and Air*, 573-581.

Zank, G. P. and **W. H. Matthaeus** (1990). Nearly incompressible hydrodynamics and heat conduction. *Physical review letters* **64**, 1243-1246.

Zhang, J. and **M. Small** (2006). Complex network from pseudo-periodic time series: Topology versus dynamics, *Phy. Rev. Lett.*, **96**, 238701.

Zhang, J., J. Sun, X. Luo, K. Zhang, T. Nakamura and **M. Small** (2008). Characterizing pseudoperiodic time series through the complex network approach. *Physica D: Nonlinear Phenomena*, **237**, 2856-2865.

Zorick, T., and **M. A. Mandelkern** (2013). Multifractal detrended fluctuation analysis of human EEG: preliminary investigation and comparison with the wavelet transform modulus maxima technique. PloS one, **8**, e68360.

Zukoski, E. E. and **F. E. Marble** (1955). The role of wake transition in the process of flame stabilization on bluff bodies. *AGARD Combustion Researches and Reviews*, 167-180.

LIST OF PAPERS BASED ON THESIS

Referred Journals:

1. **Murugesan, M.** and Sujith, R. I. Threshold grouping method to derive complex networks from time series. *Journal of networks and complex systems*, 4**,** 17-23, (2014).

2. **Murugesan, M.** and Sujith, R. I. Combustion noise is scale-free: transition from scale-free to order at the onset of thermoacoustic instability. *Journal of Fluid Mechanics*, 772, 225-245, (2015).

3. **Murugesan, M.** and Sujith, R. I. Detecting the onset of an impending thermoacoustic instability in a turbulent combustor using complex networks. *Journal of Propulsion and Power*, (2015 - accepted for publication).

4. **Murugesan, M.** and Sujith R. I. Physical mechanisms that cause intermittency that presages combustion instability and blowout in a turbulent lifted jet flame combustor. *Combustion Science and Technology*, (2015 - under review).

Peer-reviewed Conferences:

1. **Murugesan, M.,** and Sujith R. I. Experimental investigation of the onset of thermoacoustic instability in a turbulent combustor using complex networks. *22nd International Conference on Sound and Vibration, Florence*, Italy, July 12 –16, 2015.

2. **Murugesan, M.,** and Sujith R. I. Flow-acoustic-flame interaction during the transition to thermoacoustic instability in turbulent lifted jet flame combustor. *22nd International Conference on Sound and Vibration*, Florence, Italy, July 12 –16, 2015.

Abstract-reviewed Conferences:

1. **Murugesan, M.,** and Sujith R. I. A complex network approach to combustion dynamics. 51st AIAA/SAE/ASEE Joint Propulsion Conference, Orlando, Florida, July 27 –29, 2015.

2. **Murugesan, M.,** and Sujith R. I. Intermittency in combustion dynamics. *51st AIAA/SAE/ASEE Joint Propulsion Conference*, Orlando, Florida, July 27 –29, 2015.